UNIVERSITY OF BIRMINGHAM

PHOTONIC HYDROGEL SENSORS

By

Yousef Alqurashi

A thesis submitted to
The University of Birmingham
for the degree of

DOCTOR OF PHILOSOPHY

School of Engineering
College of Engineering
and Physical Science
University of Birmingham
April 2020

Abstract

Hydrogels are an important tools for sensing because of their sensitivity to small adjustments and reactions to physical, biological, and chemical changes. They have been used in wide range of applications such as biomedical fields for drug delivery and in diagnostics. Hydrogel-based systems are a reusable sensing platform to quantify biomarkers in high-risk patients at clinical and point-of-care settings. In this thesis, two fabrication methods have been developed to successfully detect glucose concentration, pH changes and intraocular pressure (IOP). Continuous glucose monitoring aims to achieve accurate control of blood glucose concentration to prevent hypo/hyperglycaemia in diabetic patients. Also, the development of pH changes sensing device is the key to prevent the fatal implications. The Increasing of intraocular pressure (IOP) is the main risk factor for glaucoma, which is the second major source of losing sight in the world.

The first method is to developed hydrogel-based sensor by using stamping technique. A novel glucose sensor based on hydrogel with a micro-imprinted hexagonal structure was fabricated here. Our method utilized diffraction properties of a hexagonally photonic microscale concavities to detect the changes in the glucose concentration from 1 mM to 200 mM. In addition, same method was used to design a new pH hydrogel-based sensor with imprinted Fresnel lens. The sensor was able to monitor the pH changes with respond time of 5 minutes. The sensor had pH range from 4.5 to 7 and showed an increase in the sensitivity after 10 days storage in PBS solution of pH 7.4. Also, when the effect of temperature changes was investigated in the study, the temperature effect was negligible in the performance the sensor.

The second method is Laser ablation of commercial contact lenses. Initially, CO_2 laser (HPC LS 3040) was used to modify the surface properties of the lens at selective areas by creating 1D and 2D patterns. Laser parameters (space gap between the patterns and laser power, and scan speed) were examined to find the optimal laser setting. We managed to improve the wettability properties of the lens by increasing the density of the surface. After that, we engraved two circular micro-channels on the contact lens using CO_2 laser (Rayjet laser). Three different lenses were fabricated with various spacing gap between the channels (1 mm, 1.5 mm and 2 mm). The lenses had maximum channel depth of up to 20 μm. By using laser treated lenses, a change in pressure from 12 mmHg to 22 mmHg, normal eye IOP and glaucoma patients IOP, was detect by the lenses.

In summary, this thesis presents important findings that can be recommended for application in medical point-of-care diagnostics, implantable chips, and wearable continuous monitoring devices to quantify biomarkers. These methods offer sensing devices that are easy and fast to manufacture, cost effective, fast response and noninvasive sensors.

Acknowledgements

Firstly, thanks to Almighty Allah for giving me strength and ability to understand, learn and complete this thesis. Also, I would like to give special thanks to all my family, my wife and friends who have given me support throughout the journey.

I wish to express my deepest gratitude to my supervisor **Dr. Haider Butt** for his guidance, motivation and support throughout my Ph.D. program research. His guidance helped me in all the time of research. I could not have imagined having a better supervisor my Ph.D study. Also, I would like to acknowledge the valuable input of **Dr. Khamis Essa**.

Besides my supervisors, I would like to thank **Dr. Magdolena Bajgrowicz-Cieslak, Dr. Umair Hassan** and **Dr. Ali K. Yetisen** for their insightful discussions that helped to shape this projects. My sincere thanks also goes my colleagues **Tawfiq Alqurashi, Ijaz Rashid, Mohamed Elsherif, Badr Alqattan. Yousef Alqurashi, Rajib Ahmed** and **Muhammed Waqas Khalid.**

I would like to Shaqra University, thank Saudi Arabia Cultural Bureau in London and the Saudi Government for the research funding. This thesis was partly copy-edited for the conventions of language, grammar and spelling by Janet's Proofreading Service.

Table of Contents

List of Figures

List of Tables

List of Publications

Peer-reviewed Journal Publications

[1] M. Bajgrowicz-Cieslak, **Y. Alqurashi**, M. I. Elshereif, A. K. Yetisen, M. U. Hassan, and H. Butt, "Optical glucose sensors based on hexagonally-packed 2.5-dimensional photonic concavities imprinted in phenylboronic acid functionalized hydrogel films," RSC Adv., vol. 7, no. 85, 2017. (Chapter 3).

[2] **Y. Alqurashi**, M. Elsherif, A. Hendi, K. Essa, and H. Butt, "Optical hydrogel detector for pH measurements," Sensors, 2020. (Chapter 4) This paper is still in process

[3] **Y. Alqurashi**, M. Bajgrowicz-Cieslak, M. U. Hassan, A. K. Yetisen, and H. Butt, "Laser-Induced Surface Modification of Contact Lenses," Adv. Eng. Mater., vol. 20, no. 6, 2018. (Chapter 5)

[4] **Y. Alqurashi,** M. Elsherif, M. Bajgrowicz-cieslak, M. U. Hassan, K. Essa, and H. Butt, "Contact Lenses-Based Microchannels for Continuous Monitoring of Glaucoma," Contact lens anterior eye J., 2020. (Chapter 6) This paper is still in process.

Conferences

[1] **Y. Alqurashi,** "Non-invasive Test to Monitor the Glucose Levels In the Tears", Engineering symposium, University of Birmingham, Birmingham, 2016.

[2] **Y. Alqurashi,** "Optical Glucose Sensors Based on Imprinted Nanopatterns in Hydrogel System", SETCOR Conference, Dubai, 2017.

[3] **Y. Alqurashi,** "Contact Lenses Sensor to measure IOP for Glaucoma" FESAT, London, 2019.

[4] **Y. Alqurashi,** "Measuring pH Level Using Fresnel Lens", The Chemistry Congress in London, London, 2019.

List of Nomenclatures

Δd	Change in the Groove constant
$\Delta\lambda$	Wavelength shift
θ^*	The apparent contact angle
θ_e	The equilibrium of the contact angle
θ_i	Incidence angle
θ_r	Reflection angle
θ_t	Transmission angle
θ_d	Diffraction angle
λ	Wavelength
τ	The time constant of swelling
c	The speed of light in vacuum
d	The groove constant
D_{coop}	Cooperative diffusion
D_T	Heat transfer coefficient
D_S	Mass transfer coefficient
E	Extension
F	Load
Hz	Hertz
m	Diffraction order
n	Refractive index
n_i and n_t	Refractive indexes
r	The final radius
$r_{\infty,max}$	the maximal radius in the equilibrium swelling
r_0	The initial radius
t	Time
v	Speed
v_i	The incident wave speed
v_t	The transmission wave speed

List of Abbreviations

1D	One-dimensional	2D	Two-dimensional
2.5D	2.5- dimensional	2-HMP	2-hdroxy-2-methylpropiophenone
3-APB	3-(acrylamido) phenylboronic acid	3D	Three-dimensional
3-PBA	3-(acrylamido) phenylboronic acid	AA	Acrylamide
Ag/AgCl	Silver chloride	ArF laser	Argon fluoride laser
BCR	Base curve radius	BIS	N,N'-methylenebisacrylamide
CCA	Colloidal crystal arrays	CCT	Central corneal thickness
CLS	Contact lens sensor	CO_2	Carbon Dioxide
CT	Centre thickness	DI	Deionized
DMPA	2,2-dimethoxy-2-phenylacetophenone	DMSO	Dimethyl sulfoxide
DS	mass transfer coefficient	DT	heat transfer coefficient
DTC	Diurnal tension curve	EGDMA	Ethylene glycol dimethacrylate
FDA	Food and drug administration	FITC-dextran	Fluorescein isothiocyanate dextran
FRET	Forster resonance energy transfer	FT	Fourier transforms
GA	Glutaraldehyde	GAT	Goldmann applanation tonometry
GCCA-lens	Gelated colloidal crystal attached lens	GOD	Glucose oxidase
GSH	Glucose sensitive hydrogel	HEMA	2-Hydroxyethyl methacrylate
ICU	Intensive care unit	IOP	Intraocular pressure
K+	Potassium ion	Laser	Light Amplification by Stimulated Emission of Radiation
LED	Light emitting diode	Na+	Sodium ion
Nd:YAG lasers	neodymium-doped yttrium aluminum garnet	OP	Optical power
OPL	Optical path length	PA	Polyacrylamide
PBS	Phosphate buffer saline	PC	Photonic crystal
PCCA	Polymerized crystalline colloidal array	Pd	Palladium
PDMAEMA	Poly(dimethylaminoethyl methacrylate)	PDMS	Polydimethyl siloxane

PEGDA	Polyethylene glycol diacrylate	PEGDMA	Polyethylene
PET	Polyethylene terephthalate	p-HEMA	poly-2-hydroxyethyl methacrylate
PHS	Photonic hydrogel sensor	PI	polyimide
PMMA	Polymethyl methacrylate	PNIPAAm	poly(N-isopropylacrylamide)
POC	Point-of-care	Pr	Maximum optical reflected power
PS	Photonic microstructure	Pt	Platinum
Pt	Profile of the optical transmitted power	Ptmax	Maximum optical transmitted power
PVA	Poly vinyl alcohol	RI	Refractive index
Ti	Titanium	TRITC-Con A	Tetramethylrhodamine isothicyanate concanavalin A
UV	Ultraviolet	v/v	Volume to volume ratio
vol	Volume	w/w	Weight to weight ratio

Chapter 1: Introduction

1.1 BACKGROUND

1.1.1 Contact lenses

Contact lenses are mainly used for vision correction by millions of people worldwide. The use of contact lenses has been widely discussed and developed over the past decades. They were discovered by Leonardo da Vinci about 500 years ago [1]. Then, A.E. Fick and Edouard Kalt succeded in designing a curved and fitted lens in 1888 [2]. In 1971 the first soft contact lens, which was made from a hydrogel polymer called hydroxyl-ethyl-methacrylate (HEMA), was approved by The Food and Drug Administration in the USA and made available on the market [3]. Three different generations of a silicone hydrogel soft lens were developed between 1998 and 2007, and colourful lenses were also launched [3, 4].

The main reason for wearing contact lenses is to correct vision deficiencies [5]. However, they also have been used in a variety of applications, such as for sensors and drug delivery devices [6,7]. The design of the lens should consider the following properties: biocompatibility, oxygen permeability, transparency, and thermal and oxidative stability [5]. Nowadays the majority of contact lenses are soft and mainly made out of HEMA; only 15% are hard contact lens [8], with poly(methyl methacrylate) PMMA used to produce the hard lens [3]. The process of manufacturing a contact lens consists of additional materials to the polymers, such as cross-linkers and initiators [5, 9]. Further, the soft contact lens materials may mix with silicon polymers and phosphoryl-choline to increase, for example, the oxygen permeability and biocompatibility [9, 10].

The contact lenses can be applied as sensors to analyse tear fluid, monitor blood glucose and intraocular pressure [6, 11]. Blood, urine, saliva, and tears are often used in relation to disease diagnosis in hospitals [12, 13]. For example, a blood test is common in glucose measurement technology by finger-pricking methods [7]. However, this method seems to be invasive and a blood infection may occur during the process [13, 14]. Therefore, researchers have tried to develop a diabetic assessment that is a non-invasive test and provides continuous monitoring [6, 7, 15]. Many studies have suggested using contact lenses to trace sugar levels with assistance of the tear fluid because it is safe and convenient [6, 7, 12, 16].

Moreover, contact lenses are appropriate for ophthalmic drug delivery as a treatment method [11, 17, 18]. This delivery system has grown fast and became attractive to researchers. However, the common method is still eye drops, which dominates about 90% of the treatment [17, 19]; despite the fact that the eye drops' technique has possible side effects, and is less efficient [18, 20]. The lens delivery system faces a main problem in that the drugs' release time is short [17]. Thus, it becomes necessary to develop a material such that the release rate can be managed. Some studies have recommended a specific material such as poly-2-hydroxyethyl methacrylate (p-HEMA) hydrogels [17, 21]. This material has improved the drug release rate in the contact lens for few days. Others explored different processes to control the release rate, by immersing a soft contact lens in drug solutions [18, 20].

1.1.2 Hydrogel sensors

Polymers that react to stimuli are plastic materials with molecular chains cross-linked to a 3-dimensional system, structured by a cross-linking interaction of polymer chains [22]. Usually, all polymers are solvophilic to a specific solution. In the company of these solvents'

solutions, non-cross-linked polymers are dissolvable; whereas cross-linked polymers will just swell and absorb the solvents because of the polymer chains' interconnections. They are called hydrogels if they swell in the water [23, 24].

Hydrogels are hydrophilic and water-swelling polymers that can transform chemical energy into mechanical energy [25]. They are chemically or physically cross-linked polymer systems in three dimensions that are capable of swelling up to 99% of their dry weights without dissolution [25–27]. The hydrogel's physical activity depends on its balance and dynamic swelling and shrinking activity in water [26]. These activities allow the polymer to respond to the changes in the surrounding environments [28]. The swelling and deswelling process also helps in the drug release [29]. Figure 1.1 shows the swelling and shrinking activities of a hydrogel system that occurred due to the effect of changes in temperature and pH [30].

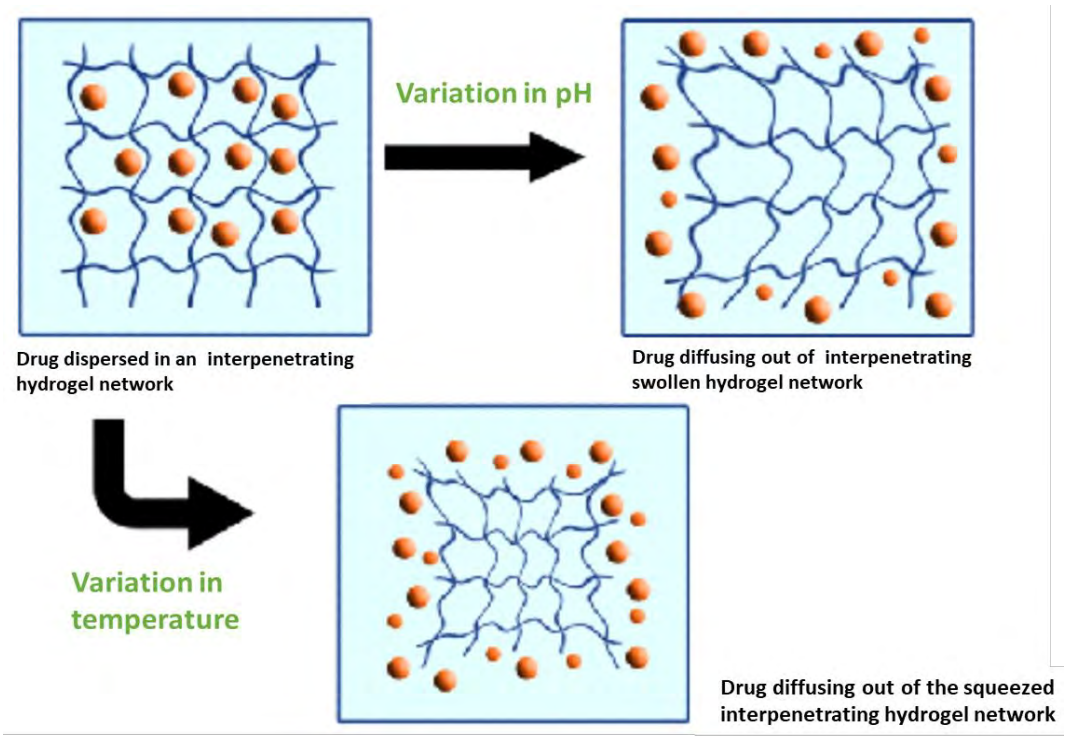

Figure 1.1: Presentation of the swelling and deswelling process of a hydrogel network affected by changes in temperature and pH

Hydrogels are an important tool for sensing because of their sensitivity to small adjustments and reactions to physical changes (e.g. pressure and temperature), biological changes (e.g. pH), or chemical changes (e.g. glucose) [31–35]. Additionally, they have been used in biomedical fields for drug delivery, and in diagnostics [26, 27]. Therefore, it is important to know and study which polymer is suitable to react to the desired sensor. Table 1.1 shows different hydrogels used to track and sense changes. Moreover, the preparation of a hydrogel sensor may include crosslinking with UV light and the use of other agents, such as adding phenylboronic acid in order to make glucose sensors [26, 36].

Table 1.1: list of hydrogels' composition and their applications

Hydrogel Composition	**Stimulus**	**Ref.**
N-isopropyl acrylamide	Temperature	[36]
poly(N-isopropylacrylamide) (PNIPAAm)	Temperature	[37]
HEMA	Glucose, sensitivity range 10 µM–40 mM	[38]
Polypyrrole	Glucose, sensitivity range up to 15 mM	[39]
Polyethylene glycol dimethacryalte (PEGDMA)	pH, swelling at pH 7.4, and deswelling at pH 1.2	[40]
Poly(dimethylaminoethyl methacrylate) (PDMAEMA)	pH, when PDMAEMA is mixed with acrylic acid, it can swell at low pH	[36]

Various types of measurement methods have been developed to determine hydrogels' changes, such as optical and mechanical methods [25, 36]. The optical approaches were

investigated extensively using different techniques such as reading the changes of fluorescence intensity with respect to the hydrogel's swelling [36]. Additionally, an interferometric method has been used to determine the hydrogel's swelling, in which a thin optical film network within the hydrogel transfers the volume changes to spectral information [36]. Another useful optical technique is tracking the shift in the wavelength of the diffraction light, referred to as Bragg diffraction [41]. The shift starts to happen due to the swelling and shrinking processes of the hydrogel. Figure 1.2 represents the typical wavelength shift in the diffraction, which is driven by Bragg's law (Equation 1.1) [25, 41]:

$$m\lambda = 2nd\ sin\ \theta_d \qquad \text{Equation 1.1}$$

where m is the diffraction order λ is the wavelength of light; n is the refractive index; d is the groove constant; and θ_d is the diffraction angle.

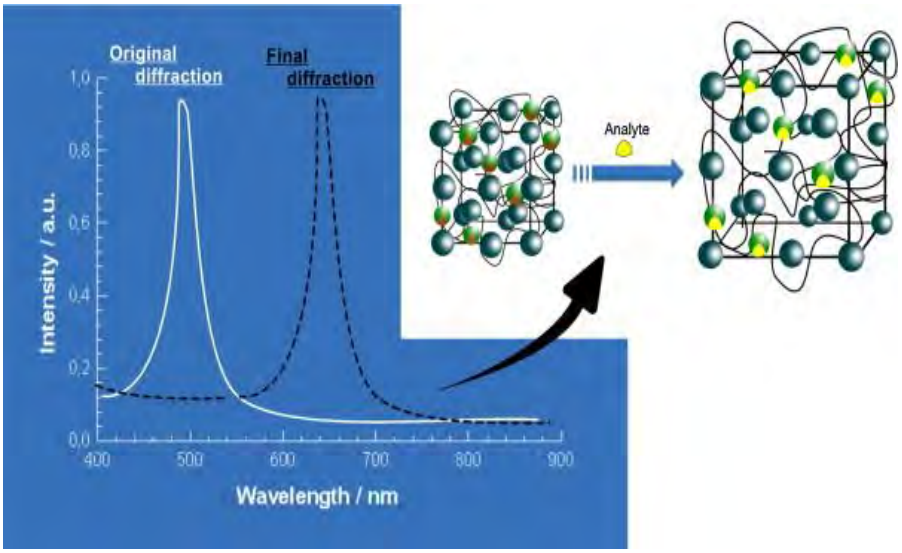

Figure 1.2: the typical shift in the wavelength of the diffraction light during swelling of the hydrogel

Hydrogels' swelling and shrinking processes are time-consuming and involve a transport of matter. Two transmission mechanisms have to be considered for starting a volume matter

transition. Firstly, the initiating stimuli, such as differences in temperature, solvents or ions which are related to the change of the pressure balance, must be passed into the hydrogel. This happens either by heat transfer (heat transfer coefficient, D_T) or by the continuous mass diffusion of a substance into the hydrogel (mass transfer coefficient, D_S). The second factor is to obtain the swelling equilibrium. During swelling and shrinking, the polymer chains must be relocated to new positions. Both the solvent diffusion and the chains' movement create a model called cooperative diffusion D_{coop}. (Figure 1.3). The time then can be defined by determining the time constant of swelling (τ) and the hydrogel radiuses during the swelling and shrinking by the following equations [24, 42, 43]:

$$\tau = \frac{r^2}{D_{coop}} \qquad \text{Equation 1.2}$$

where r is the final radius and the characteristic dimension. The radius of the hydrogel during the swelling and the shrinking are expressed in Equations 1.3 and 1.4, respectively:

$$r(t) = r_0 + (r_{\infty,max} - r_0) \cdot \left(1 - e^{-\frac{t}{\tau}}\right) \qquad \text{Equation 1.3}$$

$$r(t) = r_0 + (r_{\infty,max} - r_0) \cdot e^{-\frac{t}{\tau}} \qquad \text{Equation 1.4}$$

where r_0 is the initial radius; $r_{\infty,max}$is the maximal radius in the equilibrium swelling.

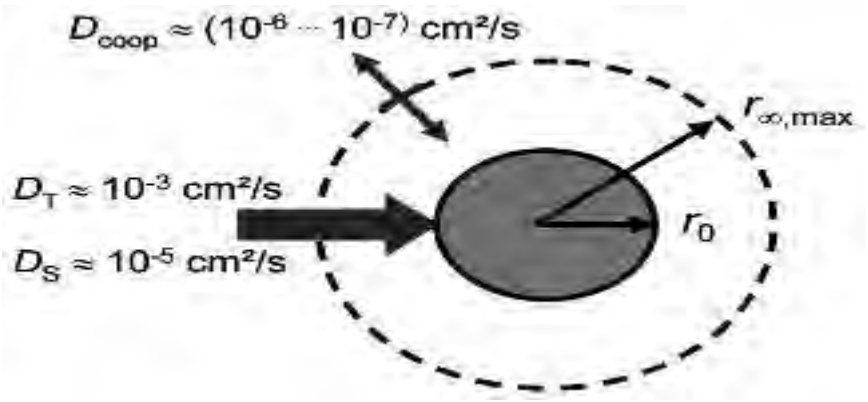

Figure 1.3: Schematic illustration of the transport operations at hydrogel swelling and shrinking status [24]

1.2 MOTIVATION

The demand for contact lenses is expected to rise due to the increase of eye-related conditions, lens-based sensing and diagnostics, controlled drug release, and contact lens based electronic interfaces [44, 45]. Structural integrity, comfort and vision correction are the main keys to determine the quality of the contact lenses [5, 46]. Lack of comfort has been the most common reason for the discontinuation of wearing contact lenses [47, 48]. Hydrophobic contact lenses lead to unclear vision, a sensation of dryness, and discomfort. Consequently, improved surface wettability and hydrophilicity are found to increase the comfort for contact lens wearers [49]. Typically, two methods are established to slightly increase the wettability of contact lenses. One is routine rewetting drops using a lens solution, which helps to increase the tear film naturally between the contact lens and the eye's surface; while the other is to adjust the lens material (plasma treatment) [50, 51]. However, chemical modifications have been used to develop hydroxyl groups to improve the wettability of the lens [52].

Contact lenses have been used to measure intraocular pressure (IOP) for glaucoma patients. In 2012, a contact lens sensor named "CLS; SENSIMED Triggerfish, Sensimed AG" was developed to detect intraocular pressure (IOP) continuously for 24 hours [53–55]. Traditionally, Goldmann applanation tonometry (GAT), is the most widely known method to measure IOP [54]. The principal limitation of GAT is that it is influenced by the static nature of the eye (central corneal thickness (CCT), ocular rigidity, and mechanical properties) [56, 57]. Moreover, the current general techniques for testing the IOP pattern in glaucoma patients over the 24-hour period are through a stress curve during the daytime or hospitalised in a sleep laboratory [58–60]. Only diurnal IOP values are established in the former process; whereas the other method costs substantially and may possibly cause stress-related issues because patients

have to be woken up several times during the night/sleep sessions[61]. The main weakness of both approaches is that IOP assessments are not practical during calm sleep and IOP readings achieve the highest value when patients are in a supine positioned during the nocturnal/sleep period [58, 62].

Moreover, currently the most common method of monitoring glucose concentration is the finger prick test which is an electrochemical method based on enzymes such as glucose oxidase, glucose dehydrogenase [63]. This procedure is inconvenient for patients, invasive, and may lead to infections. Additionally, it does not allow real-time measurements and sensors cannot be reused, due to the irreversibility of reactions [64]. Recent advances in photonics and polymer chemistry have enabled the fabrication of photonic sensors on soft hydrogel materials and have led to an increased interest in hydrogel-based optical glucose sensors [64]. Hydrogels can be designed to respond to certain stimuli such as glucose and pH. One promising approach for glucose detection using hydrogels is the covalent incorporation of boronic acids in a copolymer matrix [65, 66]. Upon the binding of the boronic acid copolymer with glucose, the polymer network swells and alters its physical and optical properties. It can be used for glucose quantitative analyses and incorporated into photonic devices. Such photonic devices work through controlling and manipulation of the propagation of light [23, 66–68]. Over the last two decades, many approaches including laser writing, self-assembly, and layer-by-layer deposition have been demonstrated to create Bragg diffraction gratings, micro-lenses, etalons and plasmonic structures in hydrogels. However, no commercial device has been released yet due to unsatisfactory sensitivity and specificity issues [69].

Additionally, accurate pH assessment is necessary for a variety of applications from chemistry to medical science. On the one hand, Traditional approaches and devices for measuring pH, such as pH paper strips and pH meters, are available. However, they may offer low sensitivity and can also be a little expensive [70, 71]. On the other hand, pH-responsive hydrogels are significantly valuable because they can be easily manufactured in small sizes, have resistance to electromagnetism and are biocompatible [70]. Moreover, optical fibre sensors are both cost-effective and reliable [71]. The pH-responsive hydrogels can be incorporated with acidic groups for sensing at high pH, or the basic hydrogels are more suitable for low pH [72]. Usually, these hydrogels exhibit significant sensitivity and have a working range which is determined by the ionisable component [24]. When the pH-sensitive hydrogel is in contact with the solution, the quantity of dissociated carboxylic ions will change depending on the pH of the solution which alters the volume and refractive index [70].

1.3 AIMS AND OBJECTIVES

This thesis aims to develop optical sensors that are able to detect glucose, pH and intraocular pressure (IOP) changes. The current methods of monitoring these biological changes (e.g. pH) and chemical changes (e.g. glucose) are inconvenient for patients, are invasive and may cause infections [30–33]. They do not allow real-time monitoring and the sensors are not reusable [63, 64]. Different methods have already been reviewed in order to reach a sustainable solution [73–76]. Optical sensors seemed to have tackle the weaknesses of the current sensors, because they can offer fast, quantitative, real-time and reversible approaches [77, 78]. In this thesis, two methods were applied to fabricate such sensors. The first is a stamping technique in which micro or nano structures were printed on contact lens material. The other method is using a laser to modify the hydrogel (contact lenses in our case)

to engrave and create micro-channels on the surface of the lenses. Using a laser is a faster method to develop a sensor compared to the stamping method. Up to 10 contact lenses would be fabricated in one session using laser engraving; whereas it would take a few hours to produce one sample by the other approach. The following steps have been taken to achieve the aim of this thesis:

1. Reviewing the contact lenses' design and advantages, hydrogel-based sensors for the glucose, pH and IOP, and the laser ablation systems; presented in Chapter 2.
2. Studying the principle of the optical diffuser, including the light propagation and the law of reflection and refraction; presented in Chapter 2.
3. Inventing a novel stamping method in order to replicate a hexagonal 2.5D grating to glucose sensitive hydrogel (GSH).
4. Probing and measuring the quality of the replication process using an angle-resolved far-field diffraction experiment and SEM scanning; described in Chapter 3.
5. Copying the Fresnel lens structure on the pH sensitive hydrogel, as in Chapter 4.
6. Using a CO2 laser to fabricate a nano/micro structure on the surface of contact lenses.
7. Finding the ideal set ups for texturing the surface of the commercial contact lens; presented in Chapters 5 and 6.
8. Fabricating 1D and 2D arrays of differently grooved channels in selective areas of the contact lens.

9. Inventing ring-shaped channels on the contact lens's surface to mentor the curvature changes.
10. Studying the optical properties of the micro/nano structure of all the fabricated sensing systems.
11. Investigating the performance of the sensors using optical microscopy, spectroscopy and optical characterisation for diffraction measurements.
12. Performing contact angle measurements to study the surface hydrophilicity; described in Chapter 5.

1.4 THESIS OUTLINE

The thesis is structured in seven chapters and is based on four publications:

Chapter 1 introduces an overall summary and some background related to contact lenses and hydrogel sensors. This chapter describes the main contribution, aims and objectives of the project. Finally, it provides the outline of this thesis.

Chapter 2 provides the literature review related to glucose sensors, pH sensors, optical sensors and IOP sensors. It covers hydrophilic and hydrophobic devices, contact angle measurements, and the lotus effect. It will also review the use of CO_2 laser treatment.

Chapter 3 presents the fabrication of a new optical glucose sensor based on a hexagonal diffraction grating imprinted on a flexible hydrogel. Here, an imprinting method was created to rapidly produce 2.5D photonic concavities in phenylboronic acid functionalized hydrogel films.

Chapter 4 demonstrates the possibility of using hydrogels to sense changes in pH for application in the coronary artery of diabetic patients. The fabricated hydrogel was based on a composition of hydroxyethyl methacrylate (HEMA). The proposed sensor exhibited good sensitivity with a quick response time. In addition to this, the recorded responses were also reproducible, meaning the hydrogel could be reused.

Chapter 5 reports on the laser-induced modification of the surface properties of contact lenses. Selective areas of the surface of commercial silicon-hydrogel contact lenses are patterned in array formats, using different powers of the CO_2 laser. One-dimensional arrays of different groove densities, channels, and 2D intersecting architecture are fabricated. Contact angle measurements are taken to measure the surface hydrophilicity. The extent of the hydration is linked with the surface profile properties and the space gap between the fabricated patterns, which are controlled by the beam exposure time, beam power, and scan speed. Laser treatment of contact lenses results in improved hydration proportional to the density of the laser-ablated segments on the surface.

Chapter 6 investigates the possibility of using laser-engraved contact lenses to measure intraocular pressure (IOP) changes for glaucoma patients. In this work, an easy method to fabricate channels in contact lenses using CO_2-laser treatment is developed.

Chapter 7 concludes and highlights the essential findings in this work; discusses the limitations of the current projects; and proposes potential future work.

REFERENCES

[1] W. Schifrin, L. and Rich, *The contact lens industry*. Washington, D.C.: Congress of the U.S., Office of Tehnology Assessment, 1984.

[2] N. Efron, “Centenary Celebration of Fick’s Eine Contactbrille,” *Arch. Ophthalmol.*, vol. 106, no. 10, pp. 1370–1377, 1988.

[3] J. Bergin, “Contact Lenses Polymers,” pp. 1–16, 2015.

[4] S. Nishimura, “The investigation of the thermal effect of contact lens wear,” no. December, 2014.

[5] C. H. Lin, Y. H. Yeh, W. C. Lin, and M. C. Yang, “Novel silicone hydrogel based on PDMS and PEGMA for contact lens application,” *Colloids Surfaces B Biointerfaces*, vol. 123, pp. 986–994, 2014.

[6] N. M. Farandos, A. K. Yetisen, M. J. Monteiro, C. R. Lowe, and S. H. Yun, “Contact lens sensors in ocular diagnostics,” *Adv. Healthc. Mater.*, vol. 4, no. 6, pp. 792–810, 2015.

[7] Y. T. T. Liao, H. Yao, A. Lingley, B. Parviz, and B. P. P. Otis, “A 3-μW CMOS glucose sensor for wireless contact-lens tear glucose monitoring,” *IEEE J. Solid-State Circuits*, vol. 47, no. 1, pp. 335–344, 2012.

[8] H. A. Stein, R. M. Stein, and M. Freeman, “Chapter 55 Basics of Soft Contact Lens Fitting,” vol. 1, 2016.

[9] P. C. Nicolson and J. Vogt, “Soft contact lens polymers: An evolution,” *Biomaterials*, vol. 22, no. 24, pp. 3273–3283, 2001.

[10] E. Y. Y.-P. M. J. Giraldez, “Hydrogel Contact Lens Surface Roughenss and Bacterial Adhesion.” Intech, 2012.

[11] J. F. Huang *et al.*, “A Hydrogel-Based Hybrid Theranostic Contact Lens for Fungal Keratitis,” *ACS Nano*, vol. 10, no. 7, pp. 6464–6473, 2016.

[12] W. G. H. J. Zhang, “CONTACT LENS INTEGRATED WITH A BIOSENSOR FOR THE DETECTION OF GLUCOSE AND OTHER COMPONENTS IN TEARS,” *Umted States Pat.*, vol. 2, no. 12, pp. 1623–1627, 2008.

[13] M. Miyashita, N. Ito, S. Ikeda, T. Murayama, K. Oguma, and J. Kimura, “Development of urine glucose meter based on micro-planer amperometric biosensor and its clinical application for self-monitoring of urine glucose,” *Biosens. Bioelectron.*, vol. 24, no. 5, pp. 1336–1340, 2009.

[14] Y. T. Liao, H. Yao, A. Lingley, B. Parviz, and B. P. Otis, “A 3-μW CMOS glucose sensor for wireless contact-lens tear glucose monitoring,” *IEEE J. Solid-State Circuits*, vol. 47, no. 1, pp. 335–344, 2012.

[15] H. Yao *et al.*, “A contact lens with integrated telecommunication circuit and sensors for wireless and continuous tear glucose monitoring,” *J. Micromechanics Microengineering*, vol. 22, no. 7, 2012.

[16] H. Yao, C. Marcheselli, A. Afanasiev, I. Lähdesmäki, and B. A. Parviz, “A soft hydrogel contact lens with an encapsulated sensor for tear glucose monitoring,” *Proc. IEEE Int. Conf. Micro Electro Mech. Syst.*, no. February, pp. 769–772, 2012.

[17] D. Gulsen and A. Chauhan, “Ophthalmic drug delivery through contact lenses,” *Investig. Ophthalmol. Vis. Sci.*, vol. 45, no. 7, pp. 2342–2347, 2004.

[18] X. Hu *et al.*, “Hydrogel contact lens for extended delivery of ophthalmic drugs,” *Int. J. Polym. Sci.*, vol. 2011, 2011.

[19] J. F. F. Huang *et al.*, “A Hydrogel-Based Hybrid Theranostic Contact Lens for Fungal Keratitis,” *ACS Nano*, vol. 10, no. 7, pp. 6464–6473, 2016.

[20] F. Yañez *et al.*, “Supercritical fluid-assisted preparation of imprinted contact lenses for drug delivery,” *Acta Biomater.*, vol. 7, no. 3, pp. 1019–1030, 2011.

[21] C. C. S. Karlgard, N. S. Wong, L. W. Jones, and C. Moresoli, “In vitro uptake and release studies of ocular pharmaceutical agents by silicon-containing and p-HEMA hydrogel contact lens materials,” *Int. J. Pharm.*, vol. 257, no. 1–2, pp. 141–151, 2003.

[22] K. Arndt, T. Schmidt, A. Richter, and Dirk Kuckling, “High response smart gels: synthesis and application,” *Macromol. Symp.*, vol. 207, pp. 257–268, 2004.

[23] D. Buenger, F. Topuz, and J. Groll, “Hydrogels in sensing applications,” *Prog. Polym. Sci.*, vol. 37, no. 12, pp. 1678–1719, 2012.

[24] A. Richter, G. Paschew, S. Klatt, J. Lienig, K. Arndt, and H. P. Adler, “Review on Hydrogel-based pH Sensors and Microsensors,” *sensors*, vol. 8, pp. 561–581, 2008.

[25] D. Buenger, F. Topuz, and J. Groll, “Hydrogels in sensing applications,” *Prog. Polym. Sci.*, vol. 37, no. 12, pp. 1678–1719, 2012.

[26] B. D. Ratner, A. S. Hoffman, and F. J. Schoen, *BlOMATERIALS SCIENCE An Introduction to Materials in Medicine Edited by*. 1996.

[27] D. Xu, J. Huang, D. Zhao, B. Ding, L. Zhang, and J. Cai, “High-Flexibility, High-Toughness Double-Cross-Linked Chitin Hydrogels by Sequential Chemical and Physical Cross-Linkings,” *Adv. Mater.*, vol. 28, no. 28, pp. 5844–5849, 2016.

[28] K. Trabbic-Carlson, L. A. Setton, and A. Chilkoti, “Swelling and mechanical behaviors of chemically cross-linked hydrogels of elastin-like polypeptides,” *Biomacromolecules*, vol. 4, no. 3, pp. 572–580, 2003.

[29] F. Yañez *et al.*, “Supercritical fluid-assisted preparation of imprinted contact lenses for drug delivery,” *Acta Biomater.*, vol. 7, no. 3, pp. 1019–1030, 2011.

[30] F. Puoci and M. Curcio, “Hydrogels: Smart Materials for Drug Delivery,” *Smart Mater. Drug Deliv. Vol. 2*, vol. 2, pp. 153–179, 2013.

[31] K. K. Lee, E. L. Cussler, M. Marchetti, and M. A. McHugh, “Pressure-dependent phase transitions in hydrogels,” *Chem. Eng. Sci.*, vol. 45, no. 3, pp. 766–767, Jan. 1990.

[32] R. Yoshida *et al.*, “Comb-type grafted hydrogels with rapid deswelling response to temperature changes,” *nat*, vol. 374, no. 6519, pp. 240–242, Mar. 1995.

[33] K. M. Gupta *et al.*, “Temperature and pH Sensitive Hydrogels: An Approach Towards Smart Semen-Triggered Vaginal Microbicidal Vehicles,” *J. Pharm. Sci.*, vol. 96, no. 3, pp. 670–681, Mar. 2007.

[34] X. J. Ju, L. Y. Chu, L. Liu, P. Mi, and Y. M. Lee, “A novel thermoresponsive hydrogel with ion-recognition property through supramolecular host-guest complexation,” *J. Phys. Chem. B*, vol. 112, no. 4, pp. 1112–1118, 2008.

[35] B. Xing, C. W. Yu, K. H. Chow, P. L. Ho, D. Fu, and B. Xu, “Hydrophobic interaction and hydrogen bonding cooperatively confer a vancomycin hydrogel: A potential candidate for biomaterials,” *J. Am. Chem. Soc.*, vol. 124, no. 50, pp. 14846–14847, 2002.

[36] H. J. Van Der Linden, S. Herber, W. Olthuis, and P. Bergveld, “Stimulus-sensitive hydrogels and their applications in chemical (micro)analysis,” *Analyst*, vol. 128, no. 4, pp. 325–331, 2003.

[37] S. Lanzalaco and E. Armelin, “Poly(N-isopropylacrylamide) and Copolymers: A Review on Recent Progresses in Biomedical Applications,” *Gels*, vol. 3, no. 4, p. 36, 2017.

[38] T. Kajisa and T. Sakata, “Glucose-responsive hydrogel electrode for biocompatible glucose transistor,” *Sci. Technol. Adv. Mater.*, vol. 18, no. 1, pp. 26–33, 2017.

[39] S. Reiter, K. Habermüller, and W. Schuhmann, “A reagentless glucose biosensor based on glucose oxidase entrapped into osmium-complex modified polypyrrole films,” *Sensors Actuators B-chemical - Sens. ACTUATOR B-CHEM*, vol. 79, pp. 150–156, Oct. 2001.

[40] L. K. Tomar, C. Tyagi, Y. E. Choonara, P. Kumar, and V. Pillay, “Rheological and Swelling Behavior of pH Sensitive Hydrogel Particles,” *APCBEE Procedia*, vol. 9, no. Icbee 2013, pp. 192–196, 2014.

[41] J. Tavakoli and Y. Tang, “Hydrogel based sensors for biomedical applications: An updated review,” *Polymers (Basel).*, vol. 9, no. 8, pp. 1–25, 2017.

[42] T. Tanaka, L. O. Hocker, and G. B. Benedek, “Spectrum of light scattered from a viscoelastic gel,” *J. Chem. Phys.*, vol. 59, pp. 5151–5159, 1973.

[43] T. Tanaka and D. J. Fillmore, “Kinetics of swelling of gels,” *J. Chem. Phys.*, vol. 70, no. 3, pp. 1214–1218, 1979.

[44] C. Chao, K. Richdale, I. Jalbert, K. Doung, and M. Gokhale, “Non-invasive objective and contemporary methods for measuring ocular surface inflammation in soft contact lens wearers – A review,” *Contact Lens Anterior Eye*, vol. 40, no. 5, pp. 273–282, 2017.

[45] F. H. Nasr, S. Khoee, M. M. Dehghan, S. S. Chaleshtori, and A. Shafiee, “Preparation and Evaluation of Contact Lenses Embedded with Polycaprolactone-Based Nanoparticles for Ocular Drug Delivery,” *Biomacromolecules*, vol. 17, no. 2, pp. 485–495, 2016.

[46] M. J. Giraldez and E. Yebra-Pimentel, “Hydrogel Contact Lenses Surface Roughness and Bacterial Adhesion,” *Intech, Croat.*, 2012.

[47] F. Stapleton *et al.*, “Risk factors and causative organisms in microbial keratitis in daily disposable contact lens wear,” *PLoS One*, vol. 12, no. 8, p. e0181343, 2017.

[48] P. Situ, T. Simpson, and C. Begley, “Hypersensitivity to Cold Stimuli in Symptomatic Contact Lens Wearers,” *Optom Vis Sci.*, vol. 176, no. 10, pp. 139–148, 2016.

[49] B. Caffery *et al.*, “Contact Lens Comfort,” *Optom. Vis. Sci.*, vol. 93, no. 8, p. 790—792, Aug. 2016.

[50] J. J. Nichols, C. W. Lievens, M. R. Bloomenstein, H. Liu, P. Simmons, and J. Vehige,

"Dual-polymer drops, contact lens comfort, and lid wiper epitheliopathy," *Optom. Vis. Sci.*, vol. 93, no. 8, pp. 979–986, 2016.

[51] G. Qin, Z. Zhu, S. Li, A. M. McDermott, and C. Cai, "Development of ciprofloxacin-loaded contact lenses using fluorous chemistry," *Biomaterials*, vol. 124, pp. 55–64, 2017.

[52] H.-Y. Li, W.-J. Ting, Y.-C. Lai, and H.-Y. Chang, "Method for Manufacturing Hydrophilic Silicone Macromer," p. EP2610281 B1, 2015.

[53] Young G, Coleman S, "Poorly fitting soft lenses affect ocular integrity.," *CLAO J*, vol. 27, no. 2, pp. 68–74, 2001.

[54] K. Mansouri, F. A. Medeiros, A. Tafreshi, and R. N. Weinreb, "Continuous 24-hour monitoring of intraocular pressure patterns with contact lens sensor: Safety, tolerability, and reproducibility in patients with glaucoma," *Arch. Ophthalmol.*, vol. 130, no. 12, pp. 1534–1539, 2012.

[55] M. Leonardi, E. M. Pitchon, A. Bertsch, P. Renaud, and A. Mermoud, "Wireless contact lens sensor for intraocular pressure monitoring: Assessment on enucleated pig eyes," *Acta Ophthalmol.*, vol. 87, no. 4, pp. 433–437, 2009.

[56] J. Liu and C. Roberts, "Influence of corneal biomechanical properties on intraocular pressure measurement:: Quantitative analysis," *J. Cataract Refract. Surg.*, vol. 31, pp. 146–155, Feb. 2005.

[57] N. Ehlers, T. Bramsen, and S. Sperling, "Applanation Tonometry and Central Corneal Thickness," *Acta Ophthalmol.*, vol. 5, no. 512, pp. 34–43, 1975.

[58] J. H. K. Liu, F. A. Medeiros, J. R. Slight, and R. N. Weinreb, "Diurnal and nocturnal effects of brimonidine monotherapy on intraocular pressure," *Ophthalmology*, vol. 117, no. 11, pp. 2075–2079, 2010.

[59] K. Mansouri, R. N. Weinreb, and J. H. K. Liu, "Effects of aging on 24-hour intraocular pressure measurements in sitting and supine body positions," *Investig. Ophthalmol. Vis. Sci.*, vol. 53, no. 1, pp. 112–116, 2012.

[60] Y. Barkana, S. Anis, J. Liebmann, C. Tello, and R. Ritch, "Clinical Utility of Intraocular Pressure Monitoring Outside of Normal Office Hours in Patients With Glaucoma," *JAMA Ophthalmol.*, vol. 124, no. 6, pp. 793–797, Jun. 2006.

[61] J. H. K. Liu and R. N. Weinreb, “Monitoring intraocular pressure for 24 h,” *Br. J. Ophthalmol.*, vol. 95, no. 5, pp. 599–600, 2011.

[62] J. H. K. Liu, X. Zhang, D. F. Kripke, and R. N. Weinreb, “Twenty-four-hour intraocular pressure pattern associated with early glaucomatous changes,” *Investig. Ophthalmol. Vis. Sci.*, vol. 44, no. 4, pp. 1586–1590, 2003.

[63] K. Tonyushkina and J. H. Nichols, “Glucose Meters: A Review of Technical Challenges to Obtaining Accurate Results,” *J. Diabetes Sci. Technol.*, vol. 3, no. 4, pp. 971–980, 2009.

[64] A. K. Yetisen *et al.*, “Photonic hydrogel sensors,” *Biotechnol. Adv.*, vol. 34, no. 3, pp. 250–271, 2016.

[65] R. Nishiyabu, Y. Kubo, T. D. James, and J. S. Fossey, “Boronic acid building blocks: tools for sensing and separation,” *Chem. Commun.*, vol. 47, no. 4, p. 1106, 2011.

[66] Y. Dong *et al.*, “Injectable and Glucose-Responsive Hydrogels Based on Boronic Acid-Glucose Complexation.,” *Langmuir*, vol. 32, no. 34, pp. 8743–8747, 2016.

[67] E. F. Banwell *et al.*, “Rational design and application of responsive ?-helical peptide hydrogels,” *Nat. Mater.*, vol. 8, no. 7, pp. 596–600, 2009.

[68] E. Yablonovitch, “Photonic crystals: semiconductors of light.,” *Sci. Am.*, vol. 285, no. 6, pp. 47-51,54-55, 2001.

[69] R. V Kuranov, V. V Sapozhnikova, D. S. Prough, I. Cicenaite, and R. O. Esenaliev, “Prediction capability of optical coherence tomography for blood glucose concentration monitoring.,” *J. Diabetes Sci. Technol.*, vol. 1, no. 4, pp. 470–477, 2007.

[70] Y. Zhao, M. Lei, S. X. Liu, and Q. Zhao, “Smart hydrogel-based optical fiber SPR sensor for pH measurements,” *Sensors Actuators, B Chem.*, vol. 261, pp. 226–232, 2018.

[71] A. K. Pathak and V. K. Singh, “A wide range and highly sensitive optical fi ber pH sensor using polyacrylamide hydrogel,” *Opt. Fiber Technol.*, vol. 39, pp. 43–48, 2017.

[72] K. Deligkaris, T. S. Tadele, W. Olthuis, and A. van den Berg, “Hydrogel-based devices for biomedical applications,” *Sensors and Actuators, B: Chemical*, vol. 147, no. 2. Elsevier B.V., pp. 765–774, 2010.

[73] M. Shichiri, Y. Yamasaki, R. Kawamori, N. Hakui, and H. Abe, “WEARABLE

ARTIFICIAL ENDOCRINE PANCREAS WITH NEEDLE-TYPE GLUCOSE SENSOR," *Lancet*, vol. 320, no. 8308, pp. 1129–1131, 1982.

[74] E. F. Pfeiffer, "The glucose sensor: the missing link in diabetes therapy.," *Horm. Metab. Res. Suppl.*, vol. 24, pp. 154–164, 1990.

[75] K. ul Hasan *et al.*, "A Miniature Graphene-based Biosensor for Intracellular Glucose Measurements," *Electrochim. Acta*, vol. 174, pp. 574–580, 2015.

[76] S. Garg *et al.*, "Improvement in Glycemic Excursions With a Transcutaneous, Real-Time Continuous Glucose Sensor," *Diabetes Care*, vol. 29, no. 1, 2005.

[77] C. K. Ho, A. Robinson, D. R. Miller, and M. J. Davis, "Overview of Sensors and Needs for Environmental Monitoring," *Sensors (Basel).*, vol. 5, no. 2, p. 4, 2005.

[78] Y. Zhao, Z. Xie, H. Gu, C. Zhu, and Z. Gu, "Bio-inspired variable structural color materials," *Chem. Soc. Rev.*, vol. 41, no. 8, p. 3297, 2012.

Chapter 2: Literature review.

2.1 INTRODUCTION

The literature review is presented in this chapter and includes some background about contact lenses, hydrogel-based sensors and laser ablation. It starts with contact lenses' history and advantages, and brief section on the use of wearable medical devices including contact lenses. Then we review types of contact lens used in glucose sensing, including fluorescence-based sensors, photonic-based sensors and electrochemical-based sensors. The glaucoma hydrogel-based sensor is discussed in section 2.4. The following sections, 2.5 and 2.6 present the pH hydrogel-based sensor and background to the Fresnel lens. Then, the principles of an optical diffuser are reviewed in section 2.7. At the end, a laser ablation review, including CO_2 laser ablation, is presented in section 2.8. Finally, the differences between hydrophilic and hydrophobic surfaces are discussed.

2.2 CONTACT LENS

The World Health Organization has reported that 75% of the global population is determined as sub-health. However only 20% is actually required to be hospitalised [1]. Therefore, the domain of having point-of-care (POC) diagnostic devices is increasing [1, 2]. Wearable devices have attracted more attention in healthcare due to the comfort, great flexibility and long-term detection capability [3]. These devices use tear fluid, sweat, saliva and skin interstitial fluid to measure blood pressure, heart rhythm, glucose level, body temperature and intraocular pressure (IOP) [3–7]. Some devices have been developed and sold on the market; such the GluoWatch Automatic Glucose Biographer which using the skin's

interstitial fluid to monitor glucose in the body. However, this equipment had to be withdrawn from the market after patients reported irritation of the skin [8]. Moreover, wrist-worn watches have shown a potential to detect biochemical changes in sweat. The main issue here is that there is a shortage of protein biomarkers in sweat which limits any further monitoring [9]. On the other hand, tear fluid produces comparably abundant proteins that have similar elements to those in blood [10]; and thus, contact lenses are becoming the ideal tool for such diagnoses (Figure 2.1). Contact lenses have already been effectively inserted with a sensor for continuously detecting glucose and glaucoma [11].

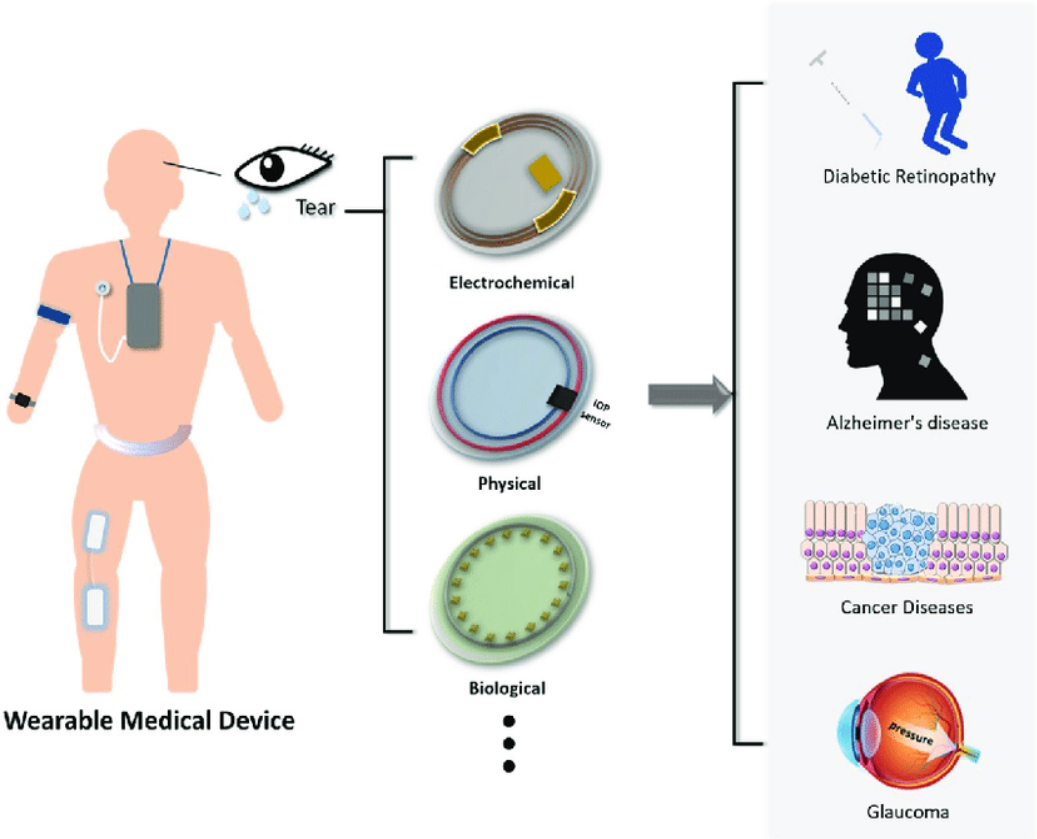

Figure 2.1: Description of wearable medical equipment based on lacrimal fluid [8]

2.2.1 Contact lens design

When designing the dimensions and features of a contact lens, four physical criteria have to be considered. The base curve radius (BCR), the contact lens diameter, the centre thickness, and the contact lens optical power (OP) are the important parameters. The curve radius ranges from 8 to10 mm, which is significant to fit the contact lens comfortably. This provides enough oxygen between the corneal cells and the surrounding air. The centre thickness, is the thickness between both the internal and the external layers through the central contact lens axis, and is about 0.1 mm. The optical power is the essential factor for vision correction [11–13].

Contact lenses are fabricated using polymer mixtures such as poly(2-hydroxyethylmethacrylate) (pHEMA), poly(vinyl alcohol) (PVA), polyacrylamide (PA), polyethylene terephthalate (PET), or polydimethylsiloxane (PDMS). These are the most common polymers to develop a sensor because of the significant oxygen permeability and consumer comfort [11, 14]. Moreover, contact lenses are cost-effective and would cost the patients roughly £2 per week [15].

2.2.2 Tear fluid

Researchers have been investigating replacement diagnosis techniques rather than using blood sampling. Although blood testing has been the standard diagnosis option in hospitals for decades, it is an invasive method and can cause some side effects [16]. By contrast, tear fluid offers diagnosis techniques in a non-invasive manner. The tear fluid contains many biological markers (proteins, lipids, enzymes, and salts) [17]. This provides a chance for disease detection. Lacrimal film has three layers, shown in Figure 2.2, which are mainly to lubricate and clean the eye [8, 18].

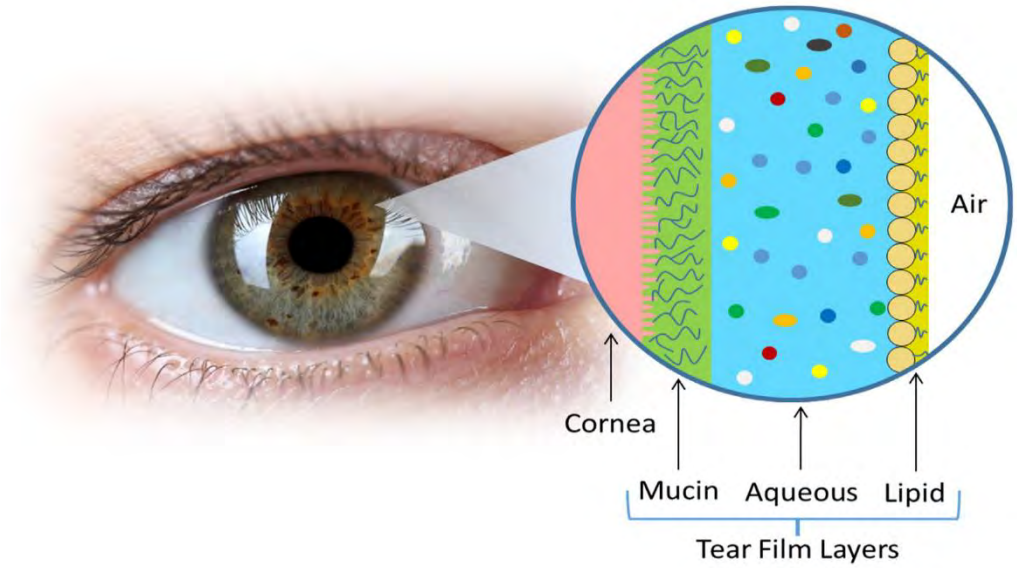

Figure 2.2: Presentation of tears' film layers [8]

Plasma leakage through the blood-tear barrier leads to tear fluid having similar components to those in the blood [11]. For example, both the blood and the tear contain glucose. However, the glucose concentrations for diabetics in blood and tears are 2-40 mM and 0.5-4 mM respectively [10, 19]. The average pH level in tears is around 7.4.

Table 2.1 shows the concentrations of biomarkers that can be found in the lacrimal fluid [10]. The tear fluid can be affected by a number of factors like low sampling size, the collection methods, variability between patinas and time to time variations. These factors cause some errors and require a highly sensitive mechanism [10], [20]. In spite of these limitations, a number of biosensors have been introduced using tear fluid to diagnose and detect disease.

Table 2.1: shows biomarkers in tear fluid compared with blood concentrations and shows the diagnostic disease for each biomarker [10, 21–24]

Component	Tear concentrations (mM)	Blood concentrations (mM)	Diagnostic disease
Glucose	0.01-0.05	3.3-6.5	Diabetes
Lactate	2.0-5.0	0.36-0.75	Cancer and liver disease
Na^+	120-165	130-145	Hypo/hypernatremia
K^+	20–42	3.5–5.0	An indicator of ocular disease
Dopamine	0.37	$475x10^{-9}$	Glaucoma
Urea	3.0-6.0	3.3-6.5	Renal function

2.2.3 Contact lens advantages

Among all wearable devices, contact lenses are the most common device developed for sight correction, and therapeutic purposes. There are more than 7 million contact lens users around the globe [11]. The intimate contact between human eyes and contact lenses can continue for a long time without causing significant irritation, and it gives an optimal platform for continuous sensing and up to 24 hours monitoring [25, 26]. Additionally, the samples remain fresh and clean throughout the collection time due to natural blinking and the tear film of the eye.

2.3 CONTACT LENS GLUCOSE SENSORS

Diabetes mellitus is a progressive metabolic disorder that affects more than 400 million people around the world. It is primarily defined by an increase in the concentration of blood

glucose [27, 28]. In 2015, the diabetes spread was reported at about 8.8% in adults and 16.2% in pregnant women. These numbers may be increased by 3% by 2040. Overall spending on diabetes care is around USD 700 billion [29]. Most of the existing POC diagnostic methods are based on invasive techniques and have limitations [30]. The contact lens sensors may serve as continuous and non-invasive diagnostic tools, using the relationship between blood and tears' glucose concentrations [27, 31]. Many types of enzyme-based electrochemical biosensors for glucose detection have been introduced and have evolved from invasive to non-invasive methods, as presented in Figure 2.3. This section reports on contact lens biosensors for continuously monitoring glucose based on different techniques, including fluorescent, holographic, and electrochemical techniques.

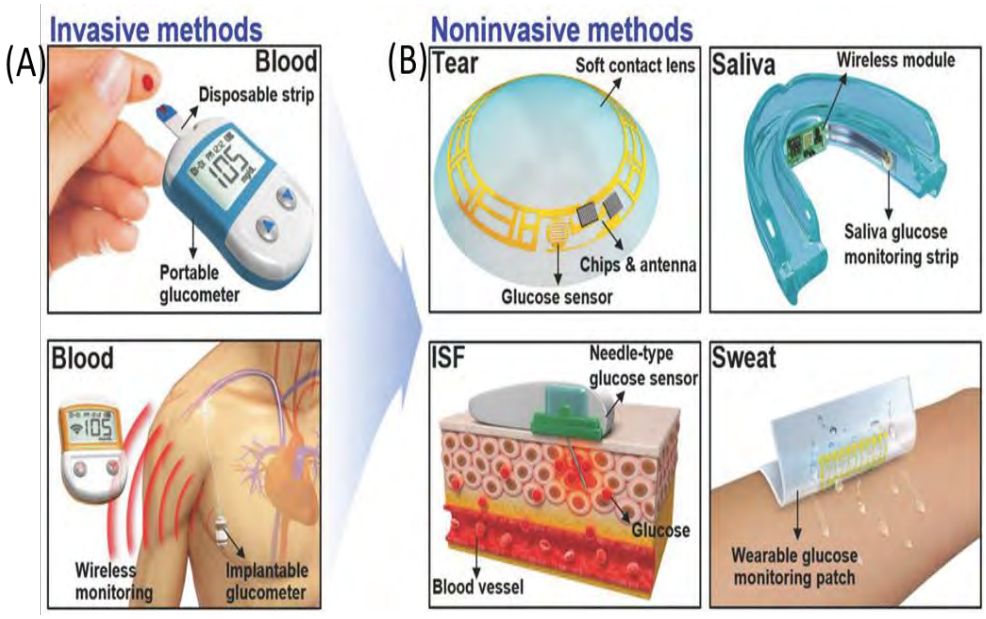

Figure 2.3: presentation of invasive to non-invasive electrochemical glucose detection devices: (A) the glucose monitoring approach in the blood directly, which is the most accurate approach but it is associated with pain and discomfort for patients; (B) a substitutional approach for non-invasive glucose monitoring using tears, saliva, interstitial fluid (ISF), and sweat [32]

2.3.1 Fluorescence-based sensors

Fluorescence-based sensors have been used in a wide range of applications due to their simplicity, flexibility and accuracy. The fluorescence occurs when excitable fluorescent

molecules absorb radiation of a specific wavelength and there is a subsequent release of photons with a greater wavelength (lower energy). Therefore, the emitted photons can be distinguished from background noise using filtering methods, which enables this monitoring method to be particularly sensitive. The chemical composition of the fluorophore affects both the excited and released wavelengths, which leads to flexible and highly specific sensing. A part of the released energy is passed from the donor fluorophore to the receiver fluorophore, and is called Förster resonance energy transfer (FRET). The transferring of the excited energy relies on the spectral overlapping between fluorophores and their interspace. In contact lens devices, March et al. developed a biosensor to monitor the glucose in tear fluid. This sensor was capable of monitoring the glucose levels of patients for more than 3 hours [33]. The biosensor was made of polymerized Nelfilcon A, which is a polyvinyl alcohol polymer that is partly converted with N-formylmethyl acrylamide and contains 69% water [34]. This polymer was incorporated into a hydrogel network that was chemically combined with tetramethylrhodamine isothicyanate concanavalin A (TRITC-Con A) and fluorescein isothiocyanate dextran (FITC-dextran) inside a contact lens mould [33]. When glucose distributes through the network, the Forster resonance energy transfer (FRET) reduces and fluorescence intensity increases due to the shift in distance between FITC-dextran molecules and TRITC-Con A. Another contact lens biosensor was fabricated by pHEMA or PDMS which had an organic dye contacting silica nanoparticles to control the quality of the sensor, and avoid early leaking [35]. The sensitivity range of this biosensor was 0.5 mM to 5 mM. Additionally, a glucose monitoring device based on boronic acid was developed by Badugu et al. and attached into commercial contact lens. It had a range from 50 μM to 100 mM with a response time of 10 min [36].

2.3.2 Photonic-based sensors

Photonic crystals (PC) can be categorised into one dimension, two dimensions and three dimensions by their optical direction [8]. When a PC network is illuminated by a wavelength beam, light is then diffracted which can calculated by Bragg's law. As a result, the colour of the diffracted light will be therefore changed due to variations in either the distance or refractive index. Use of photonic crystals has become a common method in visible medical equipment because the sensing is generally based on the changes in the colour. The advantages of this method: (1) operates without dyes or fluorophores; (2) the readouts' visibility which allow the use of readily accessible devices, like phone cameras; and (3) reusability [37, 38].

For one-dimension PC, Yetisen and his group developed a glucose sensor by functionalizing 3-(acrylamido) phenylboronic acid (3-APB) on a hydrogel network. The binding between glucose and 3-APB led to swelling of the hydrogel. The swelling then shifted the diffracted light. The sensor had a response time of 5 min for glucose concentrations between 0.1 mM and 300 mM [39]. On contact lens applications, Domschke et al. built a glucose sensitive hologram on a contact lens to measure the glucose concentrations for diabetics via tear fluid. The contact lens was able to diffract the light and in the presence of glucose the lens expanded and changed the nanoparticles' spacing. After chemical processing and sterilisation, the biosensor could still operate reversibly [40]. Another glucose sensor was designed by an imprinted photonic network with 1.6 μm on polyacrylamide (PA), which was mixed with phenylboronic acid. The structure then was fitted to a commercial contact lens. The pattern of the photonic structure was adjusted in the presence of the glucose. The sensor had glucose sensitivity up to 50 mM and a response time of about 3 s [41]. The main concern for this type of sensor is the change of intraocular pressure for glaucoma patients, as it may disturb the periodicity of the photonic structure.

Moreover, 2D and 3D photonic crystals have been fabricated for biosensors' use. Colloidal crystal arrays' (CCA) sensors have been applied for monitoring glucose levels in tear fluid. Such structures are made from crystalline nanospheres, including polystyrene or silica. Sensors based on a photonic crystal array comprises a colloidal array attached to a polymer network that diffracts light into the visible spectrum. The production of CCA includes the self-assembly of monodispersed particles using the colloidal suspension evaporation [38]. Alexeev and colleagues embedded polystyrene colloids inside a polymer mixture, PA-(bis-AA)-poly(ethylene glycol). The sensor was then functionalized with boronic acid groups like 4-amino-3-fl uorophenylboronic acid and 4-carboxy-3-fl uorophenylboronic acid which produced the opportunity to detect glucose levels at a physiological pH [42]. The measuring process includes linking glucose to boronic acid and creating additional bonds within the contact lens matrix. The structure then shrunk and altered the lattice spacing of the colloidal array. Matrix shrinkage leads to a blue shift of the diffracted light, which is related to the glucose level in the tears. The sensor had glucose sensitivity down to 0.15 mM at pH 7.4 and a response time of about 90 s to 300 s [43].

Lately, further development for this technique has been demonstrated by Ruan et al. They successfully created CCA on the surface of commercial contact lenses, using a glucose-sensitive hydrogel. Figure 2.4(A) shows the fabrication process for the sensor. The polystyrene (PS) particles were self-assembled on the surface of the contact lens. Then, the layer of the colloidal crystal was coated using a mixture of 4-boronobenzaldehyde-modified poly(vinyl alcohol) (4-BBA-PVA) in order to create the gel, which was crosslinked by glutaraldehyde (GA). This led to the designing of a hydrogel-based CCA-lens to detect the glucose in the tear fluid. The sensor had glucose sensitivity between 0.05 and 50 mM with visible diffracted light

from 0 to 3 mM between a wavelength of 567 and 468 nm and up to 10 mM (up to 567 nm wavelength), as presented in Figure 2.4 (B) [44]. Figure 2.4 (C) shows an image of the GCCA-lens sample.

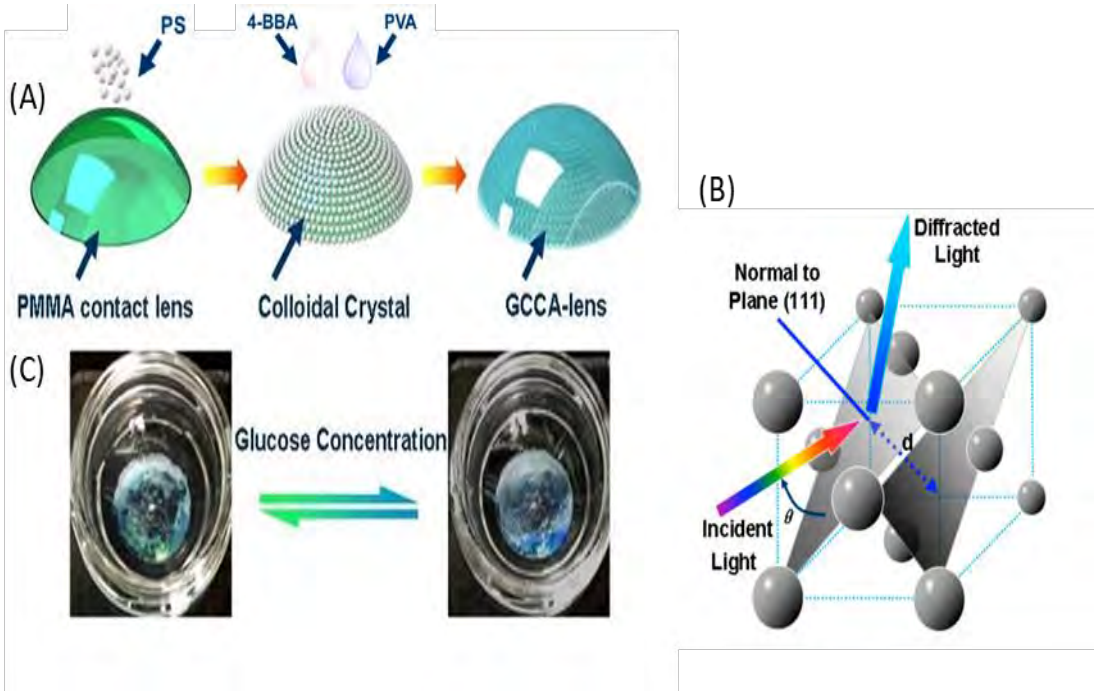

Figure 2.4: (A) the fabrication process hydrogel-based CCA-lens; (B) presentation of GCCA's diffraction wavelength from the CCA into a visible light; (C) real photographs of the GCCA-lens samples [44]

2.3.3 Electrochemically based sensors

In the previous decades, electrochemical devices for biosensor monitoring have been deeply investigated. Several manufacturing methods like the semiconductor technique are applied to develop electrochemical sensors which can be integrated into contact lenses. Electrochemical biosensors have been used to detect many biomarkers like glucose, lactate, and intraocular pressure. Such a technique can demonstrate high selectivity by using enzymes that can stimulate the electrochemical sensing reactions. Electrochemical devices have

attracted more interest due to their rapid response time, low cost, flexibility, small size of the sensors, good sensitivity and capability to provide direct biological measurements [32, 45–48]. Basically, when glucose oxidase (GOD) breaks glucose into oxygen, hydrogen ions and electrons, then electrochemically based sensors utilize the electrons to measure the glucose concentration [10].

Electrochemical devices have also been incorporated into contact lenses to measure glucose levels in tear fluid. Yao and colleagues reported an electrochemical contact lens sensor for monitoring glucose in tears [49]. They fabricated a circuitry using photoresist into a thin chip of poly(ethylene terephthalate) (PET) film. Then three layers of titanium (Ti), palladium (Pd) and platinum (Pt) were deposited on the outside surface of the PET chip and covered by a thin metal film. Having a layer of Pd between the Ti and Pt increases the signal stability [50]. Finally, the chip was heat-moulded in order to create a contact lens shape, as shown in Figure 2.5. The sensor showed a fast response time about 20 s and a detection range between 0.1 mM and 0.6 mM. Furthermore, Chu et al. designed an electrochemically based sensor on a contact lens to detect glucose in tears. They built a flexible hydrogen peroxide electrode, which had a Pt working electrode and a silver chloride (Ag/AgCl) reference/counter electrode, on PDMS film as the contact lens material. The sensitivity range of the biosensor was between 0.03 and 5.0 mM. This biosensor was tested on a rabbit's eyeball to monitor the tear glucose. It was successfully able to detect the glucose changes with a response time of 10 minutes [51].

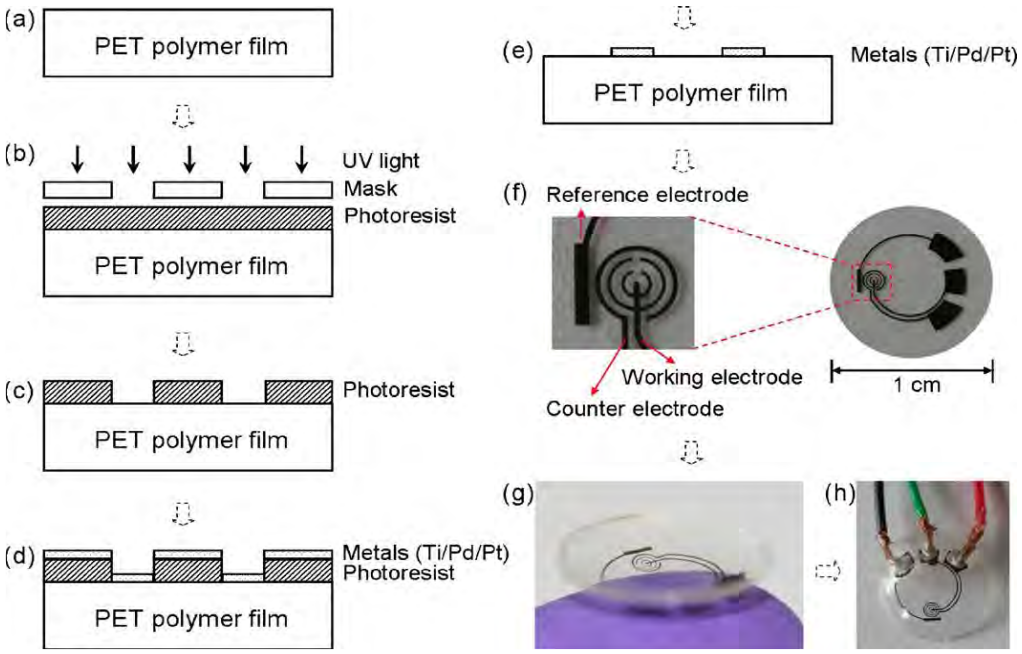

Figure 2.5: the route to fabricate an electrochemical sensor on a contact: (a) preparing the PET substrate; (b) the substrate was cured by UV light; (c) the electrodes were created using 10 nm of Ti, 20 nm of Pd and 100 nm of Pt; (d) the surface of the sample was covered by thin metal film; And (e) the sensor was heated and cut into a contact lens shape; (f-h) show images of the sensor [49].

Recently, Kim et al. introduced a wearable contact lens sensor that can detect glucose and intraocular pressure using different electrical reactions. The sensor contained graphene and silver nanowires which can serve as a field-effect transistor sensor. The graphene-silver nanowires' structure provides a measurement of electrical and mechanical properties. They demonstrated real-time measurement in a live rabbit and successfully monitored glucose concentrations from 1mM to 10 mM. Figure 2.6 shows a schematic diagram of the graphene-silver nanowires' biosensor integrated into a contact lens [52].

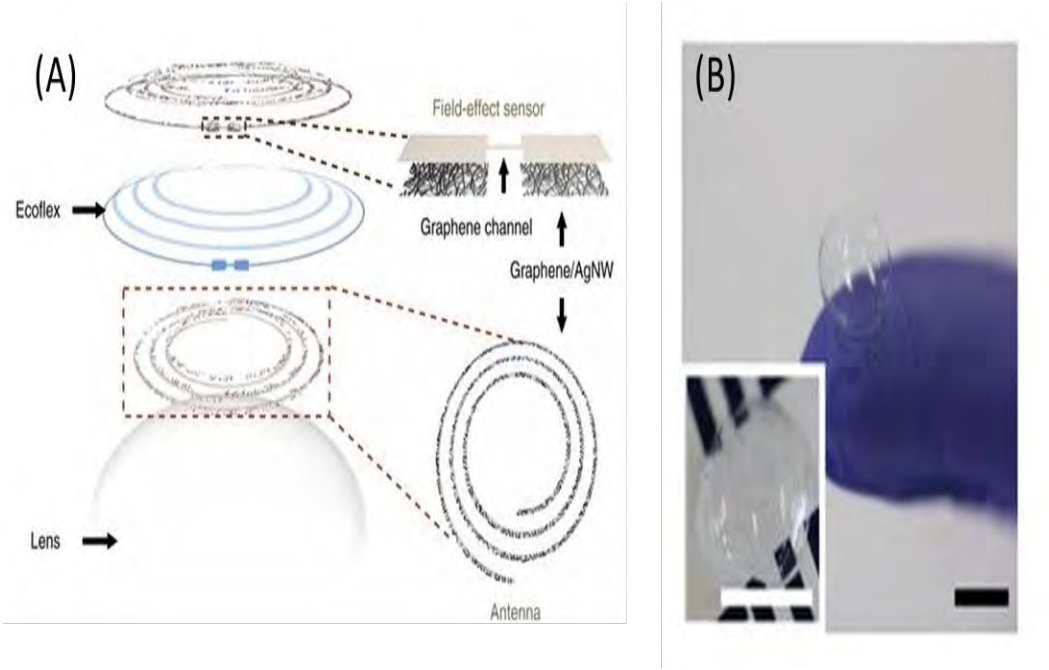

Figure 2.6: (A) Presents a schematic diagram of the graphene-silver nanowires' biosensor integrated into a contact lens; (B) presents a photograph of the sensor [52]

2.4 GLAUCOMA HYDROGEL-BASED SENSOR

Glaucoma has become one of the main causes of blindness, it influences the optic disc and harms the optic nerve due the increase of the intraocular pressure (IOP), see Figure 2.7(A) [53–55]. The World Health Organisation (WHO) stated that glaucoma is currently the second major source of sight loss worldwide, after cataracts [55]. The number of people affected by glaucoma is approximately 80 million around the world by 2019 [54]. Glaucoma is categorised into two different groups: open-angle glaucoma and angle-closure glaucoma. Although both types can damage the sight, the cause of the disease varies [56–59]. The relation between the eye fluid secretion and its discharges defines each type. In open-angle glaucoma patients the fluid outflow is blocked by the trabecular meshwork leading to bulked fluid in the eye chamber, see Figure 2.7(B). On the other hand, the eye fluid is blocked by reducing the angle between the iris and the cornea in angle-closure glaucoma patients see Figure 2.7(C) [53, 60–62].

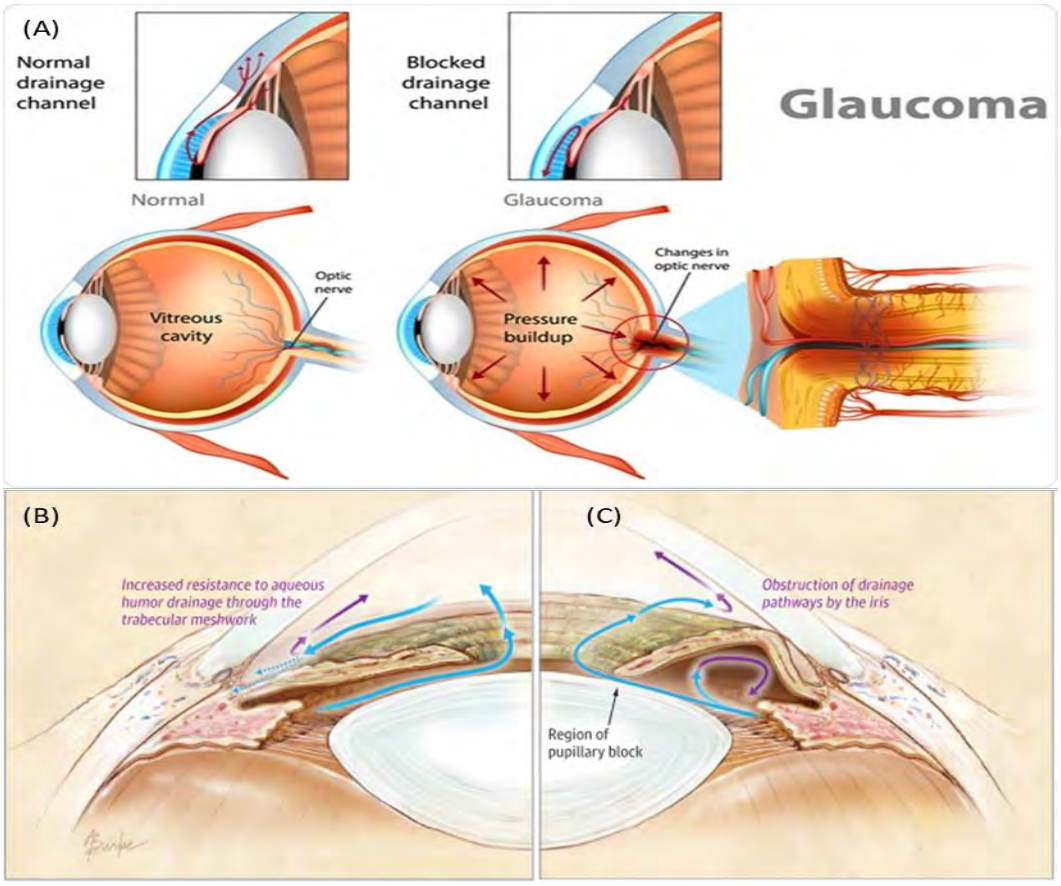

Figure 2.7: presentation of the glaucoma condition: (A) shows an illustration of the eye for a healthy person and glaucoma patients [59]; (B) shows the open-angle glaucoma condition in which the eye fluid is blocked by the trabecular meshwork; (C) shows the angle-closure glaucoma condition in which the iris-cornea angle stops the fluid outflow [53]

The main modifiable risk factor for glaucoma development is the intraocular pressure (IOP) which is associated with the curvature of the corneal radius [63–65]. An increase in IOP of 1 mmHg leads to 3 µm increase in the curvature of the corneal [62, 66]. An IOP above 21 mmHg is the indication level of developing glaucoma [67]. Thus, accurate evaluation of the IOP is significantly important in controlling glaucoma. The most common tool to measure the IOP is Goldmann applanation tonometry (GAT) [58, 67]. This measurement technique is more than 50 years old, imprecise, uses a single measurement, is only done at a specific time (i.e. during clinics hours only), and results are affected by the dynamic of the eye. The GAT method assumes the cornea is flattened in a certain area and is also thin, elastic and flexible. These assumptions are not accurate. There is also essential evidence confirming that many glaucoma

patients experience the peak of IOP values outside of clinics hours [68–70]. Another issue when using GAT is that the IOP varies during the day, so a single measurement cannot give an accurate diagnosis [67]. Therefore, many researchers have focused on developing a 24-hour IOP measurement. Continuous IOP detectors can give significant resources to understand more about 24-hour IOP variations and improve glaucoma treatments [71].

The first hydrogel-based IOP sensor was developed in 1976 by Collins who built a pressure sensor on a contact lens [62]. After that, there were many attempts to design a continuous IOP monitoring system based on contact lens. In 2002, Leonardi et al. introduced their contact lens sensor to detect IOP continuously [72]. They built a microstructure strain gauge on the lens to measure the cornea curvature changes according to IOP changes. The sensor was the first device to record 24-hour IOP measurements, and the first to confirm that the IOP value during the night is higher than the daytime values (clinic hours) [73]. Moreover, the Sensimed Company proposed and published new microprocessor strain gauges instilled in contact lenses, called Sensimed Triggerfish CLS, to record the change in the cornea limbus, see Figure 2.8 (A-C). The sensor is the only available device on the market after it had been approved with a European Conformity Declaration [62, 74]. The main issue with the Sensimed Triggerfish sensor is the IOP values' validation, i.e. the pressure units of the device are in millivolts or arbitrary units instead of mmHg. Several reports indicate negative IOP results or an IOP above 30 mmHg, which is biologically unlikely to happen [62]. Similarly, Chen et al. fabricated a pressure sensor based on a contact lens, see Figure 2.8(D-F). It was composed of silicone of medical standard with transition moulding, and the electrodes and inductive coils were made of copper foil [11].

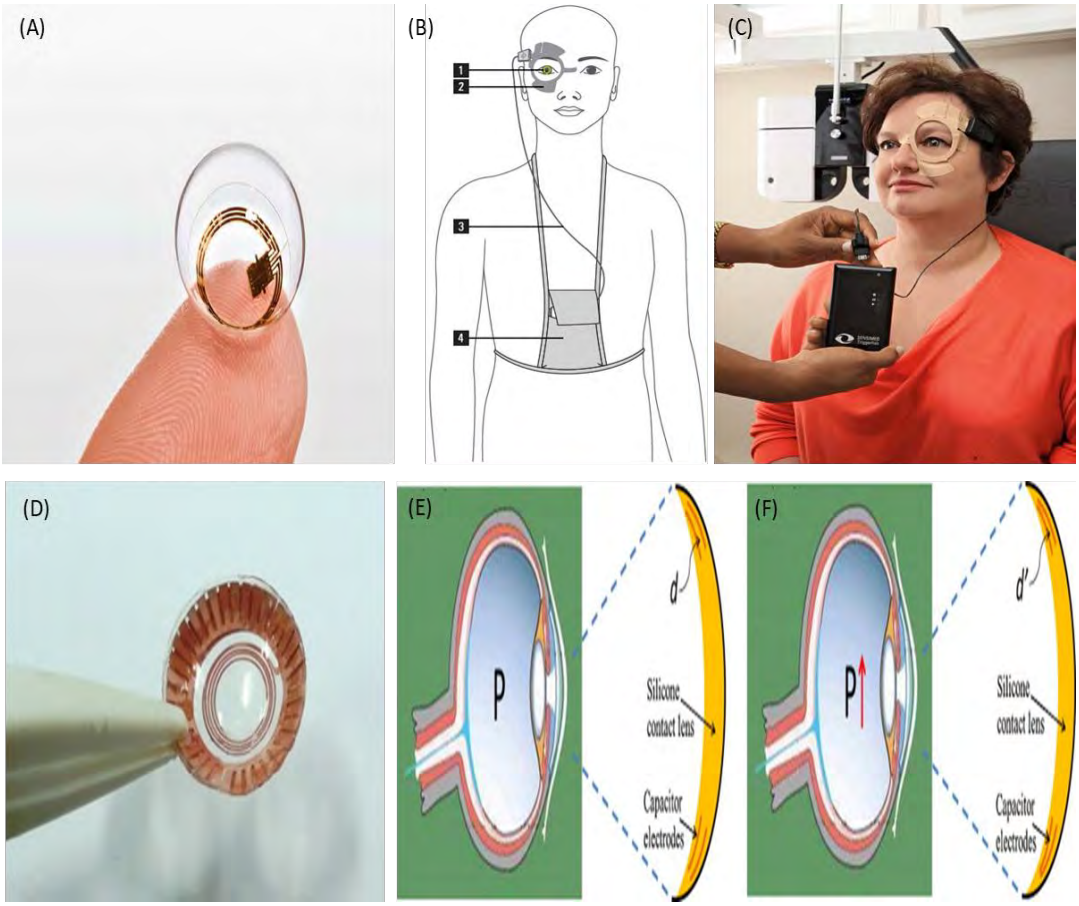

Figure 2.8: presentation of some contact lens sensors to detect IOP continuously: (A) an image of the SENSIMED Triggerfish lens to measure IOP; (B) schematic image of the device, (1) contact lens sensor (2) wireless system to transfer the data (3) a cable (4) portable recording device; (C) a real image of the device on a glaucoma patient [11], [67]; (D) a picture of a contact lens sensor to measure IOP developed by Chen et al.; (E) and (F) the mechanism of the sensor, the sensor behaviour with normal IOP values and with high IOP, in which the distance between the electrodes is decreased with IOP increase [11]

2.5 pH HYDROGEL-BASED SENSORS

Measuring pH has been a crucial factor in the evaluation of health issues, in the toxicity of environmental substances and in food safety. In fact, a change of pH is generally correlated with development and growth of bacteria [75–77]. Hydrogels that are sensitive to pH have become promising materials for a wide variety of applications because these hydrogels reversibly adjust their thickness, mass and elasticity due to the change in pH values [78–80].

The effect of pH changes in hydrogel swelling can be detected by a variety of methods such as diffraction wavelength, resonance frequency changes, or silicon layer deflection [81, 82]. This method has several benefits, such as easy and rapid production procedure, low cost, easy digital integration, chemical and biological compatibility [80].

Generally, pH hydrogel-based sensors contain polymer with acidic or basic group, which provides the pH sensitivity. All materials should be mixed, dried and cross-linked. Then, they should be cross-linked and exposed to UV light [83–85]. The selection of the polymer is important, as the delamination of the polymer layer affects the measurements' accuracy and the stability of the sensor. This can be avoided by applying a long spacer adhesion promoter, using extremely thin hydrogel layers [83, 86]. The mechanical properties and sensitivity of the sensor can be modified by adjusting the ratio between the polymer and the ionisable group, or the cross-linking parameters. Therefore, a wide range of hydrogel-based pH sensors have been developed and tested over the past decades [78, 87, 88].

Table 2.2: Hydrogel-based pH sensors along with their dimensions, sensitivity range, response time and detection method

Hydrogel material	Thickness	pH range	Response time	Sensor type	Detection method	Ref.
HEMA-DMAEMA[1]	300 nm	7-7.75	≈ 80 s	Refractometric	refractive index	[89]
PHEMA-co-MAA[2]	10 μm	5-7	≈ 4 m	Holographic	wavelength	[90]
PAAm-PCCA[3]	125 μm	4-8.5	10 m	Holographic	wavelength	[91]
HEMA-DMAEMA[4]	8 μm	7-8	≈ 6 m	Conductimetric	resistance	[92]
poly(AA-co-IOA)[5]	1.4 μm	4-8.5	2 m	Magnetoelastic	frequency	[87]
AAm-DMAEMA[6]	15 μm	6-9	15 m	Microcantilever	deflection	[93]
AAM-BAAM[7]	125 μm	8-10	20 s	Optical	wavelength	[78]
PVA-PAA[8]	390 nm	2.55-3.45	500 ms	Quartz crystal micro	frequency damping	[88]

[1,4] 2-hydroxyethyl methacrylate - *N,N*-dimethylaminoethyl methacrylate

[2] Poly(hydroxyethyl methacrylate-*co*- methacrylic acid)

[3] Poly(acrylamide)-polymerised crystalline colloidal array

[5] Poly(acrylic acid-co-isooctyl acrylate)

[6] Acrylamide-*N,N*-dimethylaminoethyl methacrylate

[7] Acrylamide-N, N'-methylene diacrylamide

[8]Poly(vinyl alcohol)-poly(acrylic acid)

It can be observed from Table 2.2 that the pH working range varies from sensor to senor due to the selection of the ionisable hydrogel network. Mostly, it relates directly to the pKa value of the ionic group used within the network. The response time is affected by the hydrogel thickness, the ionic group strength, and the mechanical properties of the swelling and shrinking. The sensors with thicknesses in the nm range responded faster than other sensors. Also, the strong ionic strength had the shortest response time, whereas the low strength was time consuming. Additionally, the sensors that relied on the swelling and the shrinking of the hydrogel were shown. Thong et al. reported that the shrinking time was significantly faster than the time taken in swelling, due to the associated elastic force with the process [94]. On the other hand, sensors that were not based on the swelling of the gel showed no significant gap in the time [88]. Figure 2.9 shows an example of the preparation process and swell/shrink behaviour of hydrogel based pH sensor [79].

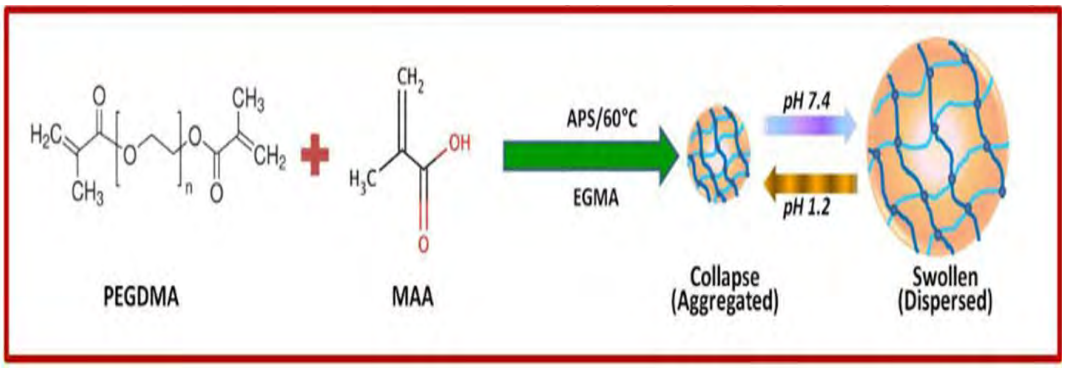

Figure 2.9: presentation of the preparation and behaviour of a hydrogel based pH sensor

2.6 FRESNEL LENS

Augustin-Jean Fresnel invented the Fresnel lens made of glass in 1822 and its first application was in a lighthouse due to its capability of attracting more light and its long range of visibility [95, 96]. In the 1950s, polymethylmethacrylate (PMMA) was used as Fresnel lens

material, providing an alternative option which was lighter and a more stable polymer [96–98]. Usually, Fresnel lenses contain distinct focused prism components in a superstrate design, in which the light becomes more focused in the central area. Figure 2.10(A and B) show the profile of a typical Fresnel lens [96, 99]. In general, a Fresnel lens is an optical function that can be used as a cost-effective, durable option to traditional optical lenses, Figure 2.10(C) displays the differences between Fresnel and standard lenses in shape and thickness. It has been used in a wide variety of applications such as solar power, photography, imaging (i.e. magnifier) and illumination (i.e. car headlights) [95, 98–100]. Moreover, in a study carried out by Espírito-Santo and colleagues, a Fresnel lens was built within a thermal energy system in order to focus the light, increase or decrease the temperature within the system and generate the power to activate a pH smart sensor to detect the pH level in water; Figure 2.10(D) presents an image of the system [101].

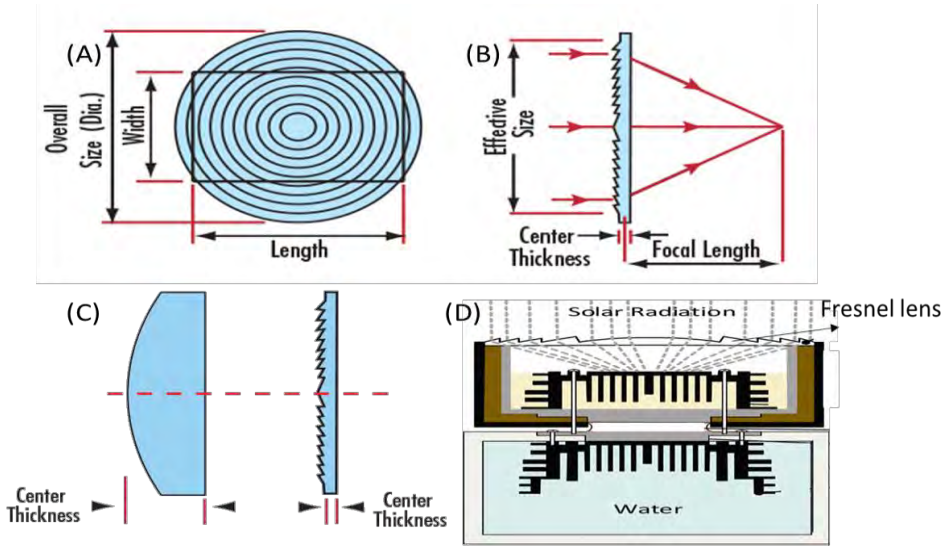

Figure 2.10: (A and B) show a typical Fresnel lens; (C) displays the differences between Fresnel and standard lenses [102]; (D) shows a Fresnel lens used to generate a pH smart sensor [101]

2.7 PRINCIPLES OF AN OPTICAL DIFFUSER

2.7.1 Brief background

Kuhn explained the history of light discovery in his book, In Quest of the Universe [103]. In 1666, Newton said that light has small and fast particles, which lead to vibration of the aether. Then, in 1890, Maxwell found that light is an electromagnetic wave. Maxwell's idea led Hertz to discover radio waves in 1888. In 1900, Planck highlighted that the energy of these waves is a continuously varying signal and is related to frequency. Einstein noted that if light contains massless particles, which are defined as photonics, then it should interact with matter. Figure 2.11(A) demonstrates how white light is divided into a visible spectrum when it passes through glass. A spectrum is the order of colours after the light has been separated by the glass. It can also be defined as a wavelength [103, 104].

A wavelength, λ, is the distance between two crests or troughs of a wave in which the wave starts repeating itself, as shown in Figure 2.11(B). Mehta said that the characteristics of matter can be examined by using the electromagnetic spectrum for spectroscopy [105]. Table 2.3 shows eight regions of the electromagnetic spectrum with their wavelength range and some applications, shown in Figure 2.11(C and D). This distribution of a wave is known as diffraction and occurs when a wave passes through a slit or across the edge of an object [103, 105]. The degree of diffraction depends on the size of the opening and the length of the wave. A smaller opening causes greater diffraction and a shorter wavelength leads to less diffraction [103]. Another important wave phenomenon is interference. This occurs when a pattern of tiny matter reflects light in the form of colours [105].

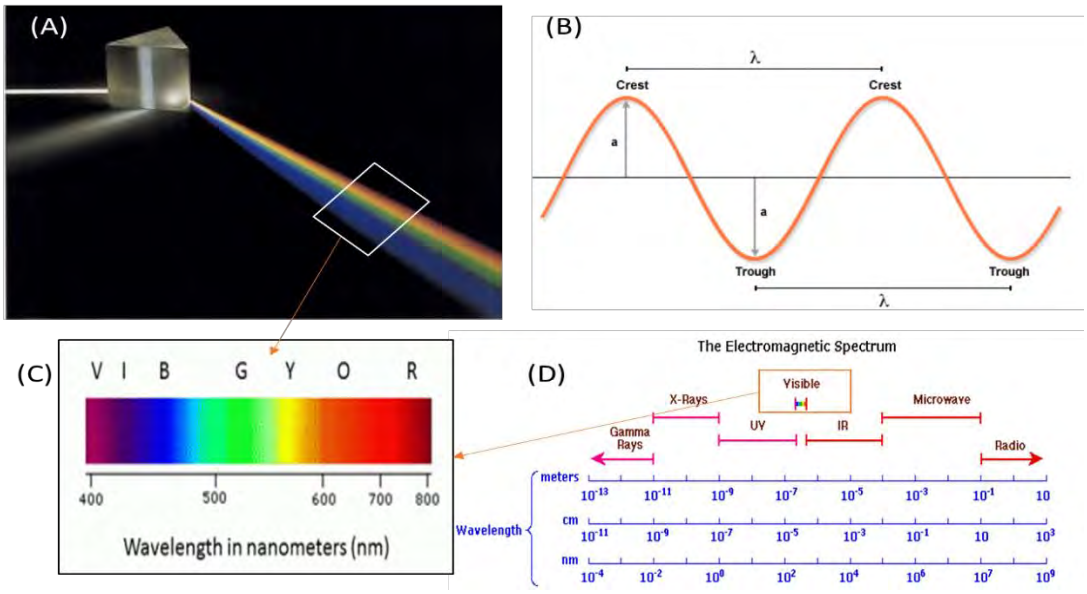

Figure 2.11: (A) presentation of glass separates a white light into its visible colours of light; (B) presentation of the wavelength λ, measured by metre (m); (C) presentation of the visible wavelength range and colours; (D) presentation of the electromagnetic spectrum order and ranges [103, 105, 106]

Table 2.3: Electromagnetic spectrum regions [103–105]

Electromagnetic spectrum	Wavelength, λ (nm)	Applications
Electric power	Above 10^9	Transfers electric energy to homes
Radio and TV	10^7-10^9	Broadcasting, communications industry
Microwave	10^6-10^7	Cooking, phones, radar
Infrared (IR)	10^3-10^6	Heating and drying, cameras, remote controls
Visible	4* 10^5 -7* 10^5	Human eye can see this range of wave
Ultraviolet (UV)	1-10^2	Germicidal, medicine
X-ray	10^{-2} -1	Medicine, remote sensing
Gamma	10^{-2}-10^{-4}	Mineral exploration

2.7.2 Light propagation

Light is defined as an electromagnetic wave consisting of coordinated pulses of electrical and magnetic fields. It transmits at light speed in a vacuum (3×10^8 m.s^{-1}). Light propagation

relates to the process when an electric wave moves its energy from one position to another. So this phenomenon refers to light interaction with material networks. Generally there are three major processes occurring when light passes through boundaries. In a transmission case, a light beam hits a transparent material such as glass. Then only a forward beam is maintained while the scattered wavelengths cancel one another. If the light beam is going across two different materials (i.e. going through the air and glass), some wavelengths are diverted back every time, the process is called reflection. When a light strikes an interface at an angle, both forward and backward beams will occur. This phenomenon is known as refraction, see Figure 2.12 [107–110].

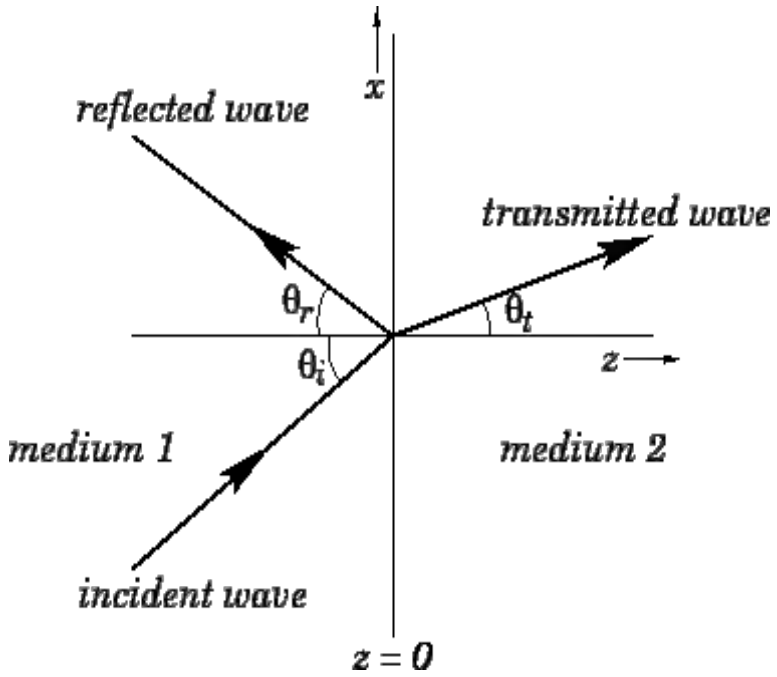

Figure 2.12: presentation of the refraction phenomenon which takes place when light strikes at an angle, showing the incident, reflected and transmitted waves [107]

2.7.3 The law of reflection

Figure 2.13(A) shows a reflected light in which the law of reflection generally assumes the reflection angle (θr) is equal to the incidence angle (θi) θr=θi. The reflected beam direction is defined by the angle-of-incidence which is the angle between the incident beam and the

surface. Figure 2.13(B and C) display the difference in the reflection behaviour between a smooth and rough surface. On the smooth surface the light will be reflected clearly and every single beam would be well-defined; this is called specular reflection. The rough surfaces would reflect the light differently and the light beams would return in all directions; this is called diffuser reflection. However, the reflection angle will be equal to the incidence angle for each beam [107, 109].

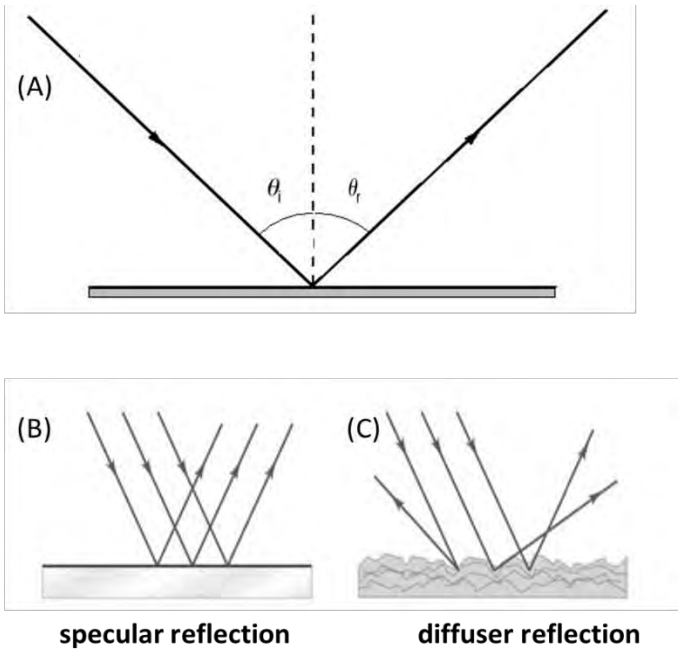

Figure 2.13: (A) the angle-of-incidence is similar to the angle-of- reflection; (B) and (C) show a presentation of specular and diffuser reflection

2.7.4 The law of refraction

Snell's law defines the law of refraction in which the beam may be reflected and transmitted at any time to form secondary wavelets [107, 109]. It states that the time *t* in which the light beam is travelling at a speed (v) to move from one point to another between two different transparent mediums with refractive indexes (n_i and n_t). The transmitted wave would reach a point at speed (v_t). The incident wave speed can be defined by $v_i = c/n_i$, and the speed

within the transmission can be defined by $v_t = c/n_t$, where c is the speed of light in vacuum. If the $n_t > n_i$ would make $v_i < v_t$. Then the Snell's law will be as

$$n_i \sin\theta_i = n_t \sin\theta_t \qquad \text{Equation 2.1}$$

2.7.5 Interference and diffraction

Interference refers to a process where two waves from two different sources converge to create a subsequent wave of larger or smaller amplitude. Whereas diffraction refers to the results of two secondary wavelets interacting from two various points of the same wave. Huygens's principle said that diffraction occurs when the wave passes or bends around an obstacle's edges or a small opening. The principle states that each point on a wavefront can serve as a source of secondary wavelets. These wavelets scatter in all directions at a speed equal to the original source [107, 108]. Figure 2.14 presents Huygens's principle of diffraction.

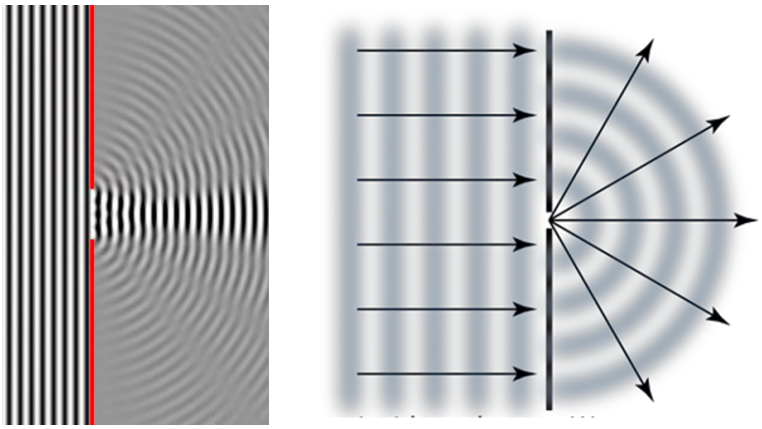

Figure 2.14: presentation of Huygens's principle of diffraction

2.8 LASER ABLATION

The term laser is formed from the initial letters of "Light Amplification by Stimulated Emission of Radiation". The accurate meaning of the expression is essential to understand when considering lasers' reaction with other materials; which makes laser energy remarkable in comparison to other forms of light energy [111, 112]. Lasers produce light power in the shape of a combination of photons from a medium that can be solid, liquid or gas. This medium defines the laser's name and the exact wavelength generated by the laser. For instance, the medium in a ruby laser is a synthetic ruby crystal and diffuses at 0.694 μm wavelength (infrared region). Moreover, the medium in a CO_2 laser is carbon dioxide gas and produces energy at 10.6 μm wavelength (far-infrared region) [112–115]. Lasers are found widely in industries such as laser drilling, laser cutting, laser milling and laser etching. Laser machining operations provide a better surface finishing for difficult to machine materials (like titanium and super alloys) compared to traditional machining operations [116–119]. These laser procedures include a popular phenomenon called laser ablation.

Laser ablation is a method of substance removal carried out by focussing a laser beam. Ablation happens only when the substance receives enough energy to melt or evaporate part of the material partially or fully [112, 115, 120]. The development of laser ablation started in 1960, when the ruby laser was discovered. Then the discovery was followed by several studies to define the fundamental features of laser removal: such as collecting the optically scattered light released from ablated metals in 1962; the foundation for the emission of a laser microprobe in 1963; and the detection of electrons' photoemission in 1963 [121]. In 1965, Smith and Turner recorded the first application of laser ablation for optically thin films made of powdered materials [122]. Currently, laser ablation is commonly utilised in metal, glass,

polymer production, and medical fields [112, 123, 124]. In past decades, laser ablation on polymers has received immense attention because of the polymers' potential to fabricate micro/nano structures such as microfluidic channels [114]. Polymers attract considerable interest because of their special characteristics including their light weight, corrosion resistance, and wide range of applications. The first use of laser ablation on polymers was published in 1978 by Cozzens and Fox. They applied an infrared laser of 10.6 μm wavelength to 11 different polymers [120].

There has also been a significant increase in studying the effect of laser types on the performance and durability of ablated properties of polymer materials. Poly(methyl methacrylate) (PMMA) is the most common polymer that has been ablated by different types of lasers such as an excimer laser (krypton fluoride laser and argon fluoride laser) and a CO_2 laser. Danielzik and his group ablated PMMA with an ArF excimer laser at a wavelength of 193 nm with a high speed to investigate the impact of laser speed on the ablation process [125]. Moreover, Nayak et al. used a CO_2 laser to fabricate micro-channels on PMMA of various molecular weights, to study the effect of the material choice on the manufacture of the microchannels [126]. Polydimethylsiloxane (PDMS) was ablated by a CO_2 laser and a femtosecond pulsed laser to produce microfluidic channels. Both laser types showed the ability to generate the channels [80, 127, 128]. Furthermore, there have been studies of laser ablation of polyimide (PI) using an excimer laser, and Nd:YAG lasers. It can be found in the literature that laser ablation has been an effective tool for the manufacture of micro and nano structures on diverse polymers. It is important to highlight that both the laser variables and material characteristics influence the laser ablation performance.

2.8.1 Mechanisms of laser ablation

All laser systems like laser milling, drilling and laser cutting mainly have the same laser ablation mechanisms. Ablation is a mixture of vaporisation and a melting process. If a focussed laser beam hits a target, laser photons excite the electrons existing in the substratum, see Figure 2.15 [129–131]. The excitement generates heat production due to the photon energy absorption. This energy can be defined by the Beer–Lambert law, which stated that the amount of the light absorbed relies on the substrate thickness and the light intensity [114, 132]. The heating impact leads to melting or evaporating of the substance, which causes selective areas to be removed from the surface of the substrate. Then, a plasma plume is created during the solid-gas transition [133, 134]. The process for ablation may be completely photochemical, photothermal or a mixture of both, depending on the laser parameters such as fluence, wavelength and speed, and material properties such as absorption level and reflectivity. The chemical ablation happens as a consequence of the breaking of polymer bonds by the UV photons' energy; whereas the thermal ablation occurs as a result of the breaking of polymer bonds by thermalizing the UV photons [135–138].

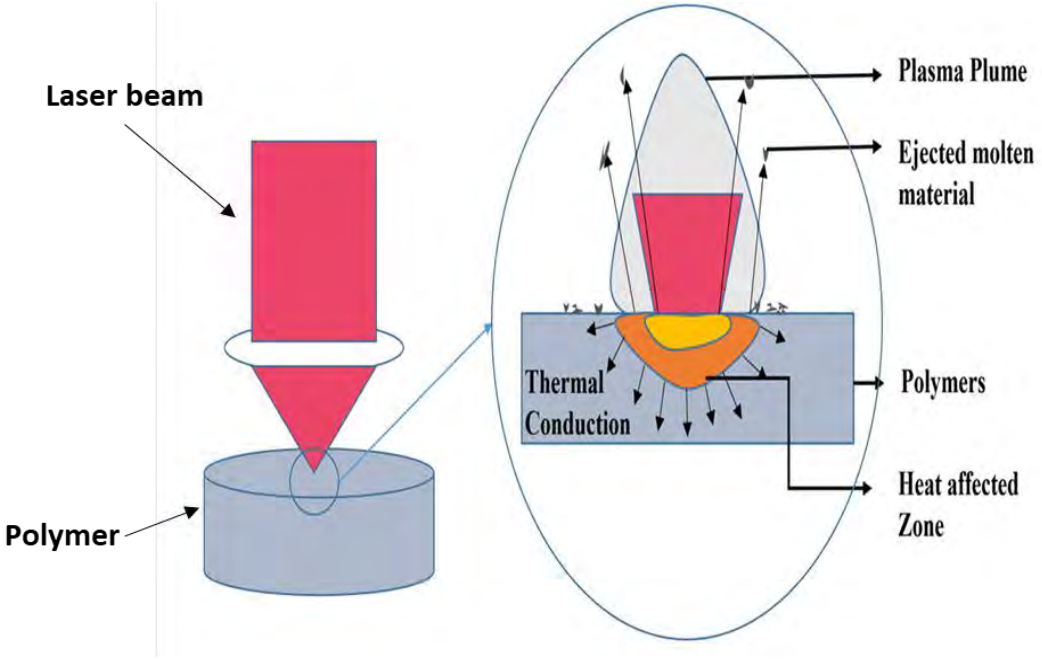

Figure 2.15: presentation of the laser ablation mechanisms [121]

2.8.2 CO_2 laser ablation

The CO_2 lasers have demonstrated outstanding performances in machining many materials. The CO_2 laser is a continuous wave laser with an infrared wavelength of 10.6 µm and are the most common laser system for cutting metal [114, 139, 140]. Stournaras et al. studied a CO_2 laser's quality in cutting aluminium alloy AA5083. They examined the surface roughness and the heat affected zone size by adjusting the laser power from 1500 W to 1800 W, the scanning speed from 2 m/min to 4 m/min, and the frequency from 8 Hz to 10 Hz [141]. Also, Yilbas investigated the effect of a CO_2 laser's parameters on the cutting quality of carbon steel. He found that the cutting width was decreased with faster laser scanning speed, and increased with greater laser power [142]. Additionally, this laser system has been used for modifying glass-based devices. Fu et al. developed glass-based microfluidic chips to detect formaldehyde concentration. They patterned the glass using a CO_2 laser to improve the roughness of the surface and create micro-channels for the detection material [140]. Ogura and

Yoshida etched two glass types, quartz glass and Pyrex glass, using a CO_2 laser. They stated that the CO_2 laser offered better results with quartz glass than Pyrex glass [143]. Furthermore, this laser is the most popular laser treatment tool in dermatology and surgery applications [112], [144], [145]. Omi and Numano highlighted that the use of CO_2 lasers in dermatology is safe, efficient, and offers a precise method [112].

In addition, CO_2 lasers have been widely used to pattern and modify polymers. This type of laser has been applied to PMMA, PDMS, HEMA, PI and many different polymers. The CO_2 laser ablation allows the manufacture of micro and nano patterns on the polymer [146–151]. It is also easy to control the focal beam precisely on the surface. Additionally, the water in the polymers helps to absorb the laser energy and minimise the damage to the polymer. Hong et al. used CO_2 laser ablation to structure microfluidic chips in PMMA for methanol detection. The study showed that CO_2 laser system has less surface in comparison to other laser ablation systems [151]. Also, Nan et al. created micro-channels on a commercial contact lens, which was made of HEMA, PEGDA, EDMA and 2-HMP, using a CO_2 laser at 30 W [114]. Liu et al. reported on the use of a CO_2 laser in cutting and patterning polydimethylsiloxane (PDMS). They fabricated a number of microstructures with different thickness from 2 μm to 3.6 mm on the PDMS layer [150]. Additionally, Riahi fabricated a 3D pattern on PMMA and PDMS by utilizing CO_2 laser removal [149].

Most of research facilities and manufacturing industries have in fact switched to CO_2 lasers because of their low cost, extremely fast fabrication and flexibility [152]. Moreover, CO_2 lasers can replace other systems without the need for equipment changes, clean room centres or professional staff. The researchers have been able to develop microfluidic structures to be

used in devices within less than 45 minutes [151–153]. The cost of the CO_2 laser ablation system is 10 times less than other ablation lasers such as the excimer laser, the femtosecond laser [140]. However, the CO_2 laser has several challenges which affects its capability. Firstly, it is hard to define the interaction between the laser and the material at the ablation point. This is because the ablation mechanism varies from one polymer to another [121, 152]. It is important to control the heat affected zone in order to avoid creating cracks and non-uniformity, to lead to a better polymer resolution [127, 132]. Moreover, one of the main challenges is getting the desired dimensions (depth and width) because currently there is no optimal for the CO_2 removal of each polymer [112]. This leads to not having a good quality finish, which is greatly required in manufacturing micro or nano structures. Controlling the laser parameters such power and speed would increase the quality of the fabrication structures [153–155]. The laser power is the main cause of the heat during the process. Some of this heat will be absorbed by the polymer in the desired location, but the rest may create cracks around the removal spots on the surface. Also the scanning speed is responsible for the surface cracks, because it has been found that the less time the laser spends in contact with the samples leads to reducing the risk of developing cracks on the surface [114, 121, 131, 149].

2.8.3 Hydrophilic and hydrophobic surfaces

The phrases "hydrophilic surface" and "hydrophobic surface" are widely used to define water behaviour on the surface of the materials. Hydrophilic surfaces have a good liquid attraction, while hydrophobic surfaces repel liquid [156, 157]. However, each material has its own wetting characteristics which classifies its surface type [158]. Applications of hydrophilic surfaces can be found in anti-fogging applications and the biomedical field. Also, hydrophobic surfaces have been used in oil removal, self-cleaning applications and waterproof solutions

[114, 159–161]. The main factor in the wetting characteristics is the surface roughness. The water spreading on the surface can be controlled by the surface roughness [162, 163]. In fact, most organic and artificial materials may be classified into the hydrophilic group. Also, the majority of polymers could be classified in this group [156].

The main criterion used to determine whether the surface is hydrophilic or hydrophobic is by measuring the contact angle. The contact angle (θ) is the angle at which the water or liquid meets the solid surface. The material is categorised according to the contact angle of the water droplet; the material will classify as hydrophilic when the angle is between 0° and 90°, and as hydrophobic when the angle is above 90° [157, 164, 165]. The material will be more water repellent as the angle gets bigger. Therefore, some authors have used various wetting classifications in which they introduced new terms like superhydrophilic ($\theta \approx 0°$), ultrahydrophobic ($120° < \theta < 150°$) and superhydrophobic ($\theta > 150°$), see Figure 2.16(A) [157, 166]. Drelich et al. reported that increasing the surface roughness will increase the contact angle. Figure 2.16(B) shows the relationship between the water-surface contact angle and the surface roughness.

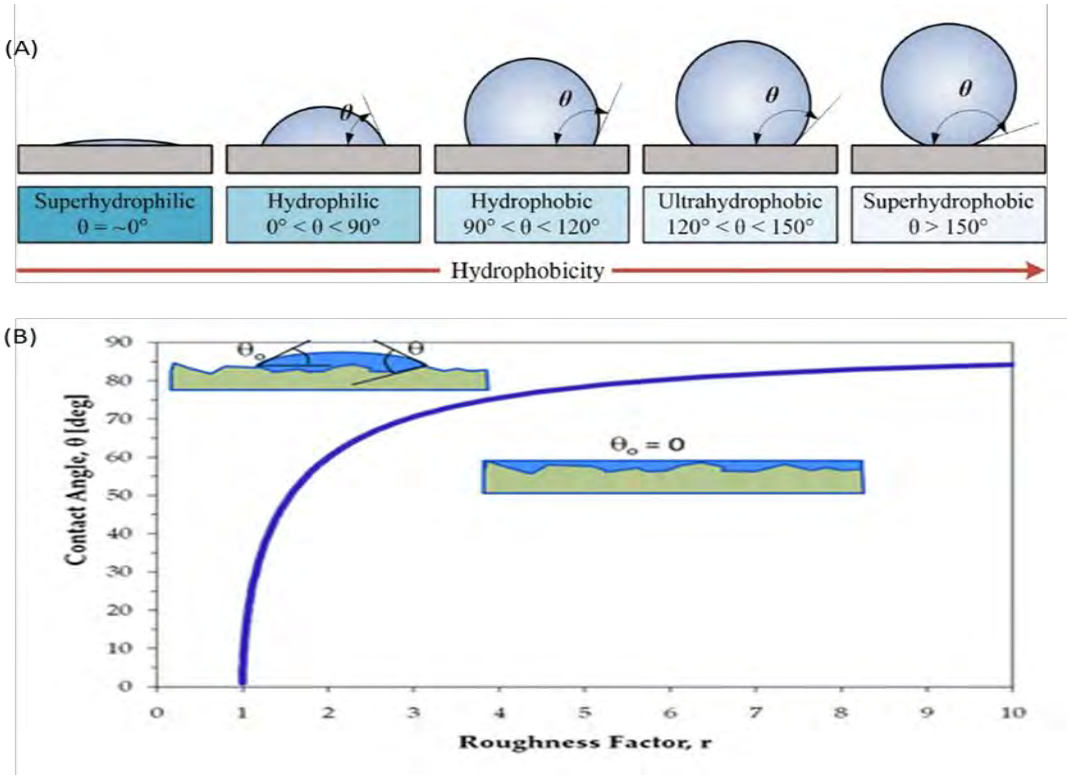

Figure 2.16: the contact angle of the liquid droplet: (A) shows the contact angle properties from superhydrophilic to superhydrophobic [157]; (B) shows the surface roughness and the contact angle correlation [156]

Laser ablation affects the surface roughness of the desired material. Therefore, it is essential to take the wettability conditions into consideration [121]. There are many studies on the influence of ablation on the surface wettability of different polymers, and on changing the polymers from the hydrophilicity region to the hydrophobicity region [167–171]. The modification of the polymer surface has attracted many researchers over the past years due to its wide applications in biomedical, coating systems and adhesion. Waugh and Lawrence investigated the effect of CO_2 lasers on the wettability characteristics of PMMA. They were able to increase the surface roughness by 3 µm by patterning structures on the surface using the laser. They managed to shift the contact angle slightly into the hydrophobic region [167]. In addition, Khorasani et al. fabricated a superhydrophobic layer on PDMS by CO_2 laser treatment [172]. Moreover, Kim et al. reported that a contact lens made of pHEMA can extend drug release time by treating the surface of the lens [171].

2.9 SUMMARY

This chapter covered the background of contact lenses and their design, hydrogel based sensors, the principles of an optical diffuser, and laser ablation. It showed that tear fluid could replace the blood sampling method in some cases. Then, contact lens sensors for glucose were studied in depth and presented. The current glucose testing methods, which are merely based on blood samples, provide only single reading, and uncomfortable, causing side effects. Over the last two decades this has encouraged researchers to look into alternative techniques. Hydrogel-based sensors for measuring IOP, which is related to glaucoma issues, were discussed. Here, we reported three methods based on contact lenses for continuous glucose monitoring. Furthermore, pH hydrogel-based sensors were reviewed in the chapter and several studies were summarized in Table 2.2 where we described the hydrogel material and detection approach in each study. Additionally, a brief background of the Fresnel lens and its applications were presented as well. Then, the principles of the optical diffuser were reviewed, including the subject of light propagation, the law of reflection and refraction. Moreover, this chapter has comprehensively studied the laser ablation systems and presented some examples of using such laser especially the CO_2 laser on polymer treatment. Furthermore, the mechanisms of the laser removal were discussed. Finally, hydrophilic hydrophobic surfaces were explained in terms of the effect of laser treatment on polymers.

REFERENCES

[1] P. B. Luppa, C. Müller, A. Schlichtiger, and H. Schlebusch, “Point-of-care testing (POCT): Current techniques and future perspectives,” *TrAC - Trends Anal. Chem.*, vol. 30, no. 6, pp. 887–898, 2011.

[2] P. Yager, G. J. Domingo, and J. Gerdes, “Point-of-Care Diagnostics for Global Health,” *Annu. Rev. Biomed. Eng.*, vol. 10, no. 1, pp. 107–144, 2008.

[3] J. Andreu-Perez, D. R. Leff, H. M. D. Ip, and G. Z. Yang, “From Wearable Sensors to Smart Implants-Toward Pervasive and Personalized Healthcare,” *IEEE Trans. Biomed. Eng.*, vol. 62, no. 12, pp. 2750–2762, 2015.

[4] Y. Yonezawa *et al.*, “A new intelligent bed care system for hospital and home patients.,” *Biomed. Instrum. Technol.*, vol. 39, no. 4, pp. 313–319, 2005.

[5] M. Leonardi, E. M. Pitchon, A. Bertsch, P. Renaud, and A. Mermoud, “Wireless contact lens sensor for intraocular pressure monitoring: Assessment on enucleated pig eyes,” *Acta Ophthalmol.*, vol. 87, no. 4, pp. 433–437, 2009.

[6] K. G. Ng, S. T. Wong, S. M. Lim, and Z. Goh, “Evaluation of the Cadi ThermoSENSOR Wireless Skin-Contact Thermometer Against Ear and Axillary Temperatures in Children,” *J. Pediatr. Nurs.*, vol. 25, no. 3, pp. 176–186, 2010.

[7] Y. T. Liao, H. Yao, A. Lingley, B. Parviz, and B. P. Otis, “A 3-μW CMOS glucose sensor for wireless contact-lens tear glucose monitoring,” *IEEE J. Solid-State Circuits*, vol. 47, no. 1, pp. 335–344, 2012.

[8] R. C. Tseng, C. C. Chen, S. M. Hsu, and H. S. Chuang, “Contact-lens biosensors,” *Sensors (Switzerland)*, vol. 18, no. 8, 2018.

[9] S. R. Corrie, J. W. Coffey, J. Islam, K. A. Markey, and M. A. F. Kendall, “Blood, sweat, and tears: Developing clinically relevant protein biosensors for integrated body fluid analysis,” *Analyst*, vol. 140, no. 13. pp. 4350–4364, 2015.

[10] K. Mitsubayashi and T. Arakawa, “Cavitas Sensors: Contact Lens Type Sensors & Mouthguard Sensors,” *Electroanalysis*, vol. 28, no. 6, pp. 1170–1187, 2016.

[11] N. M. Farandos, A. K. Yetisen, M. J. Monteiro, C. R. Lowe, and S. H. Yun, “Contact lens sensors in ocular diagnostics,” *Adv. Healthc. Mater.*, vol. 4, no. 6, pp. 792–810, 2015.

[12] W. Douthwaite, *Contact Lens Optics & Lens Design*, 3rd ed. London, United Kingdom: Elsevier Health Sciences, 2006.

[13] G. Z. Chen, I. S. Chan, and D. C. C. Lam, “Capacitive contact lens sensor for continuous non-invasive intraocular pressure monitoring,” *Sensors Actuators, A Phys.*, vol. 203, pp. 112–118, 2013.

[14] P. C. Nicolson and J. Vogt, “Soft contact lens polymers: An evolution,” *Biomaterials*,

vol. 22, no. 24, pp. 3273–3283, 2001.

[15] N. Efron, S. E. Efron, P. B. Morgan, and S. L. Morgan, “A ‘cost-per-wear’ model based on contact lens replacement frequency,” *Clin. Exp. Optom.*, vol. 93, no. 4, pp. 253–260, 2010.

[16] C. Lin *et al.*, “Toward the Development of a Glucose Dehydrogenase-Based Saliva Glucose Sensor Without the Need for Sample Preparation,” 2018.

[17] N. V. T. Hohenstein-blaul, S. Funke, and F. H. Grus, “Tears as a source of biomarkers for ocular and systemic diseases,” *Exp. Eye Res.*, vol. 117, pp. 126–137, 2013.

[18] L. Zhou and R. W. Beuerman, “Tear analysis in ocular surface diseases,” *Prog. Retin. Eye Res.*, vol. 31, no. 6, pp. 527–550, 2012.

[19] R. Badugu, J. R. Lakowicz, and C. D. Geddes, “A glucose-sensing contact lens: From bench top to patient,” *Curr. Opin. Biotechnol.*, vol. 16, no. 1 SPEC. ISS., pp. 100–107, 2005.

[20] K. B. Green-Church, K. K. Nichols, N. M. Kleinholz, L. Zhang, and J. J. Nichols, “Investigation of the human tear film proteome using multiple proteomic approaches,” *Mol. Vis.*, vol. 14, no. October 2007, pp. 456–470, 2008.

[21] D. Harvey, N. W. Hayes, and B. Tighe, “Fibre optics sensors in tear electrolyte analysis: Towards a novel point of care potassium sensor,” *Contact Lens Anterior Eye*, vol. 35, no. 3, pp. 137–144, 2012.

[22] C. R. Taormina, J. T. Baca, D. N. Finegold, S. A. Asher, and J. J. Grabowski, “Analysis of Tear Glucose Concentration with Electrospray,” *J. Am. Soc. Mass Spectrom.*, vol. 18, no. 2, pp. 332–336, 2008.

[23] H. Yao, A. J. Shum, M. Cowan, I. Lähdesmäki, and B. A. Parviz, “A contact lens with embedded sensor for monitoring tear glucose level,” *Biosens. Bioelectron.*, vol. 26, no. 7, pp. 3290–3296, 2011.

[24] N. Thomas, I. Lähdesmäki, and B. A. Parviz, “A contact lens with an integrated lactate sensor,” *Sensors Actuators, B Chem.*, vol. 162, no. 1, pp. 128–134, 2012.

[25] K. Mansouri, F. A. Medeiros, A. Tafreshi, and R. N. Weinreb, “Continuous 24-hour monitoring of intraocular pressure patterns with contact lens sensor: Safety, tolerability, and reproducibility in patients with glaucoma,” *Arch. Ophthalmol.*, vol.

130, no. 12, pp. 1534–1539, 2012.

[26] J. R. Cope, S. A. Collier, H. Nethercut, J. M. Jones, K. Yates, and J. S. Yoder, “Risk behaviors for contact lens–related eye infections among adults and adolescents — United States, 2016,” *Morb. Mortal. Wkly. Rep.*, vol. 66, no. 32, pp. 841–845, 2017.

[27] Y. R. Lin *et al.*, “Noninvasive glucose monitoring with a contact lens and smartphone,” *Sensors (Switzerland)*, vol. 18, no. 10, pp. 1–12, 2018.

[28] B. Zhou *et al.*, “Worldwide trends in diabetes since 1980: A pooled analysis of 751 population-based studies with 4.4 million participants,” *Lancet*, vol. 387, no. 10027, pp. 1513–1530, 2016.

[29] K. Ogurtsova *et al.*, “IDF Diabetes Atlas: Global estimates for the prevalence of diabetes for 2015 and 2040,” *Diabetes Res. Clin. Pract.*, vol. 128, pp. 40–50, Jun. 2017.

[30] N. M. M. Farandos, A. K. K. Yetisen, M. J. J. Monteiro, C. R. R. Lowe, and S. H. H. Yun, “Contact lens sensors in ocular diagnostics,” *Adv. Healthc. Mater.*, vol. 4, no. 6, pp. 792–810, 2015.

[31] N. S. Oliver, C. Toumazou, A. E. G. Cass, and D. G. Johnston, “Glucose sensors: A review of current and emerging technology,” *Diabet. Med.*, vol. 26, no. 3, pp. 197–210, 2009.

[32] H. Lee, Y. J. Hong, S. Baik, T. Hyeon, and D. Kim, “Enzyme-Based Glucose Sensor : From Invasive to Wearable Device,” *Adv. Healthc. Mater*, vol. 1701150, pp. 1–14, 2018.

[33] W. March, D. Lazzaro, and S. Rastogi, “Fluorescent Measurement in the Non-Invasive Contact Lens Glucose Sensor,” *Diabetes Technol. Ther.*, vol. 8, no. 3, pp. 312–317, Jun. 2006.

[34] N. Bühler *et al.*, “Nelfilcon A, a new material for contact lenses,” *Chimia (Aarau).*, vol. 53, no. 6, pp. 269–274, 1999.

[35] R. J. Russell, M. V. Pishko, C. C. Gefrides, M. J. McShane, and G. L. Cote, “A fluorescence-based glucose biosensor using concanavalin A and dextran encapsulated in a poly(ethylene glycol) hydrogel,” *Anal. Chem.*, vol. 71, no. 15, pp. 3126–3132, 1999.

[36] R. Badugu, J. R. Lakowicz, and C. D. Geddes, “A Glucose Sensing Contact Lens: A Non-Invasive Technique for Continuous Physiological Glucose Monitoring,” *J. Fluoresc.*, vol. 13, no. 5, pp. 371–374, 2003.

[37] X. Yang, X. Pan, J. Blyth, and C. R. Lowe, “Towards the real-time monitoring of glucose in tear fluid : Holographic glucose sensors with reduced interference from lactate and pH,” vol. 23, pp. 899–905, 2008.

[38] A. K. Yetisen *et al.*, “Photonic hydrogel sensors,” *Biotechnol. Adv.*, vol. 34, no. 3, pp. 250–271, 2016.

[39] A. K. Yetisen *et al.*, “Reusable, robust, and accurate laser-generated photonic nanosensor,” *Nano Lett.*, vol. 14, no. 6, pp. 3587–3593, 2014.

[40] A. Domschke *et al.*, “Holographic Sensors in Contact Lenses for Minimally-Invasive Glucose Measurements,” *Proc. IEEE Sensors*, pp. 1320–1323, 2004.

[41] M. Elsherif, M. U. Hassan, A. K. Yetisen, and H. Butt, “Wearable Contact Lens Biosensors for Continuous Glucose Monitoring Using Smartphones,” *ACS Nano*, vol. 12, pp. 5452–5462, 2018.

[42] V. L. Alexeev *et al.*, “High ionic strength glucose-sensing photonic crystal,” *Anal. Chem.*, vol. 75, no. 10, pp. 2316–2323, 2003.

[43] V. L. Alexeev, S. Das, D. N. Finegold, and S. A. Asher, “Photonic crystal glucose-sensing material for noninvasive monitoring of glucose in tear fluid,” *Clin. Chem.*, vol. 50, no. 12, pp. 2353–2360, 2004.

[44] J. Ruan, C. Chen, J. Shen, X. Zhao, and S. Qian, “A Gelated Colloidal Crystal Attached Lens for Noninvasive Continuous Monitoring of Tear Glucose,” *Polymers (Basel).*, vol. 9, no. 125, pp. 1–12, 2017.

[45] W. Dungchai, O. Chailapakul, and C. S. Henry, “Electrochemical Detection for Paper-Based Microfluidics,” vol. 81, no. 14, pp. 5821–5826, 2009.

[46] F. Yañez *et al.*, “Supercritical fluid-assisted preparation of imprinted contact lenses for drug delivery,” *Acta Biomater.*, vol. 7, no. 3, pp. 1019–1030, 2011.

[47] J. N. Patel, B. L. Gray, B. Kaminska, and B. D. Gates, “Flexible Three-Dimensional Electrochemical Glucose Sensor with Improved Sensitivity Realized in Hybrid Polymer Microelectromechanical Systems Technique,” *J. Diabetes Sci. Technol.*, vol.

5, no. 5, pp. 1036–1043, 2011.

[48] P. Rattanarat, W. Dungchai, W. Siangproh, O. Chailapakul, and C. S. Henry, “Sodium dodecyl sulfate-modified electrochemical paper-based analytical device for determination of dopamine levels in biological samples,” *Anal. Chim. Acta*, vol. 744, pp. 1–7, 2012.

[49] H. Yao, A. J. Shum, M. Cowan, I. Lähdesmäki, and B. A. Parviz, “A contact lens with embedded sensor for monitoring tear glucose level,” *Biosens. Bioelectron.*, vol. 26, no. 7, pp. 3290–3296, 2011.

[50] W. Cheng, N. Klauke, H. Sedgwick, G. L. Smith, and J. M. Cooper, “Metabolic monitoring of the electrically stimulated single heart cell within a microfluidic platform,” *Lab Chip*, vol. 6, no. 11, pp. 1424–1431, 2006.

[51] M. X. Chua *et al.*, “Soft contact lens biosensor for in situ monitoring of tear glucose as non-invasive blood sugar assessment,” *Talanta*, vol. 83, no. 3, pp. 960–965, 2011.

[52] J. Kim *et al.*, “contact lenses for wireless ocular diagnostics,” *Nat. Commun.*, vol. 8, 2017.

[53] R. N. Weinreb, T. Aung, and F. A. Medeiros, “The pathophysiology and treatment of glaucoma: A review,” *JAMA - J. Am. Med. Assoc.*, vol. 311, no. 18, pp. 1901–1911, 2014.

[54] C. T. Supuran, A. S. A. Altamimi, and F. Carta, “Carbonic anhydrase inhibition and the management of glaucoma: a literature and patent review 2013-2019,” *Expert Opin. Ther. Pat.*, vol. 29, no. 10, pp. 781–792, Oct. 2019.

[55] D. L. Halpern and C. L. Grosskreutz, “Glaucomatous optic neuropathy: Mechanisms of disease,” *Ophthalmol. Clin. North Am.*, vol. 15, no. 1, pp. 61–68, 2002.

[56] S. Moghimi, H. Hou, H. L. Rao, and R. N. Weinreb, “Optical coherence tomography angiography and glaucoma: A brief review,” *Asia-Pacific J. Ophthalmol.*, vol. 8, no. 2, pp. 115–125, 2019.

[57] R. R. Allingham, Y. Liu, and D. J. Rhee, “The genetics of primary open-angle glaucoma: A review,” *Exp. Eye Res.*, vol. 88, no. 4, pp. 837–844, 2009.

[58] T. Realini, N. Weinreb, and S. Wisniewski, “Short-term repeatability of diurnal intraocular pressure patterns in glaucomatous individuals,” *Ophthalmology*, vol. 118,

no. 1, pp. 47–51, 2011.

[59] M. Ratan-NM, “Types of Glaucoma,” *News medical life sciences*, 2019.

[60] C. Wright, M. A. Tawfik, M. Waisbourd, and L. J. Katz, “Primary angle-closure glaucoma: An update,” *Acta Ophthalmol.*, vol. 94, no. 3, pp. 217–225, 2016.

[61] J. M. Tielsch, A. Sommer, J. Katz, R. M. Royall, H. A. Quigley, and J. Javitt, “Racial Variations in the Prevalence of Primary Open-angle Glaucoma: The Baltimore Eye Survey,” *JAMA*, vol. 266, no. 3, pp. 369–374, Jul. 1991.

[62] I. Sanchez and R. Martin, “Advances in diagnostic applications for monitoring intraocular pressure in Glaucoma: A review,” *J. Optom.*, vol. 12, no. 4, pp. 211–221, 2019.

[63] J. Crawford Downs, C. F. Burgoyne, W. P. Seigfreid, J. F. Reynaud, N. G. Strouthidis, and V. Sallee, “24-hour IOP telemetry in the nonhuman primate: Implant system performance and initial characterization of IOP at multiple timescales,” *Investig. Ophthalmol. Vis. Sci.*, vol. 52, no. 10, pp. 7365–7375, 2011.

[64] J. H. K. Liu and R. N. Weinreb, “Monitoring intraocular pressure for 24 h,” *Br. J. Ophthalmol.*, vol. 95, no. 5, pp. 599–600, 2011.

[65] A. Calikoglu, G. Dundar, A. D. Yalcinkaya, and H. Torun, “Laser-Machined Split-Ring Resonators Embedded in a Polymer Matrix for Glaucoma Monitoring,” *Proceedings*, vol. 1, no. 10, p. 531, 2017.

[66] A. K. C. Lam and W. A. Douthwaite, “The effect of an artificially elevated intraocular pressure on the central corneal curvature,” *Ophthalmic Physiol. Opt.*, vol. 17, no. 1, pp. 18–24, 1997.

[67] K. Mansouri and R. N. Weinreb, “Continuous 24 hour intraocular pressure monitoring for glaucoma with a contact lens sensor - Time for a paradigm change,” *Swiss Med. Wkly.*, vol. 142, no. MARCH, 2012.

[68] M. M. Whitacre and R. Stein, “Sources of error with use of Goldmann-type tonometers,” *Surv. Ophthalmol.*, vol. 38, no. 1, pp. 1–30, 1993.

[69] L. Quaranta *et al.*, “Untreated 24-h intraocular pressures measured with Goldmann applanation tonometry vs nighttime supine pressures with Perkins applanation tonometry,” *Eye*, vol. 24, no. 7, pp. 1252–1258, 2010.

[70] R. H. Small, G. Simon, Q. Ben, and J. Parel, “THE EFFECT OF CORNEAL HYDRATION ON APPLANATION TONOMETRY AND CORNEAL TOPOGRAPHY,” *Invest. Ophthalmol. Vis. Sci.*, vol. 33, no. 4, p. 733, 1992.

[71] J. H. K. Liu and R. N. Weinreb, “Monitoring intraocular pressure for 24 h,” *Br. J. Ophthalmol.*, vol. 95, no. 5, pp. 599–600, 2011.

[72] M. Leonardi, P. Leuenberger, D. Bertrand, A. Bertsch, and P. Renaud, “A soft contact lens with a MEMS strain gage embedded for intraocular pressure monitoring,” *IEEE TRANSDUCERS Solid-State Sensors, Actuators Microsyslem*, vol. 2, pp. 1043–1046, 2003.

[73] M. Leonardi, E. M. Pitchon, A. Bertsch, P. Renaud, and A. Mermoud, “Wireless contact lens sensor for intraocular pressure monitoring: Assessment on enucleated pig eyes,” *Acta Ophthalmol.*, vol. 87, no. 4, pp. 433–437, 2009.

[74] G. E. Dunbar, B. Y. Shen, and A. A. Aref, “The Sensimed Triggerfish contact lens sensor: Efficacy, safety, and patient perspectives,” *Clin. Ophthalmol.*, vol. 11, pp. 875–882, 2017.

[75] J. R. Sharpe, S. Booth, K. Jubin, N. R. Jordan, D. J. Lawrence-Watt, and B. S. Dheansa, “Progression of wound pH during the course of healing in burns,” *J. Burn Care Res.*, vol. 34, no. 3, pp. 201–208, 2013.

[76] R. Rahimi *et al.*, “A low-cost flexible pH sensor array for wound assessment,” *Sensors Actuators, B Chem.*, vol. 229, pp. 609–617, 2016.

[77] L. V. Thomas, J. W. T. Wimpenny, and J. G.Davis, “Effect of three preservatives on the growth of Bacillus cereus, Vero cytotoxigenic Escherichia coli and Staphylococcus aureus, on plates with gradients of pH and sodium chloride concentration,” *Int. J. Food Microbiol.*, vol. 17, no. 4, pp. 289–301, 1993.

[78] Y. Zhao, M. Lei, S. X. Liu, and Q. Zhao, “Smart hydrogel-based optical fiber SPR sensor for pH measurements,” *Sensors Actuators, B Chem.*, vol. 261, pp. 226–232, 2018.

[79] L. K. Tomar, C. Tyagi, Y. E. Choonara, P. Kumar, and V. Pillay, “Rheological and Swelling Behavior of pH Sensitive Hydrogel Particles,” *APCBEE Procedia*, vol. 9, no. Icbee 2013, pp. 192–196, 2014.

[80] M. Li, S. Li, J. Wu, W. Wen, W. Li, and G. Alici, “A simple and cost-effective method

for fabrication of integrated electronic-microfluidic devices using a laser-patterned PDMS layer," *Microfluid. Nanofluidics*, vol. 12, no. 5, pp. 751–760, 2012.

[81] A. Tamayol, M. Akbari, Y. Zilberman, M. Comotto, E. Lesha, and Ludovic. Serex, "Flexible pH-Sensing Hydrogel Fibers for Epidermal Applications," *Adv Heal. Mater*, vol. 5, no. 6, pp. 711–719, 2017.

[82] L. S. Lim, I. Ahmad, and M. A. S. M. Lazim, "PH sensitive hydrogel based on poly(acrylic acid) and cellulose nanocrystals," *Sains Malaysiana*, vol. 44, no. 6, pp. 779–785, 2015.

[83] D. Kuckling, A. Richter, and K. Arndt, "Temperature and pH-Dependent Swelling Behavior of Poly (N -isopropylacrylamide) Copolymer Hydrogels and Their Use in Flow Control," *Macromol. Mater. Eng.*, vol. 288, pp. 144–151, 2003.

[84] Gerald Gerlach, M. Guenther, G. Suchaneck, J. Sorber, K. Arndt, and A. Richter, "Application of sensitive hydrogels in chemical and pH sensors," *Symp, Macromol*, vol. 210, pp. 403–410, 2004.

[85] D. Buenger, F. Topuz, and J. Groll, "Hydrogels in sensing applications," *Prog. Polym. Sci.*, vol. 37, no. 12, pp. 1678–1719, 2012.

[86] S. Bhattacharya, F. Eckert, V. Boyko, and A. Pich, "Temperature-, pH-, and Magnetic-Field-Sensitive Hybrid Microgels," *Hybrid microgels DOI*, vol. 6, pp. 650–657, 2007.

[87] C. Ruan, K. Zeng, and C. A. Grimes, "A mass-sensitive pH sensor based on a stimuli-responsive polymer," *Anal. Chim. Acta*, vol. 497, pp. 123–131, 2003.

[88] A. Richter, A. Bund, M. Keller, and K. Arndt, "Characterization of a microgravimetric sensor based on pH sensitive hydrogels," *Sensors Actuators B*, vol. 99, pp. 579–585, 2004.

[89] R. E. Kunz, G. Jobst, I. Moser, and G. Urban, "Integrated optical pH sensor using replicated chirped grating coupler sensor chips," *Sensors Actuators B*, vol. 50, pp. 210–219, 1998.

[90] A. J. Marshall, J. Blyth, C. A. B. Davidson, and C. R. Lowe, "pH-Sensitive Holographic Sensors," *Anal. Chem.*, vol. 75, no. 17, pp. 4423–4431, 2003.

[91] K. Lee, S. A. Asher, and R. V June, "Photonic Crystal Chemical Sensors : pH and Ionic Strength," *Am. Chem. Soc.*, vol. 15260, no. 14, pp. 9534–9537, 2000.

[92] N. F.Sheppard, J. M. J. Lesho, P. McNally, and A. S. Francomacaro, “Microfabricated conductimetric pH sensor,” *Sensors Actuators B Chem.*, vol. 28, no. 2, pp. 95–102, 1995.

[93] Y. Zhang *et al.*, “A pH Sensor Based on a Microcantilever Coated with Intelligent Hydrogel A pH Sensor Based on a Microcantilever Coated with Intelligent Hydrogel,” *Instrum. Sci. Technol.*, vol. 32, no. 4, pp. 361–369, 2004.

[94] Q. Thong, G. Gerlach, J. Sorber, and K. Arndt, “Hydrogel-based piezoresistive pH sensors : Design , simulation and output characteristics,” *Sensors Actuators B*, vol. 117, pp. 17–26, 2006.

[95] A. Keshavarz and M. J. Soltanzadeh, “Designing the optimal Fresnel lenses by using Zemax software,” vol. 3, no. 2, 2018.

[96] W. T. Xie, Y. J. Dai, R. Z. Wang, and K. Sumathy, “Concentrated solar energy applications using Fresnel lenses : A review,” *Renew. Sustain. Energy Rev.*, vol. 15, no. 6, pp. 2588–2606, 2011.

[97] D. C. Miller and S. R. Kurtz, “Durability of Fresnel lenses : A review specific to the concentrating photovoltaic application,” *Sol. Energy Mater. Sol. Cells*, vol. 95, no. 8, pp. 2037–2068, 2011.

[98] H. Qandil, S. Wang, and W. Zhao, “Application - based design of the Fresnel lens solar concentrator,” *Renewables Wind. Water, Sol.*, 2019.

[99] A. Davis and F. Kühnlenz, “Optical Design using Fresnel Lenses Basic Principles and some Practical Examples,” *Opt. Photonik December*, no. 4, pp. 52–55, 2007.

[100] T. T. Pham, N. H. Vu, and S. Shin, “Design of Curved Fresnel Lens with High Performance Creating Competitive Price Concentrator Photovoltaic,” *Energy Procedia*, vol. 144, pp. 16–32, 2018.

[101] A. Espírito-Santo, S. Ambrósio, P. M. D. Serra, and R. J. C. Pinto, “Water pH Monitoring with a Smart Sensor Powered by a Thermoelectric Generator with a Phase-Change Material,” *IEEE*, pp. 5550–5555, 2019.

[102] “Advantages of Fresnel Lenses,” *Edmund Optics*, 2011. [Online]. Available: https://www.edmundoptics.com/knowledge-center/application-notes/optics/advantages-of-fresnel-lenses/.

[103] K. F. Kuhn, *In quest of the universe*, 1st ed. Sudbury, Mass.: Jones and Bartlett Publishers, 1998.

[104] S. Sankaran and R. Ehsani, "Introduction to the electromagnetic spectrum," *Imaging with Electromagn. Spectr. Appl. Food Agric.*, pp. 1–15, 2014.

[105] A. Mehta, "Introduction to the Electromagnetic Spectrum and Spectroscopy," *Pharmaxchange. info.*, vol. 11, no. 8, 2011.

[106] "Wave parameters and behaviours," *BBC*, 2014. [Online]. Available: https://www.bbc.co.uk/bitesize/guides/zq4tyrd/revision/1.

[107] E. Hecht, A. Zajac, and M. E. Cox, "Optics," vol. 921, no. 1974, 2010.

[108] M. Born and E. Wolf, "Principles of optics : electromagnetic theory of propagation, interference and diffraction of light." Cambridge : Cambridge University Press, Cambridge, 1999.

[109] Z. G. Nanfang Yu, Patrice Genevet, Mikhail A. Kats, Francesco Aieta, Jean-Philippe Tetienne, Federico Capasso, "Light Propagation with Phase Reflection and Refraction," *Artic. Sci.*, vol. 334, 2011.

[110] E. M. Purcell, "Electricity and magnetism / Edward M. Purcell, David J. Morin." Cambridge : Cambridge University Press, 2013., 2013.

[111] L. Carroll and T. R. Humphreys, "LASER-tissue interactions," *Clin. Dermatol.*, vol. 24, no. 1, pp. 2–7, 2006.

[112] T. Omi and K. Numano, "The role of the CO_2 laser and fractional CO_2 laser in dermatology," *Laser Ther.*, vol. 23, no. 1, pp. 49–60, 2014.

[113] M. C. Grossman, C. Dierickx, W. Farinelli, T. Flotte, and R. R. Anderson, "Damage to hair follicles by normal-mode ruby laser pulses," *J. Am. Acad. Dermatol.*, vol. 35, no. 6, pp. 889–894, 1996.

[114] N. Jiang, Y. Montelongo, H. Butt, and A. K. Yetisen, "Microfluidic Contact Lenses," *Small*, vol. 14, no. 15, 2018.

[115] Z. K. Wang and H. Y. Zheng, "Investigation on CO_2 laser irradiation inducing glass strip peeling for microchannel formation," *Biomicrofluidics*, vol. 6, no. 1, pp. 1–12, 2012.

[116] R. Bogue, "Lasers in manufacturing: A review of technologies and applications,"

Assem. Autom., vol. 35, no. 2, pp. 161–165, 2015.

[117] M. Kuttolamadom, J. Jones, L. Mears, T. Kurfess, and A. Choragudi, "Investigation of the Machining of Titanium Components for Lightweight Vehicles," in *SAE 2010 World Congress & Exhibition*, 2010.

[118] E. Akinlabi, M. M. Rasheedat, and A. A. Stephen, "Advanced Manufacturing Techniques Using Laser Material Processing," *IGI Glob.*, pp. 11–24, 2016.

[119] I. F. Larsson, "Method and apparatus for drilling holes by means of a focused laser beam," *US Pat. US3410979A*, vol. 28, no. 2, pp. 131–134, 1968.

[120] R. F. Cozzens and R. B. Fox, "Infrared laser ablation of polymers," *Polym. Eng. Sci.*, vol. 18, no. 11, pp. 900–904, 1978.

[121] S. Ravi-Kumar, B. Lies, X. Zhang, H. Lyu, and H. Qin, "Laser ablation of polymers: a review," *Polym. Int.*, vol. 68, no. 8, pp. 1391–1401, 2019.

[122] H. M. Smith and A. F. Turner, "Vacuum Deposited Thin Films Using a Ruby Laser," *Appl. Opt.*, vol. 4, no. 1, p. 147, 1965.

[123] H. Becker and C. Gärtner, "Polymer microfabrication methods for microfluidic analytical applications," *Electrophoresis.*, vol. 21. [Weinheim, Germany] :, pp. 12–26, 2000.

[124] G. Van Steenberge, P. Van Daele, N. Hendrickx, E. Bosman, J. Van Erps, and H. Thienpont, "Laser ablation of parallel optical interconnect waveguides," *IEEE Phot. Technol Lett*, vol. 18, no. 9, pp. 1106–1108, 2006.

[125] B. Danielzik, N. Fabricius, M. Röwekamp, and D. Von Der Linde, "Velocity distribution of molecular fragments from polymethylmethacrylate irradiated with UV laser pulses," *Appl. Phys. Lett.*, vol. 48, no. 3, pp. 212–214, 1986.

[126] N. C. Nayak, Y. C. Lam, C. Y. Yue, and A. T. Sinha, "CO_2-laser micromachining of PMMA: The effect of polymer molecular weight," *J. Micromechanics Microengineering*, vol. 18, no. 9, 2008.

[127] Z. Yan, X. Huang, and C. Yang, "Rapid prototyping of single-layer microfluidic PDMS devices with abrupt depth variations under non-clean-room conditions by using laser ablation and UV-curable polymer," *Microfluid. Nanofluidics*, vol. 21, no. 6, pp. 1–9, 2017.

[128] D. B. Wolfe, J. B. Ashcom, J. C. Hwang, C. B. Schaffer, E. Mazur, and G. M. Whitesides, “Customization of poly(dimethylsiloxane) stamps by micromachining using a femtosecond-pulsed laser,” *Adv. Mater.*, vol. 15, no. 1, pp. 62–65, 2003.

[129] J. Dowden and W. Schulz, *The Theory of Laser Materials Processing*. 2017.

[130] S. Singh, M. Argument, Y. Y. Tsui, and R. Fedosejevs, “Effect of ambient air pressure on debris redeposition during laser ablation of glass,” *J. Appl. Phys.*, vol. 98, no. 11, p. 113520, Dec. 2005.

[131] Y. Ye, X. Yuan, X. Xiang, X. Cheng, and X. Miao, “Laser cleaning of particle and grease contaminations on the surface of optics,” *Optik (Stuttg).*, vol. 123, no. 12, pp. 1056–1060, 2012.

[132] N. Ahmed, S. Darwish, and A. M. Alahmari, “Laser Ablation and Laser-Hybrid Ablation Processes: A Review,” *Mater. Manuf. Process.*, vol. 31, no. 9, pp. 1121–1142, 2016.

[133] M. S. Brown and C. B. Arnold, “Fundamentals of Laser-Material Interaction and Application to Multiscale Surface Modification BT - Laser Precision Microfabrication,” in *Laser Precision Microfabrication*, K. Sugioka, M. Meunier, and A. Piqué, Eds. Berlin, Heidelberg: Springer Berlin Heidelberg, 2010, pp. 91–120.

[134] M. Abend *et al.*, “Femtosecond laser-induced scratch ablation as an efficient new method to evaluate the self-healing behavior of supramolecular polymers,” *J. Mater. Chem. A*, vol. 7, no. 5, pp. 2148–2155, 2019.

[135] J. M. Lee, C. Curran, and K. G. Watkins, “Laser removal of copper particles from silicon wafers using UV, visible and IR radiation,” *Appl. Phys. A Mater. Sci. Process.*, vol. 73, no. 2, pp. 219–224, 2001.

[136] H. Huang, J. Lai, J. Lu, and Z. Li, “Pulsed laser ablation of bulk target and particle products in liquid for nanomaterial fabrication,” *AIP Adv.*, vol. 9, no. 1, 2019.

[137] A. Hu, M. Rybachuk, Q.-B. Lu, and W. W. Duley, “Direct synthesis of sp-bonded carbon chains on graphite surface by femtosecond laser irradiation,” *Appl. Phys. Lett.*, vol. 91, no. 13, p. 131906, Sep. 2007.

[138] A. Stephen and F. Vollertsen, “Mechanisms and processing limits in laser thermochemical machining,” *CIRP Ann. - Manuf. Technol.*, vol. 59, no. 1, pp. 251–254, 2010.

[139] A. Hasçalik and M. Ay, "CO_2 laser cut quality of Inconel 718 nickel - Based superalloy," *Opt. Laser Technol.*, vol. 48, pp. 554–564, 2013.

[140] L. M. Fu, W. J. Ju, R. J. Yang, and Y. N. Wang, "Rapid prototyping of glass-based microfluidic chips utilizing two-pass defocused CO_2 laser beam method," *Microfluid. Nanofluidics*, vol. 14, no. 3–4, pp. 479–487, 2013.

[141] A. Stournaras, P. Stavropoulos, K. Salonitis, and G. Chryssolouris, "An investigation of quality in CO_2 laser cutting of aluminum," *CIRP J. Manuf. Sci. Technol.*, vol. 2, no. 1, pp. 61–69, 2009.

[142] B. S. Yilbas, "Laser cutting quality assessment and thermal efficiency analysis," *J. Mater. Process. Technol.*, vol. 155–156, no. 1–3, pp. 2106–2115, 2004.

[143] H. Ogur and Y. Yoshida, "Hole drilling of glass substrates with a CO_2 laser," *Japanese J. Appl. Physics, Part 1 Regul. Pap. Short Notes Rev. Pap.*, vol. 42, no. 5 A, pp. 2881–2886, 2003.

[144] I. Kaplan, "The CO_2 Surgical Laser," *Photomed. Laser Surg.*, vol. 28, no. 6, pp. 847–848, 2010.

[145] A. Bergh, G. Nyman, T. Lundeberg, and S. Drevemo, "Effect of defocused CO_2 laser on equine tissue perfusion," *Acta Vet. Scand.*, vol. 47, no. 1, pp. 33–42, 2006.

[146] H. H. Hou, Y. N. Wang, C. L. Chang, R. J. Yang, and L. M. Fu, "Rapid glucose concentration detection utilizing disposable integrated microfluidic chip," *Microfluid. Nanofluidics*, vol. 11, no. 4, pp. 479–487, 2011.

[147] C. H. Yeh, P. W. Lin, and Y. C. Lin, "Chitosan microfiber fabrication using a microfluidic chip and its application to cell cultures," *Microfluid. Nanofluidics*, vol. 8, no. 1, pp. 115–121, 2010.

[148] C. K. Chung and S. L. Lin, "On the fabrication of minimizing bulges and reducing the feature dimensions of microchannels using novel CO_2 laser micromachining," *J. Micromechanics Microengineering*, vol. 21, no. 6, 2011.

[149] M. Riahi, "Fabrication of a passive 3D mixer using CO_2 laser ablation of PMMA and PDMS moldings," *Microchem. J.*, vol. 100, no. 1, pp. 14–20, 2012.

[150] H.-B. Liu and H.-Q. Gong, " Templateless prototyping of polydimethylsiloxane microfluidic structures using a pulsed CO_2 laser ," *J. Micromechanics*

Microengineering, vol. 19, no. 3, p. 037002, 2009.

[151] T. F. Hong, W. J. Ju, M. C. Wu, C. H. Tai, C. H. Tsai, and L. M. Fu, "Rapid prototyping of PMMA microfluidic chips utilizing a CO_2 laser," *Microfluid. Nanofluidics*, vol. 9, no. 6, pp. 1125–1133, 2010.

[152] S. Prakash and S. Kumar, "Experimental and theoretical analysis of defocused CO_2 laser microchanneling on PMMA for enhanced surface finish," *J. Micromechanics Microengineering*, vol. 27, no. 2, 2017.

[153] J. A. Lounsbury *et al.*, "From sample to PCR product in under 45 minutes: A polymeric integrated microdevice for clinical and forensic DNA analysis," *Lab Chip*, vol. 13, no. 7, pp. 1384–1393, 2013.

[154] K. Salonitis, A. Stournaras, G. Tsoukantas, P. Stavropoulos, and G. Chryssolouris, "A theoretical and experimental investigation on limitations of pulsed laser drilling," *J. Mater. Process. Technol.*, vol. 183, no. 1, pp. 96–103, 2007.

[155] C. H. Tsai, H. T. Chen, Y. N. Wang, C. H. Lin, and L. M. Fu, "Capabilities and limitations of 2-dimensional and 3-dimensional numerical methods in modeling the fluid flow in sudden expansion microchannels," *Microfluid. Nanofluidics*, vol. 3, no. 1, pp. 13–18, 2007.

[156] J. Drelich, E. Chibowski, D. D. Meng, and K. Terpilowski, "Hydrophilic and superhydrophilic surfaces and materials," *Soft Matter*, vol. 7, no. 21, pp. 9804–9828, 2011.

[157] N. F. Himma, N. Prasetya, S. Anisah, and I. G. Wenten, "Superhydrophobic membrane: Progress in preparation and its separation properties," *Rev. Chem. Eng.*, vol. 35, no. 2, pp. 211–238, 2019.

[158] T. A. Otitoju, A. L. Ahmad, and B. S. Ooi, "Superhydrophilic (superwetting) surfaces: A review on fabrication and application," *J. Ind. Eng. Chem.*, vol. 47, pp. 19–40, 2017.

[159] E. Ueda and P. A. Levkin, "Emerging applications of superhydrophilic-superhydrophobic micropatterns," *Adv. Mater.*, vol. 25, no. 9, pp. 1234–1247, 2013.

[160] C. Wang, C. Qiao, W. Song, and H. Sun, "Ultrafast Spreading Effect Induced Rapid Cell Trapping into Porous Scaffold with Superhydrophilic Surface," *ACS Appl. Mater. Interfaces*, vol. 7, no. 32, pp. 17545–17551, 2015.

[161] P. Patel, C. K. Choi, and D. D. Meng, “Superhydrophilic Surfaces for Antifogging and Antifouling Microfluidic Devices,” *JALA - J. Assoc. Lab. Autom.*, vol. 15, no. 2, pp. 114–119, 2010.

[162] M. Miwa, A. Nakajima, A. Fujishima, K. Hashimoto, and T. Watanabe, “Effects of the surface roughness on sliding angles of water droplets on superhydrophobic surfaces,” *Langmuir*, vol. 16, no. 13, pp. 5754–5760, 2000.

[163] E. Chibowski, “On some relations between advancing, receding and Young’s contact angles,” *Adv. Colloid Interface Sci.*, vol. 133, no. 1, pp. 51–59, 2007.

[164] B. Wu, M. Zhou, J. Li, X. Ye, G. Li, and L. Cai, “Superhydrophobic surfaces fabricated by microstructuring of stainless steel using a femtosecond laser,” *Appl. Surf. Sci.*, vol. 256, no. 1, pp. 61–66, 2009.

[165] D. Ahmad, I. van den Boogaert, J. Miller, R. Presswell, and H. Jouhara, “Hydrophilic and hydrophobic materials and their applications,” *Energy Sources, Part A Recover. Util. Environ. Eff.*, vol. 40, no. 22, pp. 2686–2725, 2018.

[166] S. Huang, J. Xu, C. Liang, and X. Zhang, “Size distribution measurement of packed tower drift based on hydrophobic materials,” *Appl. Therm. Eng.*, vol. 99, pp. 873–879, 2016.

[167] D. G. Waugh and J. Lawrence, “WETTABILITY CHARACTERISTICS VARIATION OF PMMA BY MEANS OF CO_2 LASER GENERATED SURFACE PATTERNS,” in *ICALEO*, 2009, vol. 102.

[168] T. Min, “Design and Fabrication of Super-Hydrophobic Surfaces By Laser Micro/Nano-Processing,” p. 142, 2012.

[169] V. D. Ta *et al.*, “Laser textured superhydrophobic surfaces and their applications for homogeneous spot deposition,” *Appl. Surf. Sci.*, vol. 365, pp. 153–159, 2016.

[170] G. Davaasuren, C. V. Ngo, H. S. Oh, and D. M. Chun, “Geometric study of transparent superhydrophobic surfaces of molded and grid patterned polydimethylsiloxane (PDMS),” *Appl. Surf. Sci.*, vol. 314, pp. 530–536, 2014.

[171] J. Kim, A. Conway, and A. Chauhan, “Extended delivery of ophthalmic drugs by silicone hydrogel contact lenses,” *Biomaterials*, vol. 29, no. 14, pp. 2259–2269, 2008.

[172] M. T. KHORASANI, H. MIRZADEH, and P. G. SAMMES, “LASER INDUCED

SURFACE MODIFICATION OF POLYDIMETHYLSILOXANE AS A SUPER-HYDROPHOBIC MATERIAL," *Radiat. Phys. Chem*, vol. 47, no. 6, pp. 881–888, 1996.

Chapter 3: Optical Glucose Sensors Based on Hexagonallypacked 2.5-dimensional Photonic Concavities Imprinted in Phenylboronic Acid Functionalized Hydrogel Films.

This chapter of the alternative format thesis is published in **RSC Advances.** The publication information and authors' contributions are provided here.

Magdalena Bajgrowicz-Cieslak, **Yousef Alqurashi,** Mohammed Elshereif, Ali K. Yetisen, Muhammad Umair Hassan and Haider Butt, "Optical glucose sensors based on hexagonally-packed 2.5-dimensional photonic concavities imprinted in phenylboronic acid functionalized hydrogel films," RSC Adv., vol. 7, no. 85, 2017

Authors Contributions

Y.A. and M.B. conceived the idea and deigned setups. **Y.A**. led the project, analysed the results, M.B. did the SEM imaging and M.E. provided the boronic acid ratio. **Y.A**. and M.B. wrote the article, H.B. supervised the project and reviewed the article. All authors reviewed the manuscript.

Abstract

Continuous glucose monitoring aims to achieve accurate control of blood glucose concentration to prevent hypo/hyperglycaemia in diabetic patients. Hydrogel-based systems have emerged as a reusable sensing platform to quantify biomarkers in high-risk patients at clinical and point-of-care settings. The capability to integrate hydrogel-based systems with optical transducers will provide quantitative and colorimetric measurements via spectrophotometric analyses of biomarkers. Here, we created an imprinting method to rapidly produce 2.5D photonic concavities in phenylboronic acid functionalized hydrogel films. Our method exploited diffraction properties of a hexagonally-packed 2.5D photonic microscale concavities having a lattice spacing of 3.3 μm. Illumination of the 2.5D hexagonally-packed structure with a monochromatic light source in transmission mode allowed reversible and quantitative measurements of variation in the glucose concentration based on first order lattice interspace tracking. Reversible covalent phenyboronic acid coupling with cis-diols of glucose molecules expanded the hydrogel matrix by ~ 2% and 34% in the presence of glucose concentrations of 1 mM and 200 mM, respectively. A Donnan osmotic pressure induced volumetric expansion of the hydrogel matrix due to increasing glucose concentrations (1-200 mM), resulted in a nanoscale modulation of the lattice interspace, and shifted the diffraction angle (~ 45° to 36°) as well as the interspacing between the 1st order diffraction spots (~ 8 to 3 mm). The sensor exhibited a maximum lattice spacing diffraction shift within a response time of 15 min in a reversible manner. The developed 2.5D photonic sensors may have application in medical point-of-care diagnostics, implantable chips, and wearable continuous glucose monitoring devices.

Keywords: Optical sensors, hydrogels, glucose sensing, phenylboronic acids, diabetes

3.1 INTRODUCOTION

Diabetes is one of the most serious health problems worldwide [1, 2]. It is a chronic disease characterized by disorder of glucose metabolism which is reflected in the elevated concentration of blood glucose [3, 4]. Health complications caused by diabetes include heart disease, kidney failure, blindness and increase in the disability-adjusted life years [5–7]. In 2015, the estimated diabetes prevalence was 415 million adults, which is projected to reach 642 million by 2040 [8]. This epidemic also poses an enormous economic burden on the society [9], the direct annual cost of diabetes to the world is more than $827 billion [10]. Appropriate medication and glucose concentration control can improve treatment efficacy by mitigating the symptoms and reducing the complications [5, 11–13]. For this reason, glucose monitoring is crucial in diabetes management.

Currently, the most common method of monitoring glucose concentration is the finger prick test which is an electrochemical method based on enzymes such as glucose oxidase, glucose dehydrogenase [14]. This procedure is inconvenient for patients, and due to being invasive, may lead to infections. Additionally, it does not allow real-time measurements and sensors cannot be reused, due to the irreversibility of reactions [15]. Moreover, the sensitivity of such electrochemical and enzymatic sensors is affected by numerous factors such as interference from the high partial pressure of oxygen, maltose and haematocrit [14, 15]. Hence, development of new continuous and non-invasive glucose monitoring system is necessary to overcome problems related to the conventional electrochemical method [16]. It is highly desirable that the new system would provide information about real-time fluctuations in blood glucose concentrations, which improves the accuracy of insulin administration in diabetes

management [17]. To date, different approaches have been investigated to achieve a complete solution [18–21]. Optical sensors seem to overcome the limitation of existing sensors since they can provide fast, quantitative, measurements in real-time and in a reversible manner [16, 22].

Recent advances in photonics and polymer chemistry have enabled the fabrication of photonic sensors on soft hydrogel materials and have led to an increased interest in hydrogel-based optical glucose sensors [15]. Hydrogels are highly water-absorbing polymers capable of undergoing reversible volume changes [23]. They can be designed to respond to certain stimuli (e.g. temperature, pH, ionic strength, metal ions, antigens, proteins) [24–30]. The selectivity is obtained by functionalizing hydrogels with receptor molecules that are sensitive to a particular stimulus or a molecule [31, 32]. One promising approach for glucose detection using hydrogels is the covalent incorporation of boronic acids in a copolymer matrix [33–37]. Boronic acids bind to diol-containing carbohydrate species, such as glucose, through a reversible boronate formation [38, 39]. Upon binding of boronic acid copolymer with glucose, the polymer network swells and alters its physical and optical properties, which can be used for glucose quantitative analyses [31, 32]. Glucose-responsive hydrogels can be incorporated into photonic devices. The inclusion of the photonic sensor into the hydrogel can help in the development of superior analytical devices. Such photonic devices work through controlling and manipulation of the propagation of light [40]. Over the last two decades, many approaches including laser writing, self-assembly, and layer-by-layer deposition have been demonstrated to create Bragg diffraction gratings, micro-lenses, etalons and plasmonic structures in hydrogels. Although no commercial device has been released yet due to unsatisfactory sensitivity and specificity issues [10].

In this paper, we have proposed a new optical glucose sensor based on a hexagonal diffraction grating imprinted on a flexible hydrogel. The fabrication method is quick and cost-effective. The sensor detected the changes (of overall ~ 8°) in the diffraction angle within 15 min due to the increasing glucose concentrations (1-200 mM), see Figure 3.1 for the schematic illustration of the concept. This change could also be detected clearly under an optical microscope - the minimum increase in the thickness of the hydrogel sensor was ~ 2% for the lowest concentration of 1mM. These 2.5D glucose sensors could be used multiple times as the detection was observed to be reversible as well as repeatable.

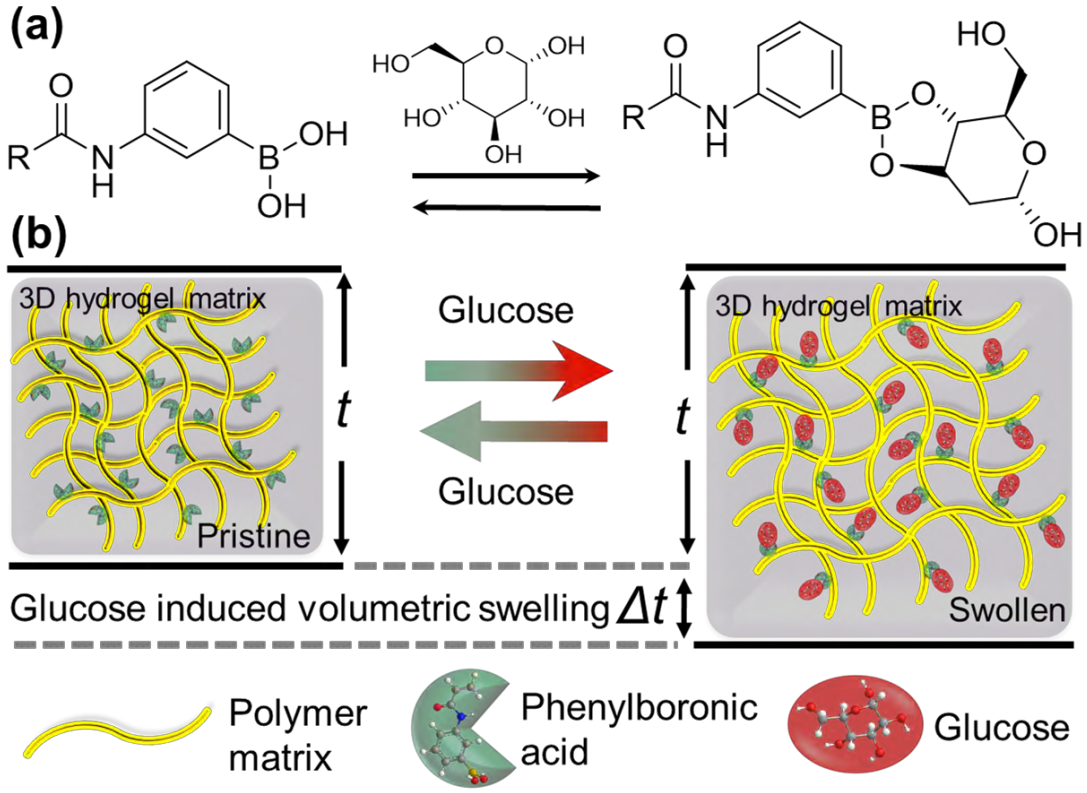

Figure 3.1: Swelling of the polyacrylamide hydrogel functionalized with 3-(acrylamido)phenyl-boronic acid, induced by the presence of glucose: (a) representation of the reversible chemical attachment of glucose at OH sites of phenylboronic acid; (b) illustration of such reversible reaction that results in a volumetric change in the boronic acid functionalized hydrogel upon glucose intake or depletion, respectively. Such volumetric modulation can be exploited for glucose sensing

3.2 METHODOLOGY

The boronic acid–diol interaction is highly pH-dependent [41]. For this reason, all measurements were conducted in phosphate-buffered saline (PBS) at a constant pH 7.4. Stock solutions of phosphate-buffered saline were prepared from PBS tablets (ThermoFisher Scientific). A high concentration glucose solution (200 mM) was prepared by dissolving D-glucose (dextrose anhydrous, Science Lab) in the PBS solution. The buffer solution containing glucose was serially diluted with the PBS to prepare various glucose concentrations in the range from 1 to 200 mM. A fresh solution was prepared for each trial and used immediately after their preparation.

A honeycomb 2.5D structure was mirror-replicated to obtain a polydimethylsiloxane (PDMS) stamp by a micro imprinting process using a honeycomb master grating [42]. The PDMS solution was prepared by mixing the PDMS base Sylgards 184 (Dow Corning) with the provided curing agent in a 10:1 (w/w) ratio and stirring the solution for 10 min at 24 °C. This solution was placed in low vacuum for 5 min to remove bubbles. The mixture was then poured on the master grating and covered with a glass slide. The sample was cured in an oven for 40 min at 60°C. The curing process solidified the PDMS, giving a mirror-replica of the parent 2.5D microstructure of the master grating for the subsequent fabrication process of the sensor, see **Error! Reference source not found.**(a-g). The micro-replication process did not damage the original 2.5D grating, such that multiple PDMS stamps could be fabricated from a single master. Subsequently, each individual PDMS stamp could be used multiple times for the preparation of glucose sensors before it starts showing some degrading.

Acrylamide, N,N'-methylenebisacrylamide, 3-(acrylamido)phenylboronic acid (PBA), dimethyl sulfoxide (DMSO) and 2,2-dimethoxy-2-phenylacetophenone (DMPA) were used as core components of our glucose sensitive hydrogel (GSH): Acrylamide (78.5 mol%), N,N'-methylenebisacrylamide (1.5 mol%) and (PBA) (20 mol%) were mixed together. A solution of 2% (w/v) DMPA in DMSO was added to the mixture at a ratio 1:1 (v/v). Subsequently, this mixture was stirred very well (120 min, at room temperature) in order to ensure good homogeneity. The resulting mixture was poured directly onto the PDMS stamp and covered with a glass slide. The thickness of the sample was controlled by controlling the space gap between glass slides by placing a fine shim of a known thickness. The sample was then moved to an ultraviolet (UV) curing chamber and cured with UV light for 5 min. Then, it was kept in DI water for 5 min and peeled off – hydrophobic nature of the surface of the PDMS stamps facilitates an easily peeling off process. Mirror-replication of the 3D structure copied from the PDMS stamp onto the GSH results in copying of the original structure of the hexagonal 2.5D master grating, see **Error! Reference source not found.**(h). All samples were hydrated overnight in deionized (DI) water before further use.

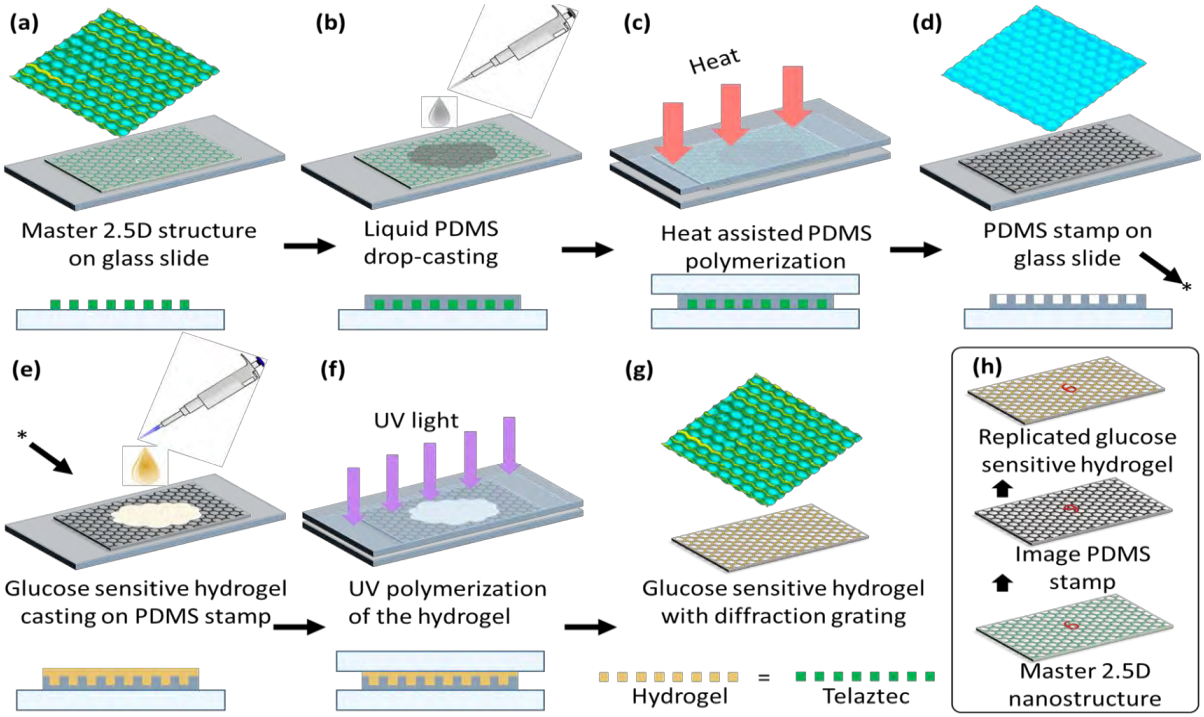

Figure 3.2: Schematic illustration of imprinting the micrograting on the glucose sensitive hydrogel: (a-d) preparation of PDMS stamp; (e-g) copying the structure from PDMS stamp on a glucose sensitive material; (h) summary of the replication process

The surface of 2.5D grating, PDMS and GSH were imaged by a scanning electron microscope (SEM) (JCM-6000PLUS NeoScope Benchtop). Before imaging, samples were coated with a gold layer (5–10 nm) using Agar sputter coater, to avoid charging effects – specimens being highly dielectric in nature result in charge accumulation and subsequently poor resolution. SEM images show that the hexagonal structure of the 2.5D mimics the true honeycomb architecture, such that the pits with certain depth covered with elevated walls around them form hexagonal cells, with an average cell constant of ~ 3.0 ± 0.3 μm and depth (/height) of ~ 1.2 μm. The mirror replication of this structure on PDMS is a conjugate fit, i.e. domes replace the pits in the mirror-replication process, and the walls in the original structure are now the deeper parts of the replica. The GHS copied from the PDMS stamp again results in the original 2.5D honeycomb (hexagonal) structure, see **Error! Reference source not**

found.(a-c). All three specimens exhibit perfect surface morphology with almost no defects suggesting a perfect copying from the 2.5D grating to the PDMS stamp and subsequently from the stamp to the GHS sensor.

The volumetric change of the GSH in the presence of glucose is also one way of measuring the glucose content in solutions, optical microscopy (Axio scope A1, Zeiss) was performed in order to determine the thickness of the pristine sample and in different conditions (after exposing to different glucose concentrations, discussed latter). We obtained the cross-section thickness of ~ 221 μm for a dry pristine GSH sensor.

Angle-resolved far-field diffraction experiment were carried out using original 2.5D grating, PDMS and GSH samples, see **Error! Reference source not found.**(d) for schematic illustration of the experiment. The sample was carefully placed in a transparent plastic cuvette, mounted on a motorized precision rotation stage and aligned normal to the incident laser beam. The intensity of each diffracted beam was measured using an image-screen place at a distance of 45 cm away from the sample, as well as, by using an optical power meter (Newport, 1918-R) traversable on a circular rail (CR) of radius of 13 cm with sample mount on its centre (the radius of CR also defines the measurement distance between the sample and the power meter). Three laser sources, red, green and blue (640, 532 and 491 nm) (Newport) were used in diffraction experiments. Measurements were recorded in dry (pristine) and soaked conditions (in PBS solution). In order to perform glucose sensing, the cuvette was filled with different solutions and the whole sample was submerged before taking the measurement. The forward-scattered spectra were collected in all cases either by rotating the cuvette or the detector itself by an increment of 1°, from 0° to 180°, relative to the sample normal. For the reference, the

intensity/power of the incident light (blank) was also recorded and percentage of the diffracted intensity for each diffraction spot was calculated. A simple method was adopted to record the glucose induced shift in the spectra: the change in the displacement between two opposite 1st order points such that the displacement line should pass through the centre (0-order) of the diffraction pattern was recorded as a function of glucose concentration. Photographs of the diffracted spectra taken on an imaging screen were also analysed with ImageJ software, and diffraction efficiency (intensity) was plotted against 1st-1st order interspace and diffraction angle.

Photographs of the master grating, PDMS and GSH took in white light revealed their diffractive properties as colors present in the incident light were resolved over space, see **Error! Reference source not found.**(e-i) for photographs of all three samples along with computationally calculated Fourier transforms (FT) of their microscopic images revealing their hexagonal architecture. **Error! Reference source not found.**(k-m) shows an example of experimentally obtained diffraction from the PDMS stamp, whereas a reverse FT can be exploited to redraw the physical structure where the light originally diffracts from. We plotted angle-resolved diffracted intensities normalize (to 1) for up to 3rd diffraction orders as the function the diffraction angle for the original 2.5D grating and PDMS stamp in **Error! Reference source not found.**(o-u). The 0-order peak was the strongest in both cases suggesting that most of the light was transmitted straight to the 0 order without being diffracted: blue, green and red illumination resulted in 0-order intensities of 29, 35 and 40% for 2.5D grating, and 16, 28 and 41% for the PDMS stamp, respectively. Intensities of increasing orders (1st, 2nd etc.) decreased with the increasing order number. Consistent with 0-order, a slight difference in diffracted intensities (e.g. for the 1st order) was also observed between both samples: blue, green and red illumination resulted in 1-order intensities of 3.2, 2.9 and 2.7%

for 2.5D grating, and 7.7, 6.8 and 6.2% for the PDMS stamp, respectively. Notice that the light distribution in diffraction depends on the incident wavelength. For shorter wavelengths, lesser transmission to the 0-order meant a stronger diffraction, such that the light was distributed more among the subsequent orders, whereas for longer wavelengths, more light was transmitted to the 0-order without being diffracted. Angle-resolved measurements confirmed that the diffraction angles for original 2.5D grating and PDMS replica were identical. The diffraction angles between normal and 1st-order peaks for different lasers, blue, red and green were 10°, 13° and 16°, respectively, consistent with the Bragg's law.

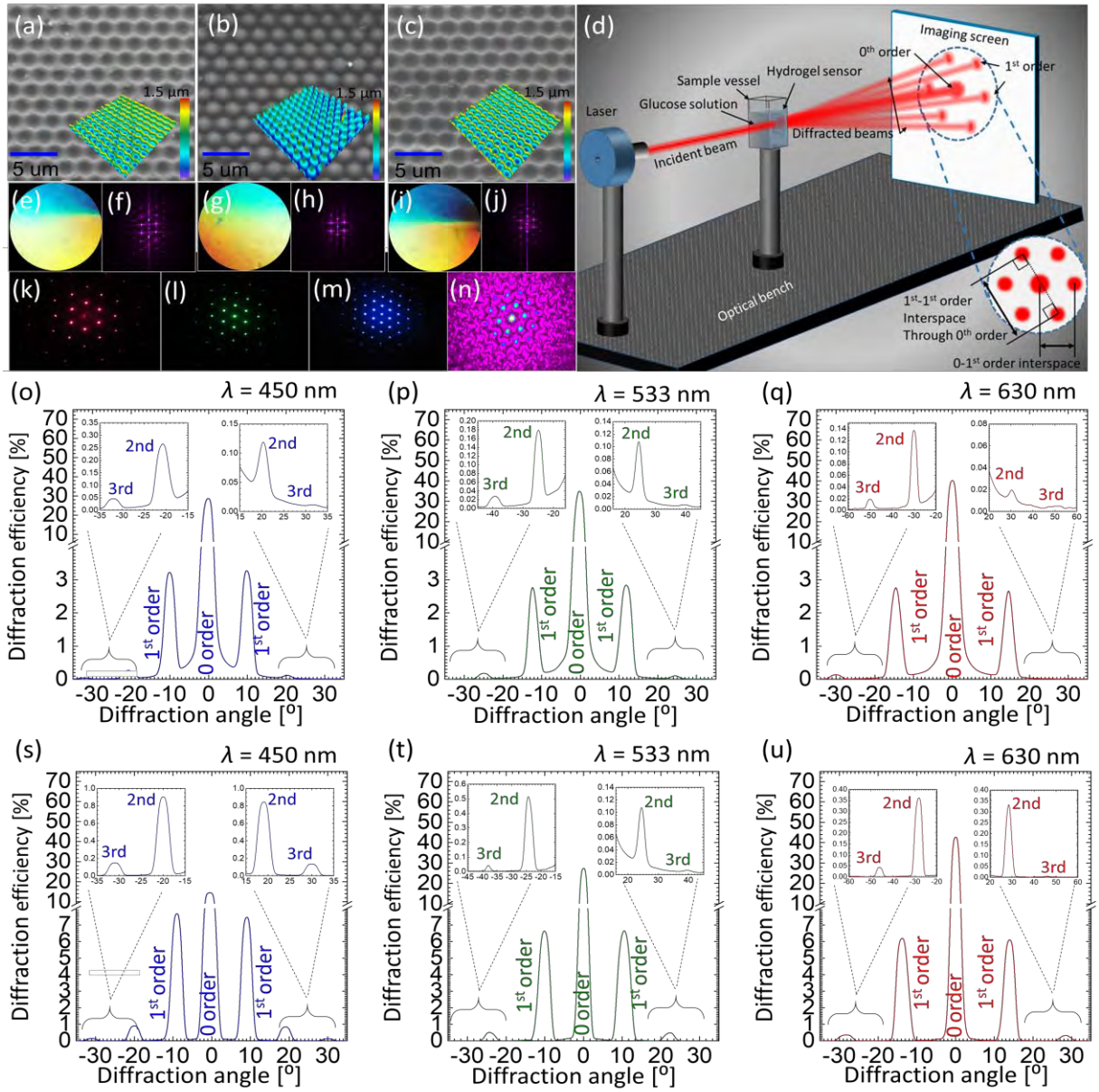

Figure 3.3: Characteristics of the original and copied honeycomb micostructures: (a-c) SEM images of the 2.5D master structure, PDMS stamp, and glucose sensitive sample, (d) Schematic illustration of optical measurement setup; (e-j) photographs taken in white-light for the surfaces of 2.5D sample, PDMS stamp and glucose sensitive sample and theoretical picture of their Fourier transforms, respectively; (k-m) Diffraction patterns generated by red, green and blue laser light transmitted through the original glucose sensitive sample; (n) Reconstruction of the glucose sensitive sample image by taking Fourier transform of the pattern itself obtained from the patterned hydrogel; (o-q) angle-resolved intensity graphs representing diffraction patterns generated by the 2.5D sample illuminated by the light of blue, green and red laser; (s-u) angle-resolved intensity graphs representing diffraction patterns generated by PDMS stamp illuminated by the light of blue, green and red laser

3.3 RESULTS AND DISCUSSION

Angle-resolved diffraction measurements were carried for the GSH in its dry and wet conditions, Figure 3.4. This was done before carrying out the glucose sensing experiment as hydrophobic nature of sensing material's resulted in an initial swelling that needed be taken into account beforehand in order to perform an error-free measurement. When the sample was soaked in PBS, it absorbed the liquid and swelled in all 3 dimensions. During the analysis, two main observations were made in the behavior of diffraction patterns: firstly, the intensity (efficiency) of the transmitted light dropped significantly when the sample was wet. For dry (wet) condition, the efficiency of 0-order spot was 64 (32), 63 (28) and 58% (34%) for blue, green and red lasers, respectively. The decrease in efficiency in the wet condition can be explained by Beer-Lambert Law, which states that increasing the thickness of the material in which light is traveling, decreases the light transmission. As soon as the sample underwent the initial swelling as the result of absorbed PBS solution, more light was absorbed by the swollen material. Secondly, the diffraction angle of the transmitted laser light decreased when the sample was in its wet condition. Diffraction angles between 1st-order spots generated by the dry (wet) sample were ~ 10° (8°), 14° (11°) and 16° (12°) for blue, green and red lasers. By the same token, the distance between 1st-order diffraction points projected on the image screen also decreased. The reason for such negative shift of the diffraction angle is the increase in the gap size (groove constant) of the micro-grating imprinted on the hydrogel.

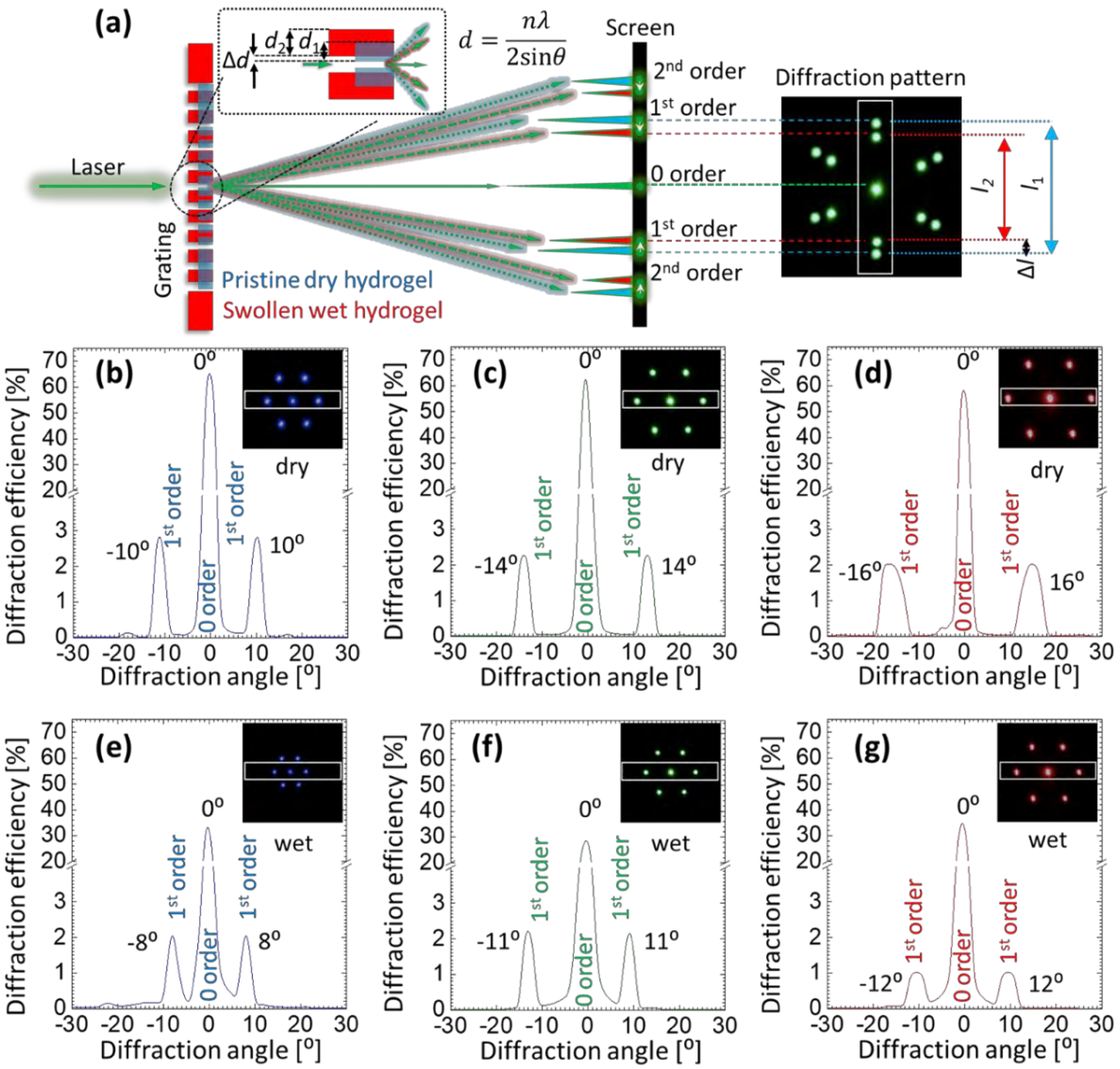

Figure 3.4 (a) Schematic illustration explaining how the volumetric change of a hydrogel influences the diffraction angle (θ) of the transmitted light by changing the groove constant of the microctructure on the surface; (b-g) angle-resolved intensity graphs of the transmitted light from the GSH in dry and wet conditions. Insets show the photographs of the diffraction patterns taken on the imaging screen. The images were obtained in transmission mode by illuminating the dry and wet samples with blue, green and red lasers, respectively

Absorption of PBS by the hydrogel sample resulted in its three-dimensional expansion, thereby, expanded the surface and the features present on the surface. According to the Braggs equation, nλ = 2dsinθ, where, n is the diffraction order, d is the groove constant, and θ is the diffraction angle, the observed shift in the diffraction pattern can be explained. Therefore,

volumetric change of the hydrogel material was detected by analyzing the changes in the diffraction pattern generated by the light transmitted through the grating imprinted on the sample. Also, it was established that the resolution of the sensor strongly depended on the wavelength of the laser light that illuminated the sample. Red laser resulted in better resolvable measurements as compared to the shorter wavelengths.

For glucose sensing, angle-resolved diffraction measurements were carried out in far-field by normally illuminating the GSH grating sensor with a green laser and recording the diffraction pattern on an imaging screen located at a distance of 45 cm away from the sensor, see Figure 3.5(a) for the snapshots of the 1st order interspace taken for increasing glucose concentration. Increasing glucose concentration can be appreciated by noticing a negative shift in the diffraction angle/1st-order interspace resulted by increasing groove constant of the illuminated GSH structure. Such observation is reversible, that is, the diffraction angle increased or decreased due to the shrinking or swelling of the grating upon exposing the same sensor to low or high glucose concentrations, respectively. Figure 3.5(b) shows the diffraction efficiency versus diffraction angle (between 0 and 1st-order) after the sensor was soaked in different solution of different glucose concentrations for 1 hr. When the sample was soaked in PBS (without glucose) the diffraction angle was ~ 28°. Subsequently, after removing the PBS solution, different glucose solutions were added one by one to examine their effect on the diffraction pattern – the diffraction angle decreased due to the increasing sensor size with a maximum change of ~ 8° for 200 mM glucose solutions. In this experiment, the lowest concentration that could be detected accurately was ~10 mM, for which the change in the 1st-order interspace was ~ 3 mm (diffraction angle ≈ 0.3°), compared with the PBS-soaked condition. However, this value of sensitivity could be improved considerably by refining

various experimental parameters, such as the laser spot size, distance between the GSH and the imaging plate and, using a more precise rotation stage.

Response time is a parameter that determines how fast does the sensor work. It is important because a quick real-time capture of the change in sugar level leads to a better treatment/management. Figure 3.5(d) represents the change in the angle over time for the 100 mM glucose concentration solution. Within first 10 min, a rapid change was observed, that moved towards the saturation at ~ 15 min, the change after 15 min was negligible. It is important to note that it is not only the interspace that could be translated to different concentrations, the time slope for different glucose concentration is also different. Therefore, the change in glucose concentration can also be measured well before 15 min by measuring the slope of the interspace-time curve. Other studies suggest that the sensors may take over 1 hr to respond [43]. In this work, we have demonstrated much faster response time as compared with previous studies. Further improvement in the response time can be achieved by using a thin GSH grating or/and a more responsive phenylboronic acid (however, this is the subject of a separate report).

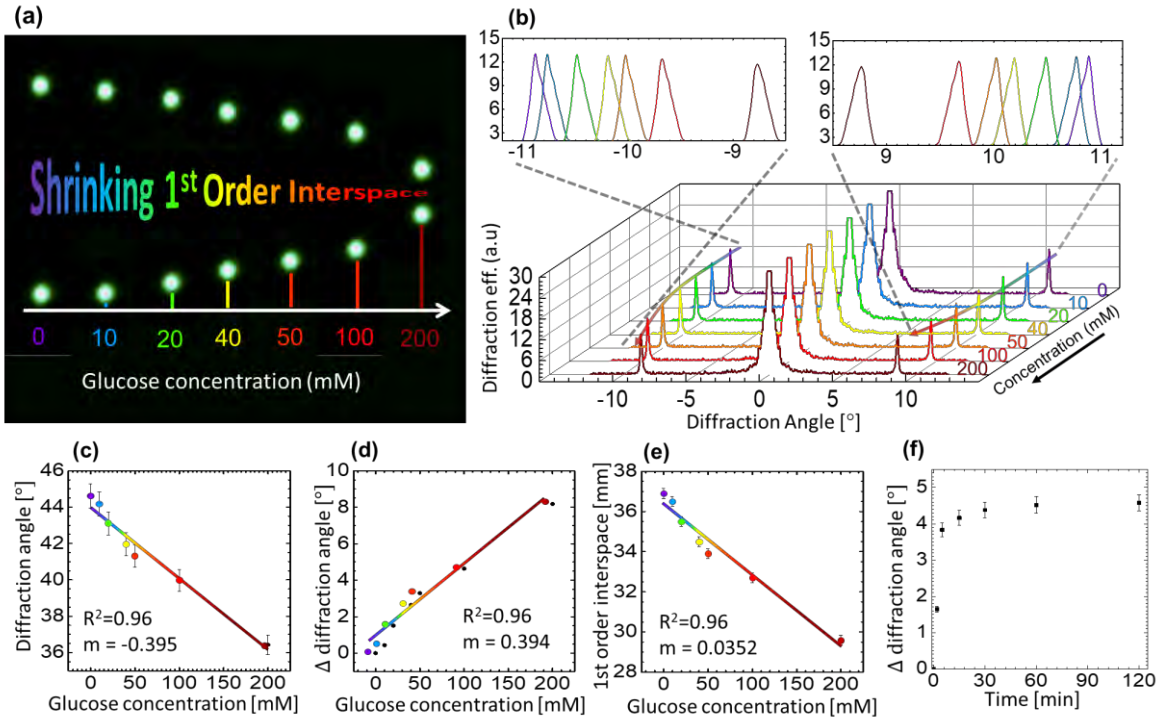

Figure 3.5: Optical sensing of glucose using GSH sensor: (a) photograph of the interspace between 1st-order points changing due to increasing glucose concentration (0-order is masked); (b-d) the change in diffraction angle of the 1st-order with increasing glucose concertation; (e) the change in the interspace of the 1st-order with increasing glucose concentration; (f) time-response of the sensor – measurements to record the change in the diffraction angle for 100 mM glucose level with time.

A thin slice was cut off the GSH sample and placed under the microscope to measure its thickness and its direct response to different glucose concentrations. The slice was placed vertically between two small glass slides and adjusted on a transparent petri dish. Then, the buffer solution of 7.4 pH was poured into the dish in order to measure the initial increase in the thickness, that is, in the presence of the buffer reference. The initial thickness of the sample without glucose was ~ 305 µm. Subsequently, the sample was soaked in different glucose solutions. With increasing glucose concentration, thickness increased, see Figure 3.6(a). The lowest detectable glucose concentration was 1 mM. For this concentration, the thickness increased by ~ 7 µm, which is ~ 2% of the initial thickness. At 200 mM, the thickness increased

by ~ 34%. A linear correlation was found between the cross-section thickness and glucose concentration at low concentrations, that is, within the range between 1 to 10 mM, see Figure 3.6(b-d). Notice that the said range is actually the physiological range and could be useful in sensing application. Extension of this work to measure the blood or urine glucose concentration are the subject our next report. It suggests that the swelling process is uniform in all 3 dimensions: from microscopic images, comparing the change in the thickness in z-axis with the change in the x-y plane extracted from the diffraction angle measurements, a linear correlation between the change in thickness and the change in the diffraction angle is obtained, see Figure 3.6(e).

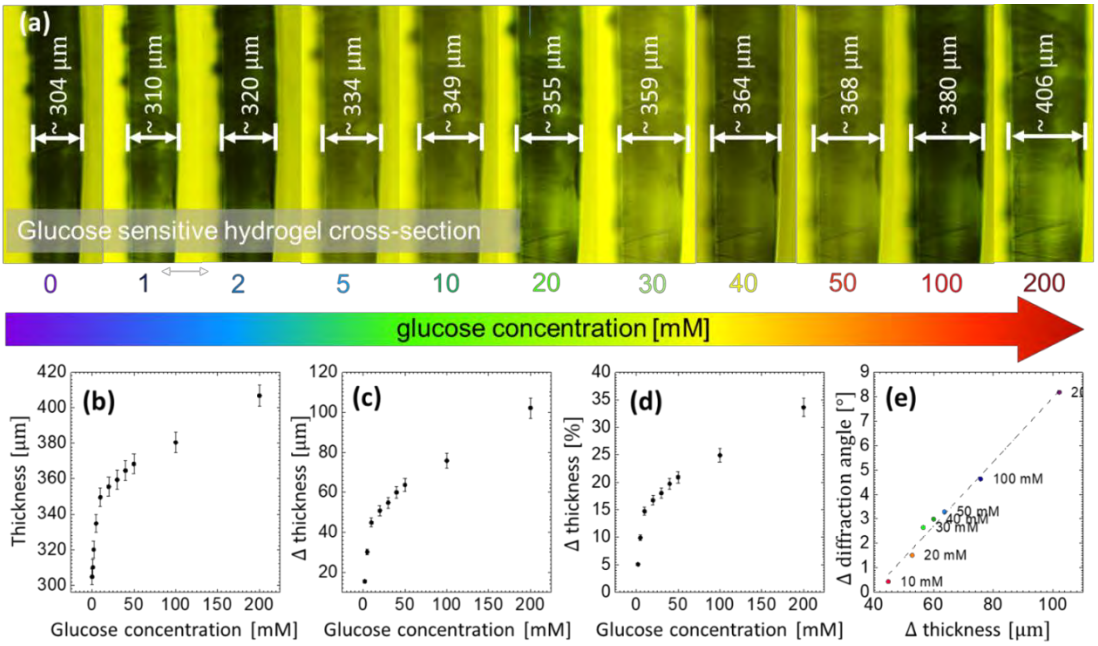

Figure 3.6: Glucose sensing via direct measurements of the dimensions (thickness) of the GSH: (a) The volumetric change of the sample in the presence of glucose at different concentration; (b-d) the change in the thickness for glucose concentration from 0 to 200 mM; (e) the correlation between the change in the diffraction angle and the change in the thickness

Although the thickness measurements gave a better resolution as compared with the optical measurements due to our experimental limitations below 10 mM, there is considerable room to refine the diffraction experiments for much higher resolution. The difficulties of

detecting the change in the diffraction angle for low concertation can be overcome by using small feature size of the diffraction grating, using longer laser wavelength and decreasing the spot size. More responsive (larger swelling coefficient) phenylboronic acids for larger glucose modulated changes in the imprinted patterns can also be used for enhanced sensitivity and improved selectively, such as 2-(acrylamido)phenylboronate, bisboronic acid, and 4-vinylphenylboronic acid [33, 41, 44, 45]. Increasing the surface area by making the nanoporous structures and introducing a gating membrane have also been proven to increase the analyte diffusion and rate of complexation [46]. Borrowing the similar techniques from previous studies can also help improving the performance of our proposed glucose sensor. Table 3.1 highlights some of the recent strategies employed to monitor glucose concentration and their challenges as compared to the standard electrochemical method. Optical detection of glucose can lead to an alternative way to the non-invasive, continuous glucose monitoring in a point-of-care setting for diabetic and non-diabetic patients in near future.

Table 3.1: Examples of different types of glucose sensors.

Type/Work Principle	Readout	Range	Advantages	Drawbacks	Ref.
Electrochemical: Measures Electrochemical potential between electrodes	Voltage vs. glucose concentration	10-1000 μM	It is capable of doing single cell measurements, Commercial use	Suffers signal bias and day to day drift	[14, 20]
Raman spectroscopic detection: Probes vibronic properties of the materials	Raman peak shift vs. glucose concentration	2-6 mM	Medium range sensitivity	Raman spectroscopy setup needed.	[47]
Holographic 2 and 3D sensors:	Colorimetric change vs glucose concentration	100 μM-100 mM	Medium range sensitivity, can be made for non-invasive use	Complex phenylboronic acid synthesis, slower response rate	[22, 29, 48]
Photonic crystal: Based on Bragg scattering					[15, 22, 29, 40]
Imprinted 1D	1 order diffraction peak; measures in 1st order interspace (angle/separation) vs. glucose concentration		Medium range sensitivity, can be made for non-invasive use Easy synthesis	Slower response rate	Present work

3.4 CONCLUSION

We have demonstrated a new glucose sensor based on a physically patterned glucose responsive hydrogel. The hydrogel was based on poly-acrylamide, N,N'-methylenebisacrylamide polymerized with a phenylboronic acid, 3-(acrylamido)phenylboronic acid. The patterning was carried out by micro-imprinting of a hexagonal structure from PDMS mirror-replica of a 2.5D honeycomb grating. Sensing was done by carrying out optical diffraction measurements from the patterned hydrogel surface in the presence of different glucose concentration. Glucose binding with phenylboronic acid resulted in physical swelling of the hydrogel, which led to the expansion of the sensor's surface imprinted with micro-patterns. This change in the Bragg diffraction was measured in a far-field transmission configuration. A clear modulation of the 1st-order interspace against varying glucose concentration was recorded. Direct observation of glucose-induced swelling of the hydrogel was carried under an optical microscope. A linear relationship between the surface and volume expansions was established. A minimum glucose concentration of 1 mM was successfully recorded suggesting the sensor's usability in physiological conditions. We demonstrated that the fabrication of such sensors is quick and cost-effective as compared to its conventional counterparts, and it is suitable for the mass production.

ACKNOWLEDGEMENTS

This work was supported by the Leverhulme Trust (RF-2016-039) and the Wellcome Trust (201929/Z/16/Z).

REFERENCES

[1] S. A. Tabish, "Is Diabetes Becoming the Biggest Epidemic of the Twenty-first

Century?," *Int. J. Health Sci. (Qassim).*, vol. 1, no. 2, pp. V–VIII, 2007.

[2] P. Lefèbvre and A. Pierson, "The global challenge of diabetes.," *World Hosp. Health Serv.*, vol. 40, no. 3, pp. 37-40,42, 2004.

[3] R. A. Defronzo, E. Ferrannini, H. Keen, and P. Zimmet, *International Textbook of Diabetes Mellitus*. Wiley-Blackwell, 2015.

[4] "Classification and diagnosis of diabetes mellitus and other categories of glucose intolerance. National Diabetes Data Group.," *Diabetes*, vol. 28, no. 12, pp. 1039–1057, 1979.

[5] G. Danaei, C. M. M. Lawes, S. Vander Hoorn, C. J. L. Murray, and M. Ezzati, "Global and regional mortality from ischaemic heart disease and stroke attributable to higher-than-optimum blood glucose concentration: comparative risk assessment," *Lancet*, vol. 368, no. 9548, pp. 1651–1659, 2006.

[6] G. Danaei *et al.*, "National, regional, and global trends in fasting plasma glucose and diabetes prevalence since 1980: systematic analysis of health examination surveys and epidemiological studies with 370 country-years and 2·7 million participants," *Lancet*, vol. 378, no. 9785, pp. 31–40, 2011.

[7] G. M. Singh *et al.*, "The Age-Specific Quantitative Effects of Metabolic Risk Factors on Cardiovascular Diseases and Diabetes: A Pooled Analysis," *PLoS One*, vol. 8, no. 7, p. e65174, 2013.

[8] L. Guariguata, D. Whiting, C. Weil, and N. Unwin, "The International Diabetes Federation diabetes atlas methodology for estimating global and national prevalence of diabetes in adults," *Diabetes Res. Clin. Pract.*, vol. 94, no. 3, pp. 322–332, 2011.

[9] J. M. Evans, R. W. Newton, D. A. Ruta, T. M. MacDonald, and A. D. Morris, "Socio-economic status, obesity and prevalence of Type 1 and Type 2 diabetes mellitus.,"

Diabet. Med., vol. 17, no. 6, pp. 478–480, 2000.

[10] R. V Kuranov, V. V Sapozhnikova, D. S. Prough, I. Cicenaite, and R. O. Esenaliev, "Prediction capability of optical coherence tomography for blood glucose concentration monitoring.," *J. Diabetes Sci. Technol.*, vol. 1, no. 4, pp. 470–477, 2007.

[11] R. B. McQueen, S. L. Ellis, J. D. Campbell, K. V Nair, and P. W. Sullivan, "Cost-effectiveness of continuous glucose monitoring and intensive insulin therapy for type 1 diabetes.," *Cost Eff. Resour. Alloc.*, vol. 9, p. 13, 2011.

[12] E. S. Huang *et al.*, "The Cost-Effectiveness of Continuous Glucose Monitoring in Type 1 Diabetes," *Diabetes Care*, vol. 33, no. 6, pp. 1269–1274, 2010.

[13] D. C. and C. T. R. Group *et al.*, "The Effect of Intensive Treatment of Diabetes on the Development and Progression of Long-Term Complications in Insulin-Dependent Diabetes Mellitus," *N. Engl. J. Med.*, vol. 329, no. 14, pp. 977–986, 1993.

[14] K. Tonyushkina and J. H. Nichols, "Glucose Meters: A Review of Technical Challenges to Obtaining Accurate Results," *J. Diabetes Sci. Technol.*, vol. 3, no. 4, pp. 971–980, 2009.

[15] A. K. Yetisen *et al.*, "Photonic hydrogel sensors," *Biotechnol. Adv.*, vol. 34, no. 3, pp. 250–271, 2016.

[16] C. K. Ho, A. Robinson, D. R. Miller, and M. J. Davis, "Overview of Sensors and Needs for Environmental Monitoring," *Sensors (Basel).*, vol. 5, no. 2, p. 4, 2005.

[17] D. C. Klonoff, "Continuous Glucose Monitoring," *Diabetes Care*, vol. 28, no. 5, 2005.

[18] M. Shichiri, Y. Yamasaki, R. Kawamori, N. Hakui, and H. Abe, "WEARABLE ARTIFICIAL ENDOCRINE PANCREAS WITH NEEDLE-TYPE GLUCOSE SENSOR," *Lancet*, vol. 320, no. 8308, pp. 1129–1131, 1982.

[19] E. F. Pfeiffer, “The glucose sensor: the missing link in diabetes therapy.,” *Horm. Metab. Res. Suppl.*, vol. 24, pp. 154–164, 1990.

[20] K. ul Hasan *et al.*, “A Miniature Graphene-based Biosensor for Intracellular Glucose Measurements,” *Electrochim. Acta*, vol. 174, pp. 574–580, 2015.

[21] S. Garg *et al.*, “Improvement in Glycemic Excursions With a Transcutaneous, Real-Time Continuous Glucose Sensor,” *Diabetes Care*, vol. 29, no. 1, 2005.

[22] Y. Zhao, Z. Xie, H. Gu, C. Zhu, and Z. Gu, “Bio-inspired variable structural color materials,” *Chem. Soc. Rev.*, vol. 41, no. 8, p. 3297, 2012.

[23] A. Bin Imran, T. Seki, and Y. Takeoka, “Recent advances in hydrogels in terms of fast stimuli responsiveness and superior mechanical performance,” *Polym. J.*, vol. 42, pp. 839–851, 2010.

[24] A. Sidorenko, T. Krupenkin, A. Taylor, P. Fratzl, and J. Aizenberg, “Reversible switching of hydrogel-actuated nanostructures into complex micropatterns.,” *Science*, vol. 315, no. 5811, pp. 487–490, 2007.

[25] A. M. Kloxin, A. M. Kasko, C. N. Salinas, and K. S. Anseth, “Photodegradable Hydrogels for Dynamic Tuning of Physical and Chemical Properties,” *Science (80-.).*, vol. 324, no. 5923, 2009.

[26] J. D. Ehrick, S. K. Deo, T. W. Browning, L. G. Bachas, M. J. Madou, and S. Daunert, “Genetically engineered protein in hydrogels tailors stimuli-responsive characteristics,” *Nat. Mater.*, vol. 4, no. 4, pp. 298–302, 2005.

[27] M. Ehrbar, R. Schoenmakers, E. H. Christen, M. Fussenegger, and W. Weber, “Drug-sensing hydrogels for the inducible release of biopharmaceuticals,” *Nat. Mater.*, vol. 7, no. 10, pp. 800–804, 2008.

[28] L. Dong, A. K. Agarwal, D. J. Beebe, and H. Jiang, “Adaptive liquid microlenses activated by stimuli-responsive hydrogels.,” *Nature*, vol. 442, no. 7102, pp. 551–554, 2006.

[29] Z. Cai, N. L. Smith, J.-T. Zhang, and S. A. Asher, “Two-Dimensional Photonic Crystal Chemical and Biomolecular Sensors,” *Anal. Chem.*, vol. 87, no. 10, pp. 5013–5025, 2015.

[30] E. F. Banwell *et al.*, “Rational design and application of responsive ?-helical peptide hydrogels,” *Nat. Mater.*, vol. 8, no. 7, pp. 596–600, 2009.

[31] D. Buenger, F. Topuz, and J. Groll, “Hydrogels in sensing applications,” *Prog. Polym. Sci.*, vol. 37, no. 12, pp. 1678–1719, 2012.

[32] E. A. Appel, J. del Barrio, X. J. Loh, and O. A. Scherman, “Supramolecular polymeric hydrogels,” *Chem. Soc. Rev.*, vol. 41, no. 18, pp. 6195–6214, 2012.

[33] R. Nishiyabu, Y. Kubo, T. D. James, and J. S. Fossey, “Boronic acid building blocks: tools for sensing and separation,” *Chem. Commun.*, vol. 47, no. 4, p. 1106, 2011.

[34] Y. Guan and Y. Zhang, “Boronic acid-containing hydrogels: synthesis and their applications,” *Chem. Soc. Rev.*, vol. 42, no. 20, p. 8106, 2013.

[35] S. Gamsey, J. T. Suri, Ritchie A. Wessling, and B. Singaram, “Continuous Glucose Detection Using Boronic Acid-Substituted Viologens in Fluorescent Hydrogels: Linker Effects and Extension to Fiber Optics,” *Am. Chem. Soc.*, vol. 22, no. 21, pp. 9067–9074, 2006.

[36] M. M. Finucane, C. J. Paciorek, G. Danaei, and M. Ezzati, “Bayesian Estimation of Population-Level Trends in Measures of Health Status,” *Stat. Sci.*, vol. 29, no. 1, pp. 18–25, 2014.

[37] Y. Dong *et al.*, “Injectable and Glucose-Responsive Hydrogels Based on Boronic Acid-Glucose Complexation.,” *Langmuir*, vol. 32, no. 34, pp. 8743–8747, 2016.

[38] H.-C. Wang and A.-R. Lee, “Recent developments in blood glucose sensors,” *J. Food Drug Anal.*, vol. 23, no. 2, pp. 191–200, 2015.

[39] K. Lacina, P. Skládal, and T. D. James, “Boronic acids for sensing and other applications - a mini-review of papers published in 2013.,” *Chem. Cent. J.*, vol. 8, no. 1, p. 60, 2014.

[40] E. Yablonovitch, “Photonic crystals: semiconductors of light.,” *Sci. Am.*, vol. 285, no. 6, pp. 47-51,54-55, 2001.

[41] X. Wu, Z. Li, X.-X. Chen, J. S. Fossey, T. D. James, and Y.-B. Jiang, “Selective sensing of saccharides using simple boronic acids and their aggregates,” *Chem. Soc. Rev.*, vol. 42, no. 20, p. 8032, 2013.

[42] A. K. Yetisen *et al.*, “Color-Selective 2.5D Holograms on Large-Area Flexible Substrates for Sensing and Multilevel Security,” *Adv. Opt. Mater.*, vol. 4, no. 10, pp. 1589–1600, 2016.

[43] Y. Takeoka and M. Watanabe, “Polymer Gels that Memorize Structures of Mesoscopically Sized Templates. Dynamic and Optical Nature of Periodic Ordered Mesoporous Chemical Gels,” *Langmuir*, vol. 18, no. 16, pp. 5977–5980, 2002.

[44] W. Zhai, X. Sun, T. D. James, and J. S. Fossey, “Boronic Acid-Based Carbohydrate Sensing,” *Chem. – An Asian J.*, vol. 10, no. 9, pp. 1836–1848, Sep. 2015.

[45] X. Yang, M.-C. Lee, F. Sartain, X. Pan, and C. R. Lowe, “Designed Boronate Ligands for Glucose-Selective Holographic Sensors,” *Chem. – A Eur. J.*, vol. 12, no. 33, pp. 8491–8497, Nov. 2006.

[46] Q. Zhang, B. Chen, L. Tao, M. Yan, L. Chen, and Y. Wei, "Microorganism inspired hydrogels: hierarchical super/macro-porous structure, rapid swelling rate and high adsorption," *RSC Adv.*, vol. 4, no. 61, pp. 32475–32481, 2014.

[47] V. K. Gupta *et al.*, "A novel glucose biosensor platform based on Ag@AuNPs modified graphene oxide nanocomposite and SERS application," *J. Colloid Interface Sci.*, vol. 406, pp. 231–237, 2013.

[48] A. K. Yetisen, I. Naydenova, F. da Cruz Vasconcellos, J. Blyth, and C. R. Lowe, "Holographic Sensors: Three-Dimensional Analyte-Sensitive Nanostructures and Their Applications," *Chem. Rev.*, vol. 114, no. 20, pp. 10654–10696, Oct. 2014.

Chapter 4: Optical Hydrogel Detector for pH Measurements.

This section of the alternative format thesis is submitted to **Sensors Journal.** The submission details and authors' contributions are provided here.

Yousef Alqurashi, Mohamed Elsherif, Asail Hendi, Khamis Essa, Haider Butt, "Optical hydrogel detector for pH measurements"

Authors Contributions

Y.A. and H.B conceived the idea and deigned setups. **Y.A.** led the project, and analysed the results, A.H. carried out the hydrogel copying process. **Y.A.** and A.H. performed the measurements and took the microscopic images. **Y.A**. wrote the article and H.B. supervised the project and reviewed the article. All authors reviewed the manuscript.

ABSTRACT

Measuring pH has become a major key for determining health conditions, and food safety. The traditional pH assessment approaches are costly and offer low sensitivity. Here, a novel pH hydrogel-based sensor has been developed. A Fresnel lens pattern was replicated on the surface of a pH-responsive hydrogel using replica mold method. The pH-responsive hydrogel is based on hydroxyethyl methacrylate (HEMA). Free standing and substrate attached hydrogel sensors were fabricated. The pH-sensors were tested in pH range of 4 – 7. Introducing various pH solutions to the pH-sensor led to volumetric shifts as the hydrogel swelled with pH. Subsequently, the dimensions of the replicated Fresnel lens changed modifying the focal lens and the focus efficiency of the optical sensor. As a result, the measured optical power at a fixed distance from the sensor changed with pH. The optical sensor showed the best performance in the acidic region when pH changed from 4.5 to 5.5 in which the recorded power increased by 7% in the first day and 13% after storing the sensor for 7 days. Microscopic images of the optical sensor were taken while the sensor was immersed in various pH solutions for understanding the working principle. The effect of the temperature on the sensor's performance was studied, and a negligible interference resulting from the temperature changes (20° – 40°) was recorded. The sensor exhibited sensitivity to pH changes with respond time within minutes in a reversible manner. The developed pH-optical sensor may have applications in medical point-of-care diagnostics, and wearable continuous pH detection devices.

KEYWORDS: Fresnel lens, hydrogel, hydroxyethyl methacrylate, pH-monitoring

4.1 INTRODUCOTION

Heart disease is a chronic condition which continues to be the primary cause of death in Europe [1]. Improved treatment methods for such disorders have been under review. Monitoring the changes in pH of blood is one way to prevent many fatal implications [2, 3]. Measuring pH has become a major signal for determining health conditions, and food safety. In food quality applications, variations in pH are generally correlated with bacteria growth and colonisation. In human blood, increasing the pH level than the normal range (7.35 – 7.45) is related to degenerative diseases and decreasing the pH level is related to lower blood flow due to excessing acid adhering to the vessel [4-8]. The pH determination is necessary in a variety of applications in many fields such as chemistry and medical research [9].

Hydrogels are three-dimensional cross-linked system that are made of water soluble polymer with characteristics enable them to be suitable for use in biomedical technologies [10–12]. They have shown reversible responses to various stimuli such as pH, temperature, and biological molecules [13, 14]. In addition, devices that use optical properties are both cost-effective and durable [15, 16]. pH-responsive hydrogels gained attention because of their ease of manufacturing, small size, and their biocompatibility [17–19]. pH-responsive hydrogels contain acidic or basic groups which respond to pH changes [11]. The selection of the polymer is critical because the delamination of the backbone polymer affects the quality and stability of the sensor. Generally, the ionisable portion of the hydrogel determines the sensitivity and the working range of pH-sensor [16]. The sensor's mechanical properties and sensitivity can be controlled by modifying the ratio between the polymer and the ionisable portion or cross-linking. Fibre optic based on hydrogels is an ideal method for remote and continuous measuring of the pH level. Their working principle relies on the change of the refractive index of the

hydrogel in presence of different pH levels which occurs due to the volumetric shift of the hydrogel network [20, 21].

In the past decades, pH-responsive hydrogels have been widely investigated for implementation in many applications. Every hydrogel sensor has its unique characteristics and working range due to the various formulations of hydrogels which provide enormous range of applications. For instant, Tamayol et al. reported a pH-hydrogel sensor for epidermal wound monitoring [22]. The pH-sensor changed its colour with pH of the wound which reflects the health conditions. Also, hydrogel based pH sensors have been developed for drug delivery. pH-sensor have been synthesised from different groups of polymers such as 2-hydroxymethacrylate, N,N`-methylenebisacrylamide, and N-isopropylacrylamide [12, 23–25]. Recently, hydrogel-based pH sensors have been used for controlling the insulin delivery [26–28].

In this paper, we presented a novel optical hydrogel sensor to monitor pH levels. The sensor is rapid to fabricate, cost-effective, and reusable. Fresnel lens was replicated on pH-sensitive hydrogel in order to monitor the volumetric changes of the responsive-hydrogel. The sensor was tested for detecting pH changes in the range of 4.5 - 7. The sensor's performance was examined under microscope and by using a practical optical setup. Testing the sensor was carried out in the temperature range of 20° - 40 °C to study the temperature influence. Moreover, effect of the shelf life on the sensor was studied.

4.2 METHODOLOGY

Materials: Fresnel lens made of acrylic polymer was purchased from Thorlabs. The lens has a focal length of 32 mm, diameter of 25 mm, and 1.5 mm thickness. Hydroxyethyl methacrylate (HEMA), ethylene glycol diamethacrylate (EGDMA), Acrylic acid (AA), 2-dimethoxy-2-phenylacetophenone (DMPA), sodium phosphate monobasic, sodium phosphate dibasic, isopropanol, 3-(trimethoxysilyl) propyl methacrylate (98%) were purchased from Sigma Aldrich and were used without further purification.

Fabrication of the pH-optical sensor: A mixer of HEMA (91.5 mol%), EGDMA (2.5 mol%), and AA (6%) was prepared. The photoinitiator (DMPA) was mixed with isopropanol in a separate plastic vial. Both mixtures were added together to form the pH-responsive gel. Approximately 40 µl of this gel was dropped on the Fresnel lens using pipette and a glass piece was gently paced on top (Figure 4.1A-E). The gel was polymerised using a UV light lamp of wavelength 365 nm for 5 minutes. The sample was kept in DI water for up to two hours to facilitate separating the sample from the master mold. In case of preparing the substrate's attached sensor, a salinized glass piece was used instead of the untreated one that was used in preparing the free standing sensor. Blu Tack was used to close some grooves of the Fresnel lens to prevent any leakage of the solution. All samples were hydrated overnight in phosphate-buffered saline (PBS) solution at pH 7.4 before any further experiment. Figure 4.1(F-I) show that the Fresnel lens pattern has been successfully copied into the pH-sensitive hydrogel.

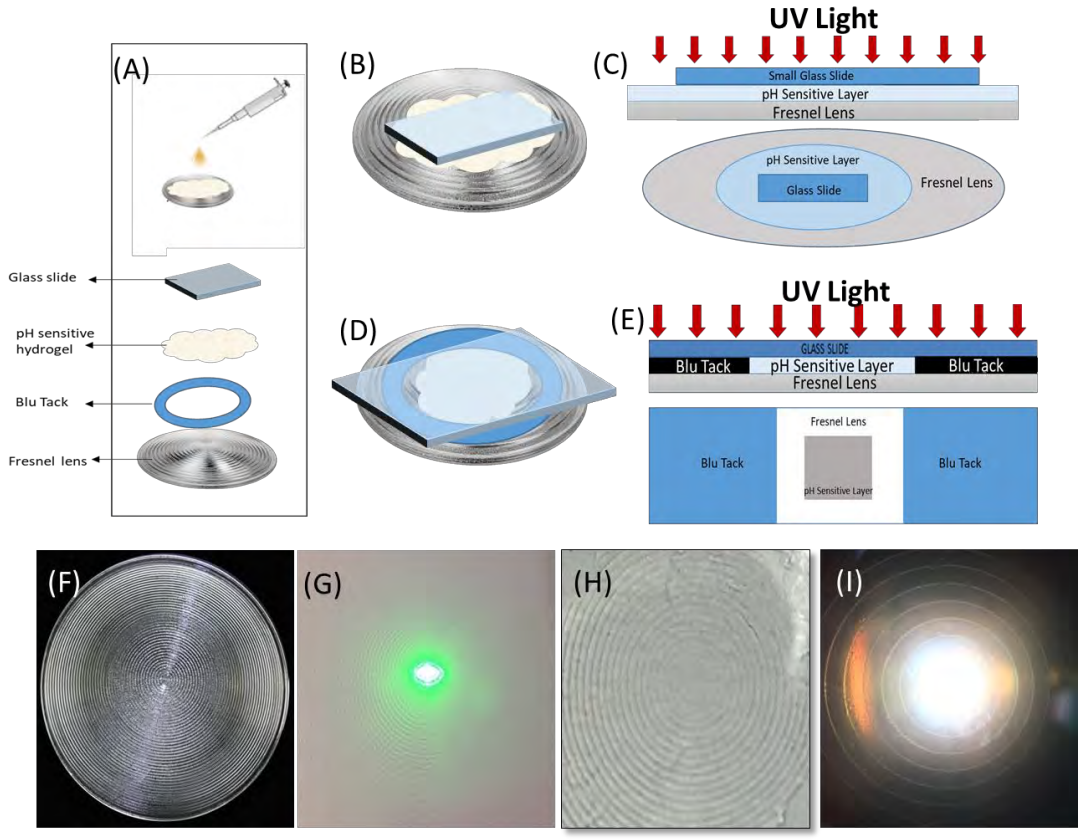

Figure 4.1: A schematic illustration of the fabrication process for replication the Fresnel lens on the pH-sensitive hydrogel; (A-E) steps of replicating the Fresnel lens on the pH-responsive hydrogel; (F-I) images of the Fresnel lens, laser beam passed through the Fresnel lens, Fresnel lens pattern replicated on the pH-responsive hydrogel, and the pH-sensor illuminated by white light beam

Measurement techniques: Computer-controlled rotation stage, laser pointer of wavelength 532 nm, and an optical power meter (Newport, 1918-R) were used for angle-resolved optical power intensity measurements. The pH-sensor was fitted in a transparent plastic cuvette filled with PBS solution, ensuring that the whole sample was submerged in the solution and aligned with the laser beam and a power meter. Then, the test started with replacing the PBS solution with the lowest pH solution (4.5). The pH-sensor was illuminated with the laser beam which was incident normal to the surface plane. The laser transmitted spectra was collected by rotating the sennsor's holder at 1° increments from 0° to 180° and the power meter was recording the light intensity at each angle. The same steps were repeated for

all tested pH solutions. Also, an optical microscope (Zeiss) was used to measure the changes in dimensions of the Fresnel lens imprinted on the pH- sensitive hydrogel. pH-sensor was placed in a transparent petri dish containing 1 ml of the tested pH solution. The free standing sensor was permitted to shrink and expand naturally in the solution.

4.3 RESULTS AND DISCUSSION

The sensitivity of the fabricated pH-sensor was investigated by detecting the optical signal transmitted through the sensor by a photodetector. A schematic illustration of the testing setup is shown in Figure 4.2(A-B). Introducing different pH solutions in the range of 4.5-7 led to change the recoded optical signals and the optical power increased with pH (Figure 4.2C). The sensor showed the highest sensitivity in the pH range of 4.5 – 5.5 as the power increased with value of $4.5 \cdot 10^{-5}$ mW which represent 7% of the reference power. In order to study the effect of the shelf life on the sensor, the pH-sensor was stored in PBS solution for 7 days and the test was repeated. Again, the recorded optical signals increased with pH; however, the sensitivity of the sensor is doubled as sensor showed an increase of 13% in the recorded power in the same pH range (4.5 – 5.5) (Figure 4.2D). The respond and saturation times for the sensor were 5, and 9 min, respectively. The response time of the stimuli-responsive hydrogels relies on the thickness of the hydrogel sensor. Since our sensor was thin, the response time was fast and immediate shifts were apparent with pH change. Figure 4.2(E) displays the recorded power measurements versus time which shows the saturation time of the sensor. The sensor also was examined daily for 10 days while it was stored in PBS buffer solution during the time between tests (Figure 4.2F). It was found that the sensitivity increased with longer storage time as well as increasing the input optical power.

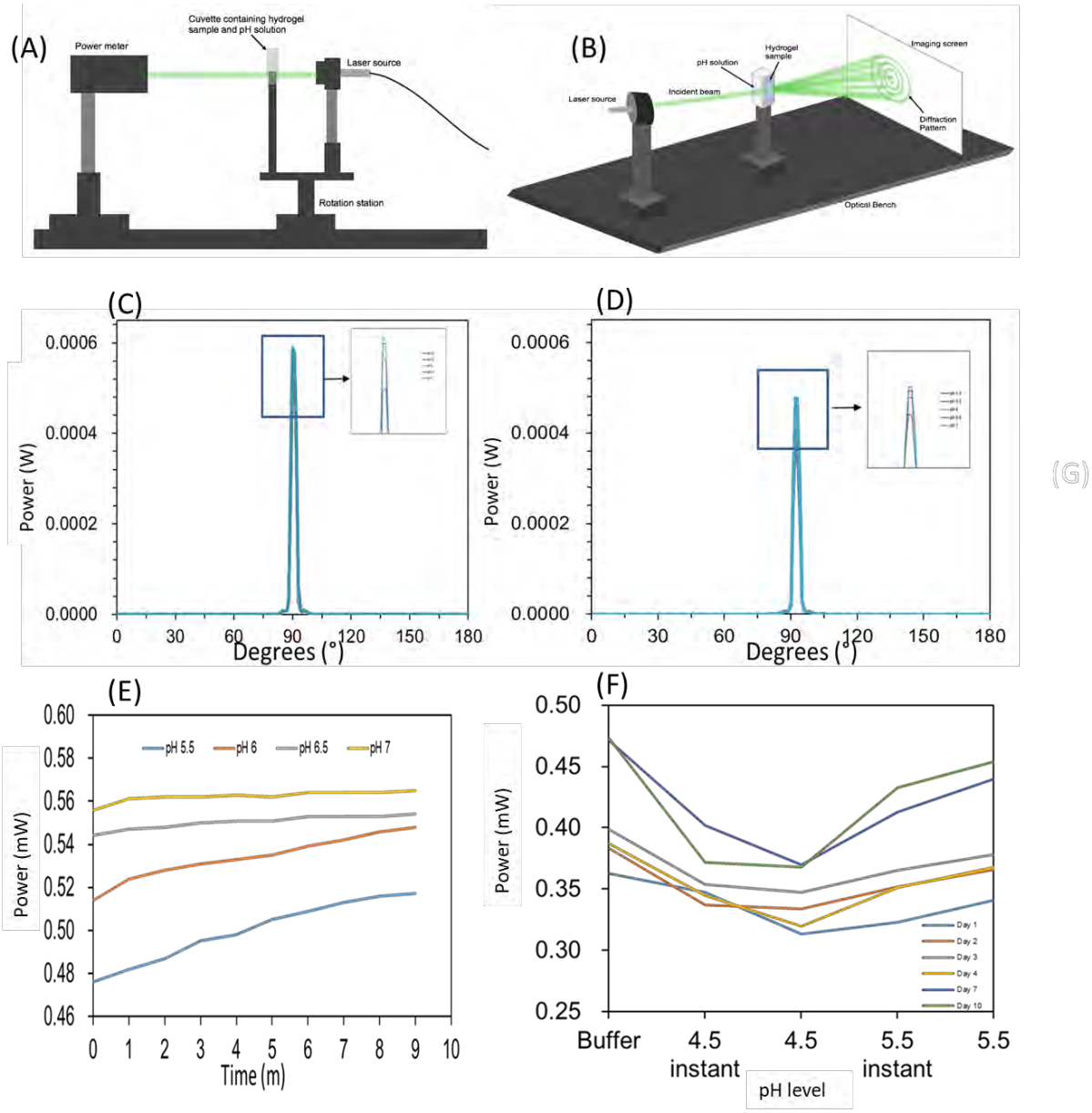

Figure 4.2: (A-B) A schematic illustration of the experiment setup; (C) profile of the measured power intensity for the constrained pH-sensor; (D) laser power profile of the laser beam passed through the confined pH-sensor which was stored for 7 days before testing; (E) response time of the sensor; (F) the effect of 10 days storing on the sensitivity of the pH-sensor

The optical microscope was used to measure and analyse the Fresnel lens dimensions which is replicated on the pH-responsive hydrogel. The test was carried out for the free-standing and the substrate-attached pH-sensors. Microscope images of the pH-sensor immersed in different pH solutions are presented in Figure 4.3(A-F). The images show that changing pH

induced a volumetric shift for the hydrogel sensor. The cuvette contained the constrained pH-sensor was sealed and placed horizontally under the microscope to measure the change in dimensions of Fresnel lens replicated on the sensor's surface when the sensor was soaked in different pH solutions. The cuvette was filled with a PBS solution of pH 7.4 and the diameter of Fresnel lens rings were measured. Then, the PBS buffer was replaced with a solution of pH 4.5 and the diameter of the Fresnel lens rings were measured. This protocol was repeated with different pH solutions (Figure 4.3A). The diameter of Fresnel lens rings at pH 7 increased ≈ 6 μm which represents 3 % of the ring diameter at pH 4.5 (Figure 4.3G). For the free standing sensor, the sensor was placed in a petri dish containing 1 ml of PBS solution having a pH 7.4 and the diameter of Fresnel lens ring was measured under the microscope, and the measured diameter was 238 μm. Different pH solutions having pH in the range of 4.5 – 7 were replaced the PBS on sequence. The initial diameter of Fresnel lens ring at pH of 4.5 was ≈ 187 μm, and at pH of 5.5 the diameter dramatically increased by 11% reached up to ≈ 213 μm. At pH 7 the measured diameter value increased by ≈ 18% (Figure 4.3G). Noticeably, the diameter of Fresnel lens rings for both sensors (free-standing and constrained) rapidly dropped due to the pH change from high pH level (PBS of 7.4 pH) to low pH level of 4.5. Overall, the results show that the constrained sensor had a much smaller diameter change comparing to the free standing sensor. Also, the free standing sensor demonstrated higher sensitivity with a significant rise in dimensions of Fresnel lens with pH.

Effect of temperature on the sensor was studied (Figure 4.3H). The senor was soaked in PBS solution and the temperature was increased from 20 to 40 °C and the transmitted optical powers were recorded. Both the attached/constrained, and free standing sensors showed that the temperature changes has no significant impact on the sensitivity. The power increased by 0.5% and 1% for the free standing, and substrate-attached sensors, respectively.

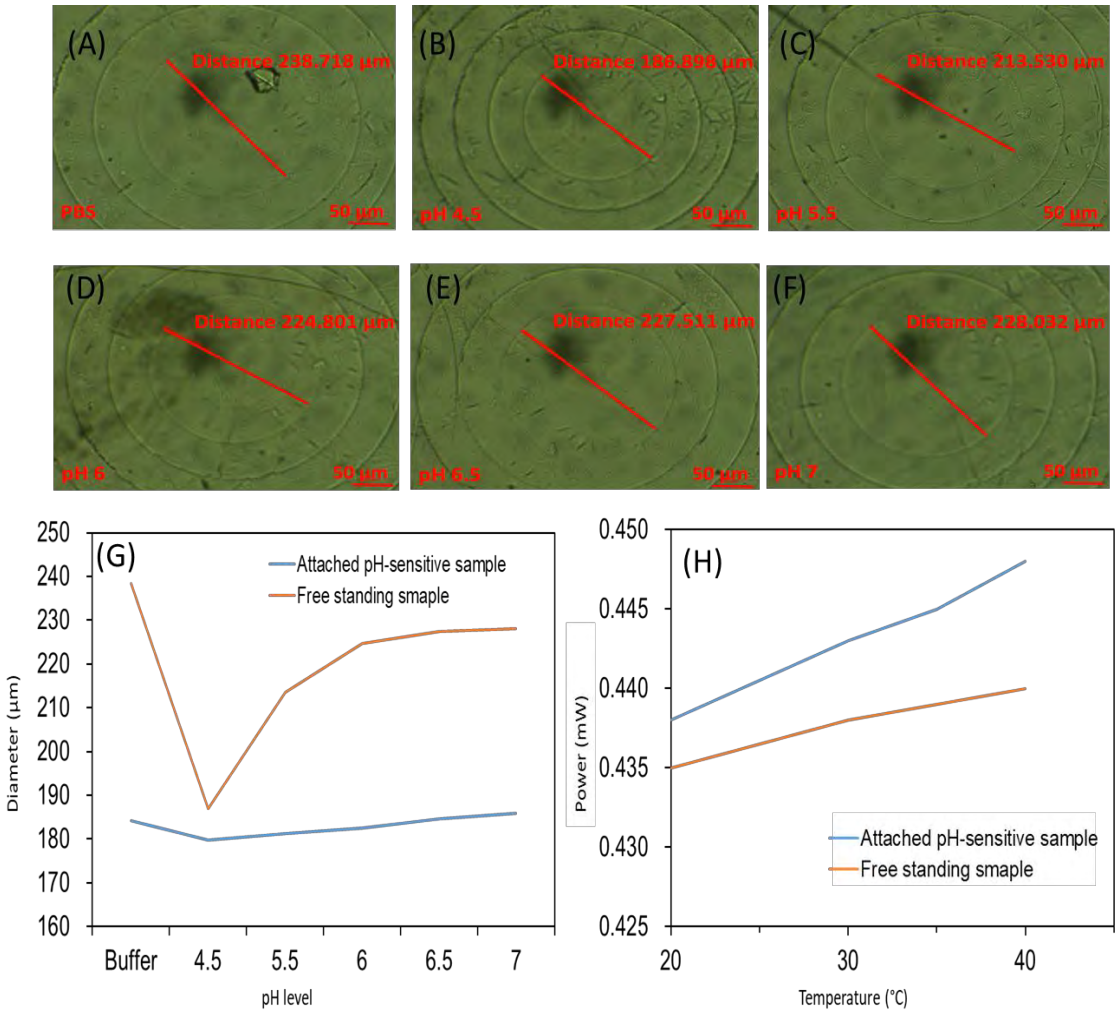

Figure 4.3: (A-F) Images snapped by the scanning electron microscope for the free standing pH-sensor at different pH levels, PBS of pH 7.4 and pH 4.5, 5.5, 6, 6.5 and 7; (G) diameter of Fresnel lens rings recoded during the change of pH levels for both sensors; (H) the impact of temperature on the pH-sensors

4.4 CONCLUSION

We have demonstrated a novel pH-optical sensor based on a combination of Fresnel lens and a pH-responsive hydrogel. A substrate-attached sensor, and a free-standing sensor were fabricated in this work. The optical sensors had a pH sensitivity range of 4.5 - 7, and recorded a respond time of 5 min. The sensors showed the highest sensitivity in the pH range of 4.5 - 5.5 and the sensitivity of the sensors increased due to storage for 10 days in a PBS buffer

solution of pH 7.4. The free standing sensor showed a three-fold higher sensitivity as compared to the substrate-attached one. The temperature changes in the range of 20 – 40 °C was found to have a negligible effect on the sensor. Also, we showed that the fabrication of such novel sensors is fast and cost-effective compared to their conventional counterpart and it could be ideal for mass production. However, optimizing the sensor sensitivity to function perfectly at the physiological pH range would candidate these sensor for monitoring the pH of human blood.

REFERENCES

[1] J. Perk *et al.*, "European Guidelines on cardiovascular disease prevention in clinical practice," *Eur. Heart J.*, pp. 1635–1701, 2012.

[2] W. Aoi and Y. Marunaka, "Importance of pH Homeostasis in Metabolic Health and Diseases : Crucial Role of Membrane Proton Transport," *Hindawi Publ. Corp.*, vol. 2014, no. Figure 1, 2014.

[3] T. Dunning and G. Ward, "Managing clinical problems in diabetes," *Blackwell Publ.*, vol. 32, no. Sep, pp. 1–2, 2008.

[4] E. Chow, D. D. Liana, B. Raguse, and J. J. Gooding, "A Potentiometric Sensor for pH Monitoring with an Integrated Electrochromic Readout on Paper," *Aust. J. Chem.*, vol. 70, no. 9, pp. 979–984, 2017.

[5] T. Wang and D. C. Jackson, "How and why pH changes with body temperature : the α -stat hypothesis," *J. Exp. Biol.*, vol. 219, pp. 1090–1092, 2016.

[6] S. Oxford, *Make Yourself Immune to Heart Attack*, First edit. ShieldCrest,

2012.

[7] G. K. Schwalfenberg, “The Alkaline Diet : Is There Evidence That an Alkaline pH Diet Benefits Health ?,” *Hindawi Publ. Corp.*, vol. 2012, pp. 1–7, 2011.

[8] D. Kuzman, T. Žnidarčič, M. Gros, S. Vrhovec, S. Svetina, and B. Žekš, “Effect of pH on red blood cell deformability,” *Pflügers Arch. - Eur. J. Physiol.*, vol. 440, no. 1, pp. R193–R194, 2000.

[9] S. Atta *et al.*, “Injectable biopolymer based hydrogels for drug delivery applications,” *Int. J. Biol. Macromol.*, vol. 80, pp. 240–245, 2015.

[10] T. R. Hoare and D. S. Kohane, “Hydrogels in drug delivery: Progress and challenges,” *Polym. with aligned carbon Nanotub. Act. Compos. Mater.*, vol. 49, no. 8, pp. 1993–2007, 2008.

[11] K. Deligkaris, T. S. Tadele, W. Olthuis, and A. van den Berg, “Hydrogel-based devices for biomedical applications,” *Sensors and Actuators, B: Chemical*, vol. 147, no. 2. Elsevier B.V., pp. 765–774, 2010.

[12] M. Rizwan *et al.*, “polymers pH Sensitive Hydrogels in Drug Delivery : Brief History, Properties, Swelling, and Release Mechanism, Material Selection and Applications,” *Polymers (Basel).*, vol. 9, no. 137, 2017.

[13] R. V. Ulijn *et al.*, “Bioresponsive hydrogels We highlight recent developments in hydrogel materials with biological,” *Mater. today*, vol. 10, no. 4, 2007.

[14] T. Miyata, T. Uragami, and K. Nakamae, “Biomolecule-sensitive hydrogels,” *Adv. Drug Deliv. Rev.*, vol. 54, pp. 79–98, 2002.

[15] A. K. Pathak and V. K. Singh, “A wide range and highly sensitive optical fi ber pH sensor using polyacrylamide hydrogel,” *Opt. Fiber Technol.*, vol. 39, pp. 43–48, 2017.

[16] A. Richter, G. Paschew, S. Klatt, J. Lienig, K. Arndt, and H. P. Adler, “Review

on Hydrogel-based pH Sensors and Microsensors," *sensors*, vol. 8, pp. 561–581, 2008.

[17] S. Bhattacharya, F. Eckert, V. Boyko, and A. Pich, "Temperature-, pH-, and Magnetic-Field-Sensitive Hybrid Microgels," *Hybrid microgels DOI*, vol. 6, pp. 650–657, 2007.

[18] D. Kuckling, A. Richter, and K. Arndt, "Temperature and pH-Dependent Swelling Behavior of Poly (N -isopropylacrylamide) Copolymer Hydrogels and Their Use in Flow Control," *Macromol. Mater. Eng.*, vol. 288, pp. 144–151, 2003.

[19] Y. Zhao, M. Lei, S. X. Liu, and Q. Zhao, "Smart hydrogel-based optical fiber SPR sensor for pH measurements," *Sensors Actuators, B Chem.*, vol. 261, pp. 226–232, 2018.

[20] N. Jiang *et al.*, "Functionalized Flexible Soft Polymer Optical Fibers for Laser Photomedicine," *Adv. Opt. Mater.*, vol. 1701118, pp. 1–10, 2018.

[21] S. Singh and B. D. Gupta, "Chemical Fabrication and characterization of a highly sensitive surface plasmon resonance based fiber optic pH sensor utilizing high index layer and smart hydrogel," *Sensors and Actuators B-chemical*, vol. 173, pp. 268–273, 2012.

[22] A. Tamayol *et al.*, "Flexible pH-Sensing Hydrogel Fibers for Epidermal Applications," *Adv. Healthc. Mater*, vol. 5, pp. 711–719, 2016.

[23] L. S. Lim, I. Ahmad, and M. A. S. M. Lazim, "PH sensitive hydrogel based on poly(acrylic acid) and cellulose nanocrystals," *Sains Malaysiana*, vol. 44, no. 6, pp. 779–785, 2015.

[24] D. Arunbabu, H. Shahsavan, W. Zhang, and B. Zhao, "Poly(AAc- co -MBA) Hydrogel Films: Adhesive and Mechanical Properties in Aqueous Medium,"

ACS Publ., vol. 117, pp. 441–449, 2013.

[25] A. Chang, “pH-sensitive starch-g-poly(acrylic acid)/sodium alginate hydrogels for controlled release of diclofenac sodium,” *Iran. Polym. J.*, vol. 24, no. 2, pp. 161–169, 2015.

[26] X. Qi *et al.*, “Salecan-Based pH-Sensitive Hydrogels for Insulin Delivery,” *ACS Publ.*, vol. 14, pp. 431–44, 2017.

[27] Y.-H. Kim, Y. H. Bae, and S. W. Kim, “pH/Temperature-sensitive polymers for macromolecular drug loading and release,” J. M. Anderson, S. W. Kim, J. Kopeček, and K. B. T.-A. in D. D. S. Knutson 6, Eds. Elsevier, 1994, pp. 143–152.

[28] A. Kikuchi and T. Okano, “Stimuli-sensitive hydrogels,” *Polym. Drug Deliv.*, pp. 275–322, 2005.

Chapter 5: Laser-Induced Surface Modification of Contact Lenses.

This chapter of the alternative format thesis is published in **Advanced Engineering Materials.** The publication information and authors' contributions are provided here.

Yousef Alqurashi, Magdalena Bajgrowicz-Cieslak, Muhammad Umair Hassan, Ali K. Yetisen, Haider Butt, "Laser-Induced Surface Modification of Contact Lenses," Adv. Eng. Mater., vol. 20, no. 6, 2018.

Authors Contributions

Y.A. and H.B conceived the idea and deigned setups. **Y.A.** led the project, and analysed the results, **Y.A.** and M.B carried out the laser treatment process, and did the SEM imaging. **Y.A**. wrote the manuscript. H.B. supervised the project and reviewed the manuscript. All authors reviewed the manuscript.

ABSTRACT

We report on the laser-induced modification of surface properties of contact lenses. Selective areas of the surface of commercial silicon-hydrogel contact lenses were patterned in array formats using different powers of the CO_2 laser. 1D arrays of different groove densities, channels, and 2D intersecting architecture were fabricated. Contact angle measurements were carried out to measure the surface hydrophilicity, and extent of hydration was linked with the surface profile properties and the space gap between the fabricated patterns, which were controlled by the beam exposure time, beam power, and scan speed. Laser treatment of contact lenses resulted in improved hydration proportional to the density of laser ablated segments on the surface. The hydration time of water droplets on different lens surfaces was also recorded – all 2D patterned lenses showed faster hydration as water quickly diffused into the bulk of the lens due to the extended interfacial area between the contact lens and the water droplet as a consequence of larger areal modification in 2D as compared with 1D patterns. The best wettability properties were obtained with 0.3 mm space gap, 9 W power, and 200 mm s^{-1} scan speed. Optical microscopy was used to image the 3D surface profiles of the modified lenses and the depth of the patterns and was correlated with the experimental observations. The maximum depth of 40 μm was observed with 0.3 mm space gap, 9 W, and 200 mm s^{-1} scan speed. Optical transmittance of broadband white light was measured to assess the surface treatment effects on the contact lenses. A large exposure and dense patterning of contact lens resulted in decreased (down to a minimum of 45%) in the light transmittance, which dictates the practical usability of such patterning. Surface treatment of contact lenses can be utilized to deposit stable conducting connection for on-lens-LEDs, displays, and communication antennas as well as for stabilizing biosensing materials and drug dispensing applications.

Keywords: contact lenses; microfluidics; channels; laser ablation; laser proccessing; contact angle.

5.1 INTRODUCTION

Contact lenses were invented by Adolf Fick in 1888, [1] and this industry is currently worth more than $9 billion as of 2017 [2]. 125 million people wear contact lenses worldwide for correcting vision or trending decorative fashion [3]. The demand for contact lenses is expected to increase due to increasing eye-related conditions, lens-based sensing and diagnostics, controlled drug release, and contact lens based electronic interfaces [1, 2, 4]. Since their first discovery, contact lenses have continually evolved, bringing numerous advantages in terms of quality, ease of use, and compatibility with eye chemistry [5–7]. Three different generations of silicone hydrogel soft lens were developed between 1998 to [8–10]. Soft contact lenses are flexible, softer, oxygen permeable, and hydrophilic [11–13]. Their quality is determined by structural integrity, comfort, and vision correction [14].

Lack of comfort is the most common cause of contact lens discontinuation [15, 16]. Hydrophobic contact lenses lead to hazy vision, a sensation of dryness, and discomfort [17, 18]. Consequently, increase in surface wettability and hydrophilicity has been known to enhance the wear comfort of contact lenses [17]. Typically, two approaches are undertaken to improve the wettability of contact lenses temporarily; one is the regular application of lens solution (rewetting drops) that replenish the naturally diminishing tear film between the contact lens and ocular surface, while the other is to modify the lens material itself (plasma treatment) [18, 19]. However, introducing hydroxyl groups through chemical modifications have been utilized to increase the water affinity of the lens's surface [20].

Here, a new laser treatment method is demonstrated to improve the wettability of commercial contact lenses. The approach was adopted to increase the surface area at selective places on the contact lens. Improved wetting properties were obtained by increasing the density

of surface patterns. The wettability was measured by depositing a controlled volume of deionized (DI) water onto a fully-hydrated lens. Correlation between the surface area and inherent wettability/contact angle was studied. Continuous monitoring of the drop-cast water droplet revealed the temporal behavior of the droplet on various laser-treated contact lens surfaces.

5.2 METHODOLOGY

A CO_2 laser (HPC LS 3040) was used to modify the surface properties of commercial silicon-hydrogel contact lenses (Narafilcon, 1-day Acuvue® TruEye®, Johnson & Johnson) (Figure 5.1a-g). Silicone hydrogel contact lenses had a center thickness of 0.09 mm. and a dioptric power of -0.5 with a base curve of 8.6 mm. The surface structures in the form of long channels were produced in an engraving mode. Laser parameters were varied to obtain different architectures: power (6, 9 W), scan speed (200, 300 mm s^{-1}), space-gap/hatch (0.1, 0.2, 0.3, 0.4, 0.5 mm). The distance (7.4 mm) between the laser-head and surface bed (height or z-axis) remained constant throughout the experiments. After the laser exposure, contact lenses were stored in DI water before characterization.

The surface morphology of laser-treated contact lenses was analysed by an optical microscope (Zeiss Axio). Also, the transmissibility of each lens was measured within the visible spectral range (400-700 nm) using a spectrophotometer (Ocean Optic DH-2000) attached to the eye-piece of the optical microscope. The topography of the modified surface of contact lenses after the laser exposure was also studied using Alicona optical microscope. 3D images were obtained to assess the depth profile of laser engraved channels. The sessile drop

method was used to measure the contact angle on laser-treated contact lenses. A customized liquid dispensing system was used to drop equal amount (5 μL) of DI water for each measurement. A digital microscope coupled with a charge-coupled device (CCD) camera was used to record time-lapse images to study the temporal response of the water drop on contact lenses. Still images were captured at 0, 15, 30, 60 and 90 s after landing the drop onto the surface. The contact angle plugin of ImageJ software (NIH) was used to analyse the images and determine the contact angles (n = 3). All the experiments were conducted at 24 °C and ~ 30% relative humidity. Figure 5.1(h-i) presents an image of CO_2 laser-patterned geometries on selective area of the lenses.

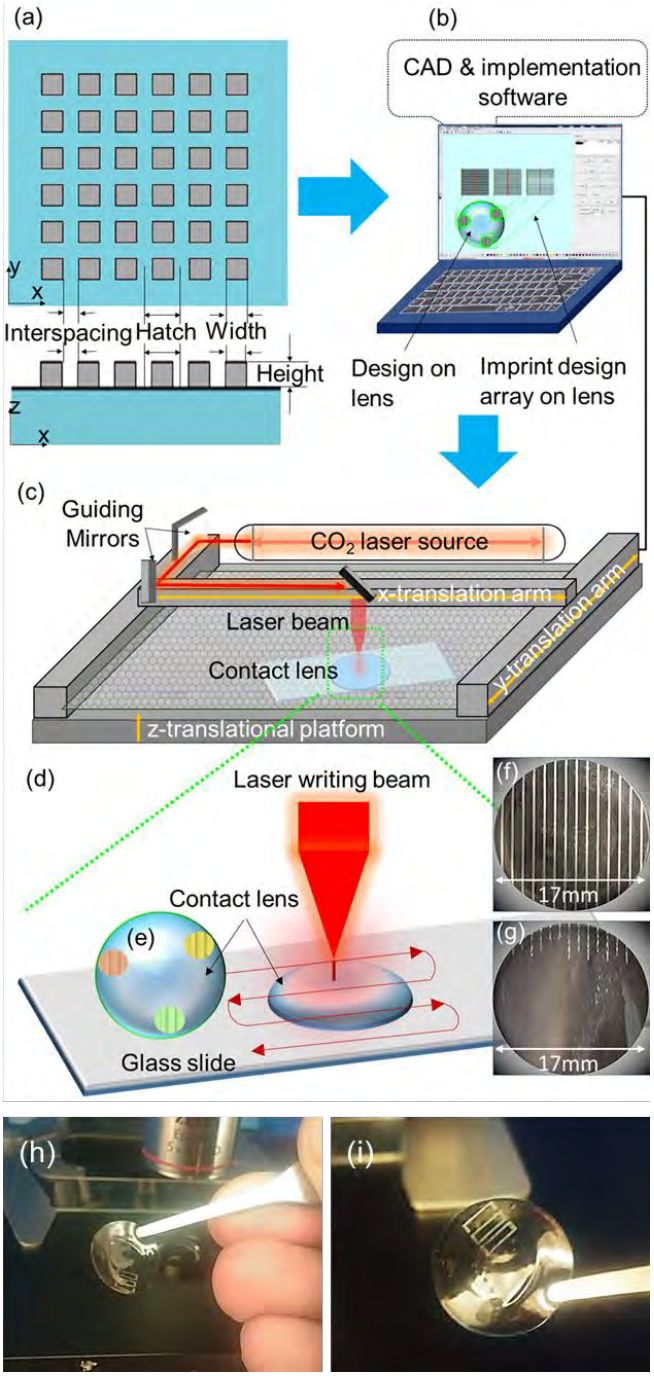

Figure 5.1. Formation of arrays and channels in contact lenses via CO_2 laser treatment: (a) The design of the desired structure; (b) the CAD and implementation software was used to design the space gap, exposure time, rate and power information to pattern through the laser; (c) the computer-controlled laser fabrication of patterns on contact lenses; (d) the illustration of laser treatment of the lens; (e) a concept figure of patterns areas to stabilize different biosensing materials on the contact due to the increased area and roughness of laser treated selective areas; (f) photograph of a contact lens with channel patterned across the entire lens (17 mm); (g) photograph of a partially patterned contact lens; (h,i) photographs of CO_2 laser-patterned geometries on selective portions of contact lenses

5.3 RESULTS AND DISCUSSION

Figure 5.2(a) shows 1D and 2D structures obtained by scan the CO_2 laser beam (with different operating conditions) on contact lens samples in xy-plane. The scan speed was controlled to achieve different desired patterns. A slow beam scan speed (200 mm s^{-1}) was utilized for pattering continuous channels. However, a faster scanning speed (300 mm s^{-1}) was used to make segregated spots/pits in the contact lens. A space gap between the scanned lines was introduced to draw the patterns with different duty cycles/groove densities. Two laser beam powers (6 and 9 W) were used for both scan speeds as well as for all space gaps. Higher power produced deeper patterns as compared to the low-power scans. This was attributed to the total energy imparted to the lens by the laser beam, namely, E = P.t, where, E is the total energy imparted by the laser, P is the beam power, and t is the active engraving time spent per pattern. Powers above 9 W, cut through the lens and no patterning could be obtained at these powers. Nevertheless, this also defined the lower limit of the power threshold that can be used to cut the lens in particular shapes if needed. In 2D patterning at 6 W, continuous channels and segregated structures were patterned without damaging the lens. At 9 W beam power, the crossing points where the laser interacted with the contact lens twice traversing from two perpendicular directions showed some damage and formed well-matrixed through holes in lenses. An optical microscope was used to analyze the maximum groove depth obtained at 200 mm s^{-1} scan speed and the beam power of 9 W. The maximum depth was recorded to be ~ 40 μm for the channels made at the scan speed of 200 mm s 1 and power of 9 (Figure 5.2b).

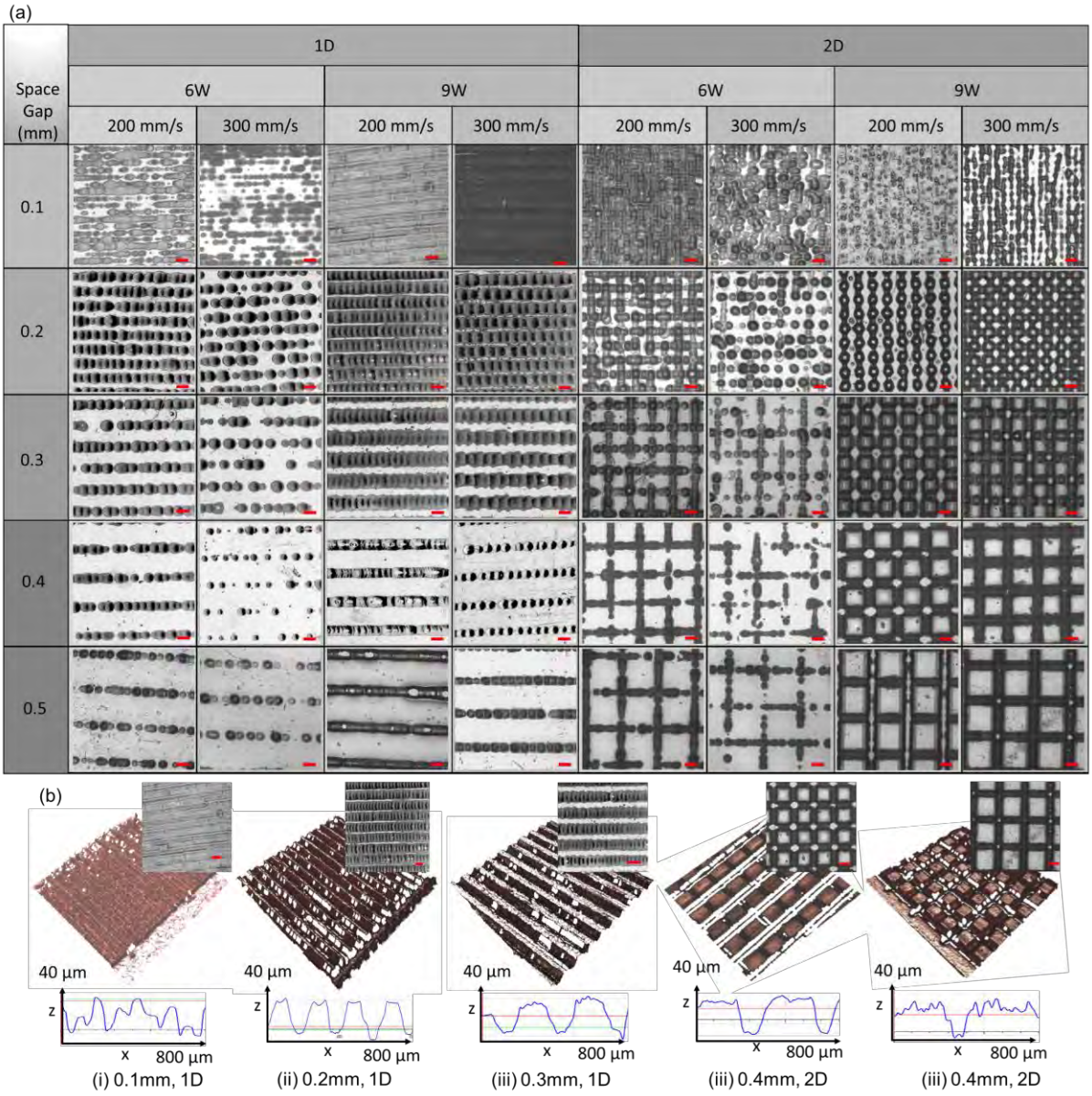

Figure 5.2: Microscopic images of laser-modified contact lenses: (a) 1D and 2D patterns were fabricated at 6 and 9 W, scan speeds (200 and 300 mm s^{-1}), and five space gaps (0.1-0.5 mm, with the increment of 0.1 mm). A fast scan speed casts distant features whereas the low speed results in channel-like structures. Scale bars=200 µm; (b) 3D microscopic images of 1D and 2D patterned surfaces produced at 200 mm s^{-1} scan speed and 9 W for different space gaps

Contact angle measurements were carried out to analyze the hydration properties of 1D and 2D patterned lenses (Figure 5.3). The behaviour is governed by $\cos\theta^* = r.\cos\theta e$, where θe

is the equilibrium of the contact angle [21, 22]. θ* is the apparent contact angle owing to the surface roughness r defined as the ratio of the actual area to the projected area of the surface. The contact angle was plotted against the groove density (1/space gap) (Figure 5.3d-k) and time (Figure 5.3l-u) after pouring a droplet on the surface. For unmodified contact lens, the initial contact angle was ~77.2°. A decrease of 3.5° (4.52%) was recorded in the contact angle within 90 s. The space gap played an important role in the surface wettability – for all samples, increasing (decreasing) space gap (groove density) from 0.1 mm to 0.3 mm (10-3 mm 1), and the recorded contact angle initially showed a decreasing (increased) trend. The initial decrease in the contact angle with increasing groove density is attributed to increasing surface roughness. As the groove density decreased from 3.33 mm^{-1} to 2 mm^{-1}, the recorded contact angles exhibited increasing trend across the entire time-frame for all samples (1 and 2D). However, hydration effects in 2D lenses were more pronounced as compared to their corresponding 1D samples. 2D-patterned contact lenses showed lower contact angles as compared to corresponding single-engraved lenses. In comparison to corresponding 1D lenses, 2D patterned lenses showed an average of ~ 21% lower contact angle (recorded after 90 s) as 2D lenses contained twice as many channels as the single engraved equivalents.

The laser energy also systematically influenced the contact angle (Supporting Information, Figure S1). Lenses subject to 9 W, as opposed to 6 W, had ~ 9% lower contact angle after 90 s of time lapse, as more energy was imparted by the laser over the same area of engraving in the case of 9 W exposure, which led to the formation of deeper channels, increasing hydration. The scan speed had also some effects on patterns produced on lenses – the lower the speed, the smaller the contact angle. The speed 200 mm s^{-1} showed ~ 4 % lower contact angle (after 90 s) as compared to patterning at 300 mm s^{-1}.

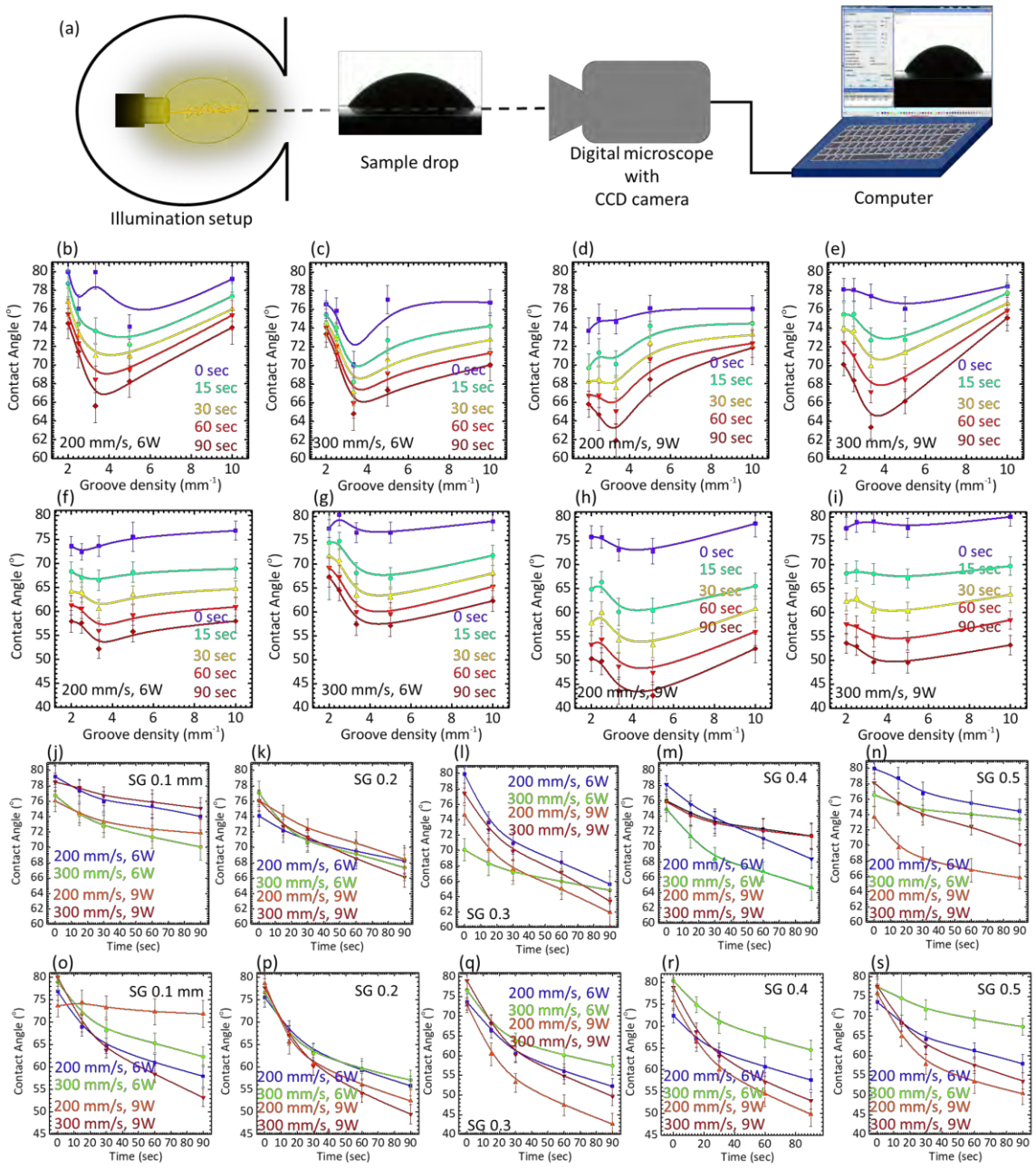

Figure 5.3: Contact angle measurements in laser-treated contact lenses: (a) schematic of the contact angle measurement setup; (b, c) photographs of contact angle measurements for 1D and 2D pattering, respectively (scan speed=200 mm s^{-1}, beam power=6 W); (d-g) contact angle versus groove density for 1D-patterned lenses; (h-k) contact angle versus groove or line density for 2D-patterned lenses; (l-p) time response of contact angle for 1D patterns; (q-u) time response of contact angle for 2D patterns

The time response of the diffusing water droplet on contact lens surfaces suggests higher diffusivity on 2D patterned contact lenses as compared with 1D patterns as slopes in contact angle-versus-time graphs show larger negative values than 1D suggesting their better

hydration. The overall contacts angle for all condition and interval of times are also smaller in 2D patterned contact lenses. The behaviour suggests that increasing the surface area by making it rougher with laser treatment provides a larger cross-section at the water-contact lens interface, increasing the diffusion rate and improving the hydration properties of these modified samples.

Broadband white-light transmission measurements were carried out to analyze the optical modification introduced by CO_2 laser patterning of contact lenses Figure 5.4. A pristine (unmodified) lens showed a transmittance of ~97% for the visible light spectrum. Increasing the space gap (0.1 to 0.5 mm) in the patterned samples showed increased transmittance, both in 1D and 2D patterned samples. The behaviour was expected because at large space gaps, the laser beam modified the surface at larger distances and there was more pristine area present between the consecutive grooves as compared with densely patterned designs. Consequently, most of the incoming light transmitted unhindered through the pristine parts of the lens. Increasing the power from 6 W to 9 W decreased the transmittance due to the wider profile of the patterns, decreasing the pristine area between the grooves, and also due to deeper engraving (consequently roughening) at higher power. 1D-patterned lenses exposed to 9 W beam power showed a ~11% lesser transmittance on average as compared to 6 W exposure. Similarly, comparison of 9 W and 6 W equivalent 2D-patterned lenses showed a decreased transmittance by ~14%. Increasing the scan speed effectively has the effect of increasing the distance between the laser patterns within a particular groove. Therefore, increased scan speed also results in increased transmission of the light as more pristine areas become available to the incoming light to pass through.

Un-patterned and patterned (1D and 2D) contact lenses were placed in front of a mobile camera to see how patterning might deteriorate the vision, though actual effects can only be realized only in clinical trials (Figure 5.4c). Photographs taken with and without un-patterned contact lens are almost of identical quality and provided a good definition of the captured objects. However, 1D and 2D patterning resulted in deterioration of the definition such that 2D-patterned contact lens resulted in a more blurred image as compared to that taken through a 1D-patterned contact lens.

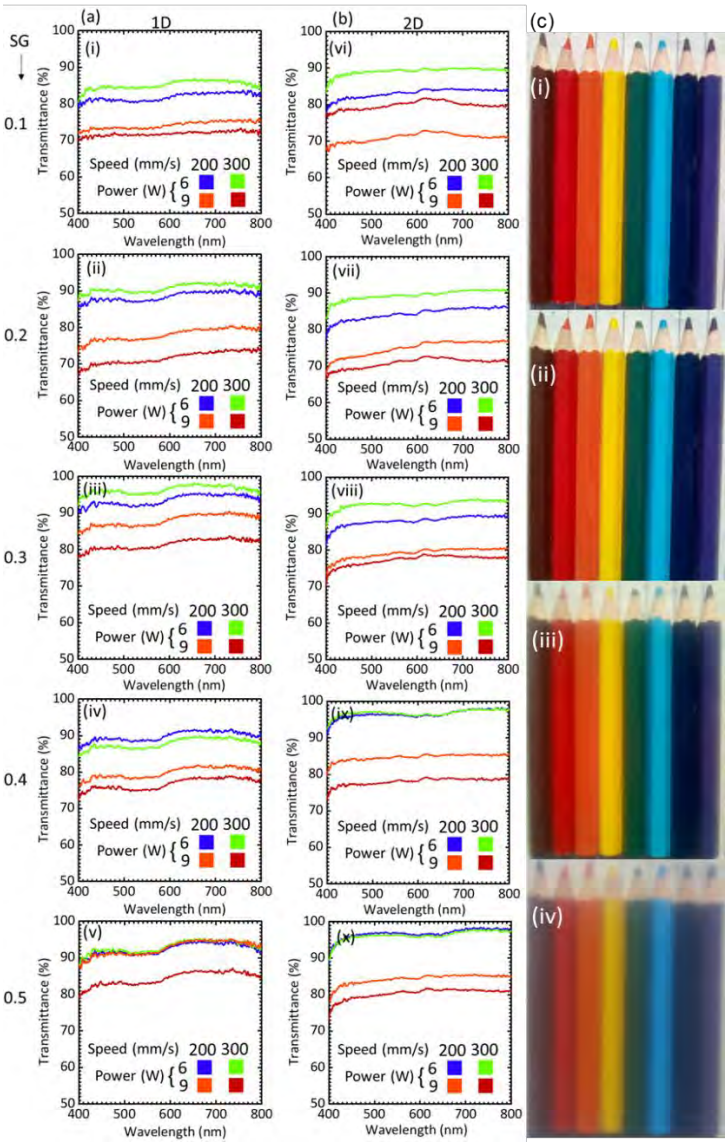

Figure 5.4: Transmission properties of the laser-treated lenses: Transmission of light within the visible range for 1D (a) and 2D (b) patterning for groove spacing between 0.1 mm to 0.5 mm

for 1D (i-v) and 2D (vi-x) patterning, respectively; (c) photographs taken from a mobile phone camera without a contact lens in front (i) with contact lens having no patterning (ii) with 1D patterned contact lens (iii), and with 2D patterning

Figure 5.5(a-d) summarizes the transmittance behaviour related to increasing space gap and energy imparted to the lens. The transmittance increased systematically with a linear trend with increasing space gap, and as an exponential function of the imparted energy. The transmittance was also related to the scan speed. In general, the low scan speed of 200 mm s^{-1} resulted in slightly lower transmittance over the whole range of space gaps than the patterns fabricated at the higher speed of 300 mm s^{-1}. These results were consistent with contact angle measurements. Decreasing contact angle suggested higher roughness which generally occurred at high power, low scan speed, and high groove density. Accordingly, the light transmittance also showed a general decreasing trend with the abovementioned parameters. Therefore, smaller the contact angle poorer the light transmission due to increasing surface roughness effects and vice versa.

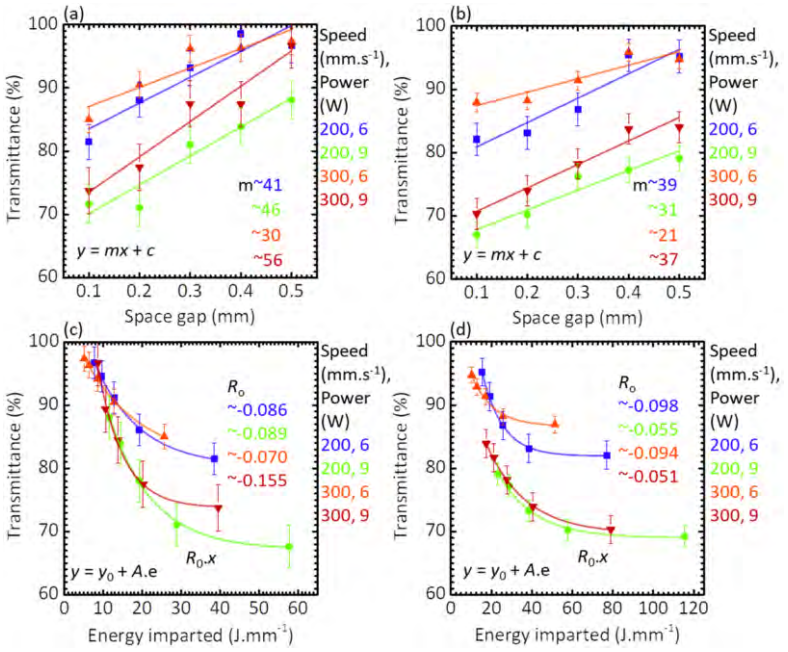

Figure 5.5: Transmittance versus space gap for 200 and 300 mm s^{-1} scan speed and at 6 W and 9 W for (a) 1D and (b) 2D patterns. Transmittance with energy imparted to the lens at scan speeds of 200 and 300 mm s^{-1} and powers of 6 and 9 W for (c) 1D and (d) 2D patterns

The impact of laser patterning on mechanical properties of modified contact lenses was studied in a load (F) versus extension (E) experiment (Figure 5.6). The lens was patterned from the middle (5×5 mm2, hatch distance 400 mm, power 6 W). The pristine lens withstood an extension of ~ 2.2 mm at which the maximum load was ~ 0.078 N. The corresponding tensile strength was ~ 0.052 N/mm2, followed by a downturn (failure) in the F-E curve. The patterned lens showed the extension of ~ 1.6 mm, where the maximum load was ~ 0.032 N, with the corresponding tensile strength of ~ 0.021 N/mm2 before the failure. Notice that 5×5 mm2 is a large area considering the dimensions of the lens. The experimental setup restrained us to carry out the measurements on a lens having patterns on its periphery. We suggest that the deterioration of the mechanical properties can be lessened by selectively premodifying the 'to-be-patterned' area of the contact lens during its fabrication process.

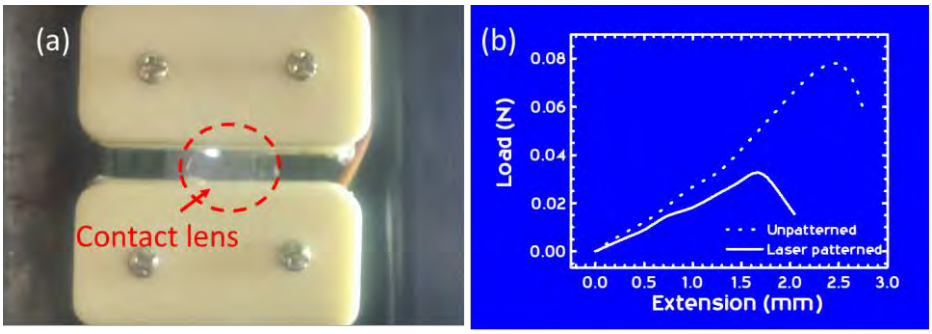

Figure 5.6 (a) Experimental setup used to measure the mechanical properties of the unpatterned and patterned cont lenses; (b) Load vs. Extension curves for unpatterned pristine contact lens (dotted line) and laser patterned contact lens (solid line)

5.4 CONCLUSION

We developed an effective low-cost and fast method of writing different structures using a CO_2 laser on the surface of commercial contact lenses for tuning the surface properties. Different parameters including the groove spacing, beam power, and scan speed were changed to study the surface roughness variation on hydrophilicity and transmission properties of contact lenses. Modifying the roughness of contact lenses by laser treatment increased hydrophilicity. The maximum power that can be used in this process was 9 W, above which laser can cut through the bulk of the lens matrix. The optimal range for the scan speed of the laser was within 200-300 $mm.s^{-1}$. The space gap and laser energy applied to the lens were critical parameters that affected the wettability significantly. For the best wettability properties as assessed by contact angle behavior, 0.3 mm space gap, 9 W power, and 200 $mm.s^{-1}$ were the optimum conditions. In the case of 2D scan the crossing-points, where the lens area was exposed twice to the laser beam, the higher power range (9 W) resulted in deeper ablation. The intense exposure led to localized cut-through areas of damage.

Laser treatment of contact lenses has its practical limitations as there was a trade-off between the wettability and transmittance. Surface areas away from the sight of vision are should be patterned to avoid specular effects such as laser processing of the periphery of the lenses can be utilized for quick hydration of the contact lens, as well as for biosensing by attaching/crosslinking colorimetric, fluorescent, or electronics within the patterned area [4]. Channels can be exploited to fabricate conducting contacts due to enhanced sticktion of such roughened surfaces [23]. Such processing can find its applications in contact lens-embedded LEDs, displays and communication systems [24, 25]. In addition, a lens containing nanoscale channels is also promising for inducing anti-bacterial properties [26]. Although a CO_2 laser was successfully employed to form channels on the contact lens surfaces, more precise

channels can be formed with higher resolution by using more advanced laser systems such as femtosecond lasers with shorter wavelengths.

SUPPORTING INFORMATION

Table S1. Specifications of commercial silicone lens.

Material	Narafilcon-A (silicon-hydrogel)
Manufacturer	Johnson & Johnson
Water content (%)	46%
FDA group	V
Center thickness (mm)	0.09
Oxygen permeability (x10-11)	100
Principal monomers	MPMDSM, DMA, HEMA, siloxane macromer, TEGDMA, PVP

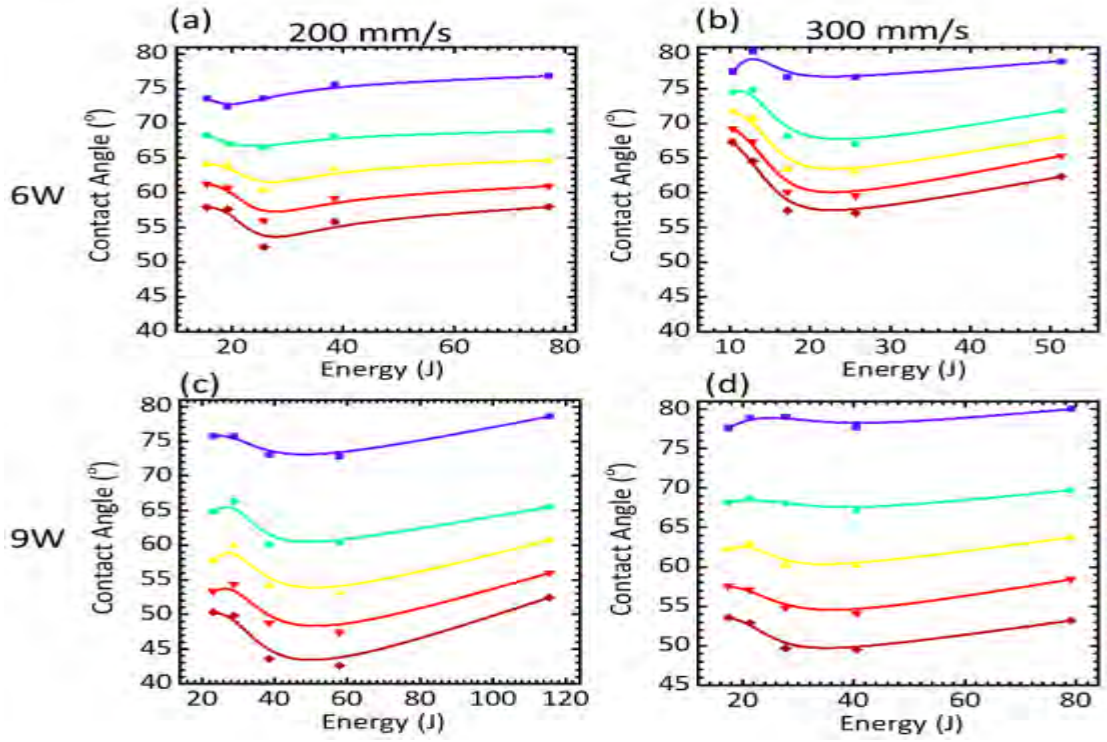

Figure S1: (a-d) Contact angle measurements versus imparted energy in laser-treated contact lenses for scan speeds of 200 and 300 mm s^{-1} and powers of 6 and 9W. Data for different groove spacing, 0.1mm (blue) 0.2mm (green) 0.3 (yellow), 0.4mm (red) and 0.5(brown), are shown.

REFERENCES

[1] R. Heitz and J. Enoch, “Leonardo da Vinci: An assessment on his discourses on image formation in the eyeNo Title,” *Adv. Diagnostic Vis. Opt.*, pp. 19–26, 1987.

[2] G. V. R. Report, “Contact Lenses Market Analysis, By Product Type, By Design Type (Spherical, Toric, Multifocal), By Usage Type (Corrective, Therapeutic, Cosmetic, Prosthetic), By Regions, And Segment Forecasts, 2014 - 2025,” 2017.

[3] C. Chao, K. Richdale, I. Jalbert, K. Doung, and M. Gokhale, “Non-invasive objective and contemporary methods for measuring ocular surface inflammation in soft contact lens wearers – A review,” *Contact Lens Anterior Eye*, vol. 40, no. 5, pp. 273–282, Oct. 2017.

[4] F. H. Nasr, S. Khoee, M. M. Dehghan, S. S. Chaleshtori, and A. Shafiee, “Preparation and Evaluation of Contact Lenses Embedded with Polycaprolactone-Based Nanoparticles for Ocular Drug Delivery,” *Biomacromolecules*, vol. 17, no. 2, pp. 485–495, 2016.

[5] G. Iskeleli, Y. Karakoç, Ö. Aydn, H. Yetik, H. Uslu, and M. Kzlkaya, “Comparison of Tear-Film Osmolarity in Different Types of Contact Lenses,” *Eye Contact Lens*, vol. 28, no. 4, 2002.

[6] P. C. Nicolson and J. Vogt, “Soft contact lens polymers: An evolution,” *Biomaterials*, vol. 22, no. 24, pp. 3273–3283, 2001.

[7] D. FONN, “Targeting Contact Lens Induced Dryness and Discomfort: What Properties Will Make Lenses More Comfortable,” *Optom. Vis. Sci.*, vol. 84, no. 4, 2007.

[8] F. Stapleton, S. Stretton, E. Papas, C. Skotnitsky, and D. F. Sweeney, “Silicone Hydrogel Contact Lenses and the Ocular Surface,” *Ocul. Surf.*, vol. 4, no. 1, pp. 24–43, 2006.

[9] L. Alvord *et al.*, “Oxygen permeability of a new type of high Dk soft contact lens material,” *Optom. Vis. Sci.*, vol. 75, no. 1, pp. 30–36, 1998.

[10] L. Kodjikian *et al.*, “Bacterial adhesion to conventional hydrogel and new silicone-hydrogel contact lens materials,” *Graefes Arch. Clin. Exp. Ophthalmol.*, vol. 246, no. 2, pp. 267–273, 2008.

[11] N. Gaylord, “Oxygen-permeable contact lens composition, methods and article of manufacture,” p. US3808178 A, 1974.

[12] E. Papas, C. Vajdic, R. Austen, and B. Holden, “High oxygen-transmissibility soft contact lenses do not induce limbal hyperaemia,” *Curr Eye Res*, vol. 16, pp. 942–948, 1997.

[13] S.-H. Hyon, W.-I. Cha, Y. Ikada, M. Kita, Y. Ogura, and Y. Honda, “Poly(vinyl alcohol) hydrogels as soft contact lens material,” *J. Biomater. Sci. Polym. Ed.*, vol. 5, no. 5, pp. 397–406, Jan. 1994.

[14] M. J. Giraldez and E. Yebra-Pimentel, “Hydrogel Contact Lenses Surface Roughness and Bacterial Adhesion,” *Intech, Croat.*, 2012.

[15] F. Stapleton *et al.*, “Risk factors and causative organisms in microbial keratitis in daily disposable contact lens wear,” *PLoS One*, vol. 12, no. 8, p. e0181343, 2017.

[16] P. Situ, T. Simpson, and C. Begley, “Hypersensitivity to Cold Stimuli in Symptomatic Contact Lens Wearers,” *Optom Vis Sci.*, vol. 176, no. 10, pp. 139–148, 2016.

[17] B. Caffery *et al.*, “Contact Lens Comfort,” *Optom. Vis. Sci.*, vol. 93, no. 8, p. 790—792, Aug. 2016.

[18] J. J. Nichols, C. W. Lievens, M. R. Bloomenstein, H. Liu, P. Simmons, and J. Vehige, “Dual-polymer drops, contact lens comfort, and lid wiper epitheliopathy,” *Optom. Vis.*

Sci., vol. 93, no. 8, pp. 979–986, 2016.

[19] G. Qin, Z. Zhu, S. Li, A. M. McDermott, and C. Cai, "Development of ciprofloxacin-loaded contact lenses using fluorous chemistry," *Biomaterials*, vol. 124, pp. 55–64, 2017.

[20] H.-Y. Li, W.-J. Ting, Y.-C. Lai, and H.-Y. Chang, "Method for Manufacturing Hydrophilic Silicone Macromer," p. EP2610281 B1, 2015.

[21] S. D. Hodgson, D. G. Waugh, A. Gillett, and J. Lawrence, "High speed CO 2 laser surface modification of iron / cobalt co-doped boroaluminosilicate glass and the impact on surface roughness , gloss and wettability," *Laser Phys. Lett. 13*, vol. 13, no. 076102, 2016.

[22] F. Heib, W. M. Munief, S. Ingebrandt, R. Hempelmann, and M. Schmitt, "Influence of different chemical surface patterns on the dynamic wetting behaviour on flat and silanized silicon wafers during inclining-plate measurements : An experimental investigation wi," *Colloids Surfaces A*, vol. 508, pp. 274–285, 2016.

[23] B. S. Cook, J. A. Herbsommer, Y. Lin, R. Zhang, A. Castro, and M. D. Romig, "PACKAGED DEVICE WITH ADDITIVE SUBSTRATE SURFACE MODIFICATION," p. US9524926 B2, 2016.

[24] C. Vanhaverbeke, R. Verplancke, J. De Smet, D. Cuypers, and H. De Smet, "Microfabrication of a spherically curved liquid crystal display enabling the integration in a smart contact lens," *Displays*, vol. 49, pp. 16–25, 2017.

[25] F. Honoré, B. Otis, and A. Nelson, "Reader Communication with Contact Lens Sensors and Display Device," p. US8922366 B1, 2017.

[26] S. Han, S. Ji, A. Abdullah, D. Kim, H. Lim, and D. Lee, "Applied Surface Science Superhydrophilic nanopillar-structured quartz surfaces for the prevention of biofilm

formation in optical devices," *Appl. Surf. Sci.*, vol. 429, pp. 244–252, 2018.

Chapter 6: Contact Lenses-Based Microchannels for Continuous Monitoring of Glaucoma.

Research work in this chapter of the alternative format thesis is submitted to **Contact lens & anterior eye Journal.** The submission details and authors' contributions are provided here.

Yousef Alqurashi, Mohamed Elsherif, Magdalena Bajgrowicz-Cieslak, Muhammad Umair Hassan, Khamis Essa, Haider Butt, "Contact Lenses-Based Microchannels for Continuous Monitoring of Glaucoma"

Authors Contributions

Y.A. and H.B conceived the idea and deigned setups. **Y.A.** led the project, fabricated the samples using CO_2 laser, and analysed the results. **Y.A**. wrote the manuscript and H.B. supervised the project and reviewed the article. All authors reviewed the article.

ABSTRACT

Glaucoma is a major cause of irreversible blindness worldwide. For diagnosis, the intraocular eye pressure (IOP) has to be measured. Unfortunately, the available diagnostic techniques are invasive, uncomfortable, and requires visiting an optician. Here, commercial contact lenses were laser-processed to be capable of monitoring the intraocular eye pressure. A ring-couple was engraved on the surface of the contact lens by using carbon dioxide laser. Changing IOP leads to shift the interspace between the ring-couple and the interspace can be detected by a smartphone camera. Three different models of the ring-couples were introduced; the interspacing distances between the ring-couples were 1 mm, 1.5 mm, and 2 mm. The laser operation conditions for engraving the rings was 40 W, and 440 mm.s^{-1}, which produced a maximum depth of 20 μm. The developed contact lenses showed a significant response to the changes of the surface curvature, which make them candidate for measuring the intraocular pressure (IOP). The developed lenses were able to respond to the change of IOP in the range of 12 - 22 mmHg which represents the normal and the risk level of intraocular eye pressure, respectively. The proposed contact lenses are cost-effective, non-invasive, reusable, and can provide continuous monitoring.

KEYWORDS: contact lenses; glaucoma, intraocular eye pressure, carbon dioxide laser

6.1 INTRODUCTION

Glaucoma has become one of the main causes of blindness, which affects over 65 million people around the world. Almost half of patients with glaucoma do not recognize that they have this disease. [1–4] The increasing of intraocular pressure (IOP) is the main risk factor for glaucoma. An IOP above 21 mmHg is considered as a risk point for having glaucoma disease [5,6]. Although the IOP fluctuates during the day in glaucoma patients, most of the eye care clinicians depend mainly on one or a few IOP assessments within regular office times. Considerable studies have indicated that glaucoma patients experience the peak level of IOP outside of office hours [5–8]. The average IOP range over a 24-hour duration has been recorded as 9.4 mmHg and it can reach the highest value any time. Also, the 24-hour IOP value can be 12 mmHg higher than IOPs measured in the clinic [9–12]. Therefore, continuous IOP detection will be essential and more useful than the current methods.

Goldmann applanation tonometry (GAT) is the most known standard test for measuring intraocular pressure (IOP) since 1940 [12,13]. The GAT measurements are based on law of Imbert-Fick. The law assumes that the eyeball is an ideal sphere and the cornea is thin and elastic.[14,15] The GAT works by flattening the cornea over a defined area with a diameter of 3.06 mm and IOP estimation is provided by the applanation pressure. However, the central thickness of the cornea, scleral rigidity, and mechanical properties of the cornea affect the GAT performance.[16–18] Currently, the most popular method for 24-hour monitoring of IOP fluctuations is the diurnal tension curve (DTC), which records several IOP measurements at different times during working hours, or in a sleep laboratory.[19,20] Both GAT and DTC offer limited IOP values, inconvenient, and expensive. The patients are required to be awake during both approaches which may then cause stress issues.[14, 21]. In the past few years, self-

tonometry has been recommended; however, it is challenging for elderly patients and does not provide IOP measurements during sleep time.[22–24].

In order to tackle these issues, the Swiss company SENSIMED Triggerfish® has developed a contact lens sensor to detect continuously the IOP changes [25]. The sensor is designed based on the idea of that the IOP fluctuations induces changes in the cornea's curvature [26]. The sensor involves a silicone soft contact lens embedded with two pressure gauges, an antenna, and a microprocessor. The gauges monitor the modifications in cornea's shape to record the IOP values. It is a safe and well tolerated device for 24-hour measuring of IOP for healthy and glaucomatous users. Although the device is minimally invasive, safe, and has limited incompliance, it has some side effects such as blurry vision as the contact lens has no vision correction option.[6, 24]. Other side effects include dry eye, eye irritation, and the eye feel scratchy were reported.

In this paper, commercial contact lenses were laser-treated to allow continuous detection of intraocular eye pressure (IOP). A ring-couple was engraved on the surface of commercial contact lenses (ACUVUE TrueEye) using a carbon dioxide laser. Fabrication of the rings on the contact lenses was carried out by using simple, easy, rapid, cost-effective, and applicable mass-production method. The interspace between the ring-couples changed upon IOP fluctuations, and was detected by a smartphone camera.

6.2 METHODOLOGY

The contact lenses used in the experiment were ACUVUE TrueEye (Johnson & Johnson, Jacksonville, FL, USA). The lenses were taken from their original packaging and stored in 46%

H_2O in buffered saline with methyl ether cellulose; each lens had a base curve of 9.0 mm and a diameter of 14.2 mm. Micro-channels were created on the surfaces of the contact lenses in a shape of a ring-couple using a CO_2 laser (Rayjet, Canada, USA The laser beam has a wavelength of 10.6 μm, a variable output power with a maximum of 80 W, and a diameter of 20 μm. The ablation process was carried out on the outer edges of the lenses to avoid blocking the vision. The distance between the contact lens and the outlet of the laser beam was kept invariable at 50 mm throughout all laser-treatment processes. Other parameters such as laser's power, and laser' s scanning speed were validated and optimised using Rayjet software in order to avoid damaging the contact lenses. A schematic illustrates the used laser system and the fabrication process is showed in Figure 6.1(A). Two circular channels (rings) were created on the surface of the contact lens at different laser operation settings (power and scanning speed) to identify the optimum conditions. The fabricated micro-channels on the surfaces of contact lenses and their geometry are displayed in Figure 6.1(B-E).

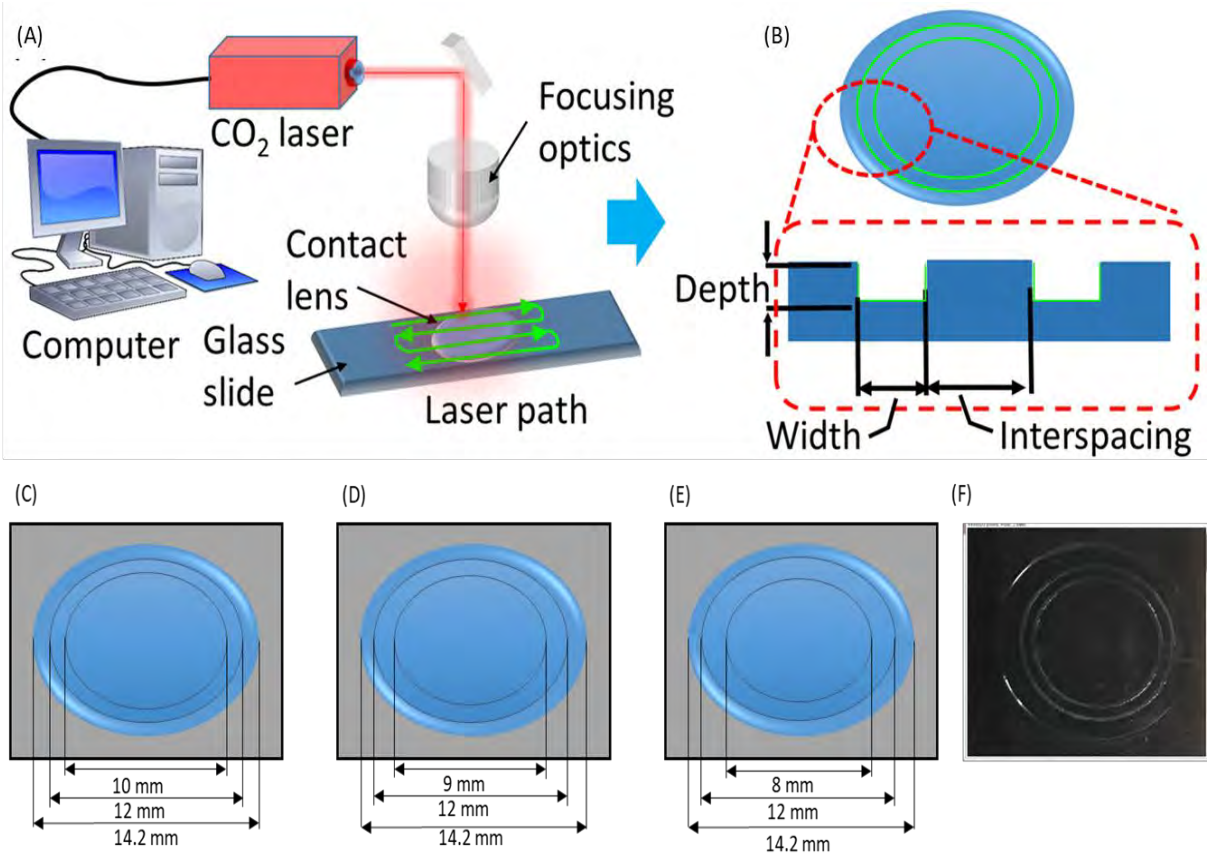

Figure 6.1: CO_2-laser for treating contact lenses: (A) Schematic of the laser system used to fabricate the micro-channel rings; (B) top and side view of the contact lens after laser-treatment; (C-E) an illustration of the geometric parameters of the engraved rings/channels; and (F) shows a real image of the laser- engraved geometries on selective portions of a contact lens

An optical microscopic (ZEISS, Jena, Germany, Zen USA software) was used to image the modified surface of the laser-treated lenses. The performance of the processed contact lenses was determined by measuring the change in the interspace between the fabricated ring-couple while the lenses fixed on surfaces of different curvature levels. The measurements were performed using an automatic calliper and a microscope. A schematic diagram of the microscope set-up and an image of the contact lens placed on the test holder is shown in Figure 6.2(A-C). The interspace between the laser-engraved rings were measured in flat and curved conditions for both the inner side and outer side of the lenses. Firstly, measurements

were performed when the lens was fixed on a flat plastic sheet (Figure 6.2D). Secondly, measurements were recorded when a force was applied on the sides of the plastic sheet in such way that the lens was curved/bent, and the distance between the top of the lens and its bottom edge was 7.7 mm, which is the typical cornea radius of curvature (Figure 6.2E) [18]. Also, measurements were taken at radius of curvature of 15 mm, which represents the extreme risk of the cornea for developing glaucoma (Figure 6.2F) [18]. The distance between the two rings was measured by using the microscope's built-in software (Zen, USA).

Another test was carried out to check performance of the lenses. The contact lenses were fixed directly on a balloon surface to examine effect of increasing the balloon's internal pressure and the balloon surface curvature on the interspace of the rings which was measured by a calliper and a smartphone (Figure 6.2G). The photos of the tested lenses were captured by a smartphone camera, then ImageJ software was used to analyse the images measuring the interspace changes. Usage of a balloon assisted to simulate the change of the curvature of eye cornea resulting from increasing of IOP. The curvature of the balloon's surface changed with the internal pressure of the balloon. As a result, the interspace between the engraved rings on the contact lens fixed on the balloon shifted. The contact lenses were examined at two conditions: at pressures of 12 mmHg, and 22 mmHg which represent the normal and risk level of the intraocular eye pressure (Figure 6.2G-I)) [5].

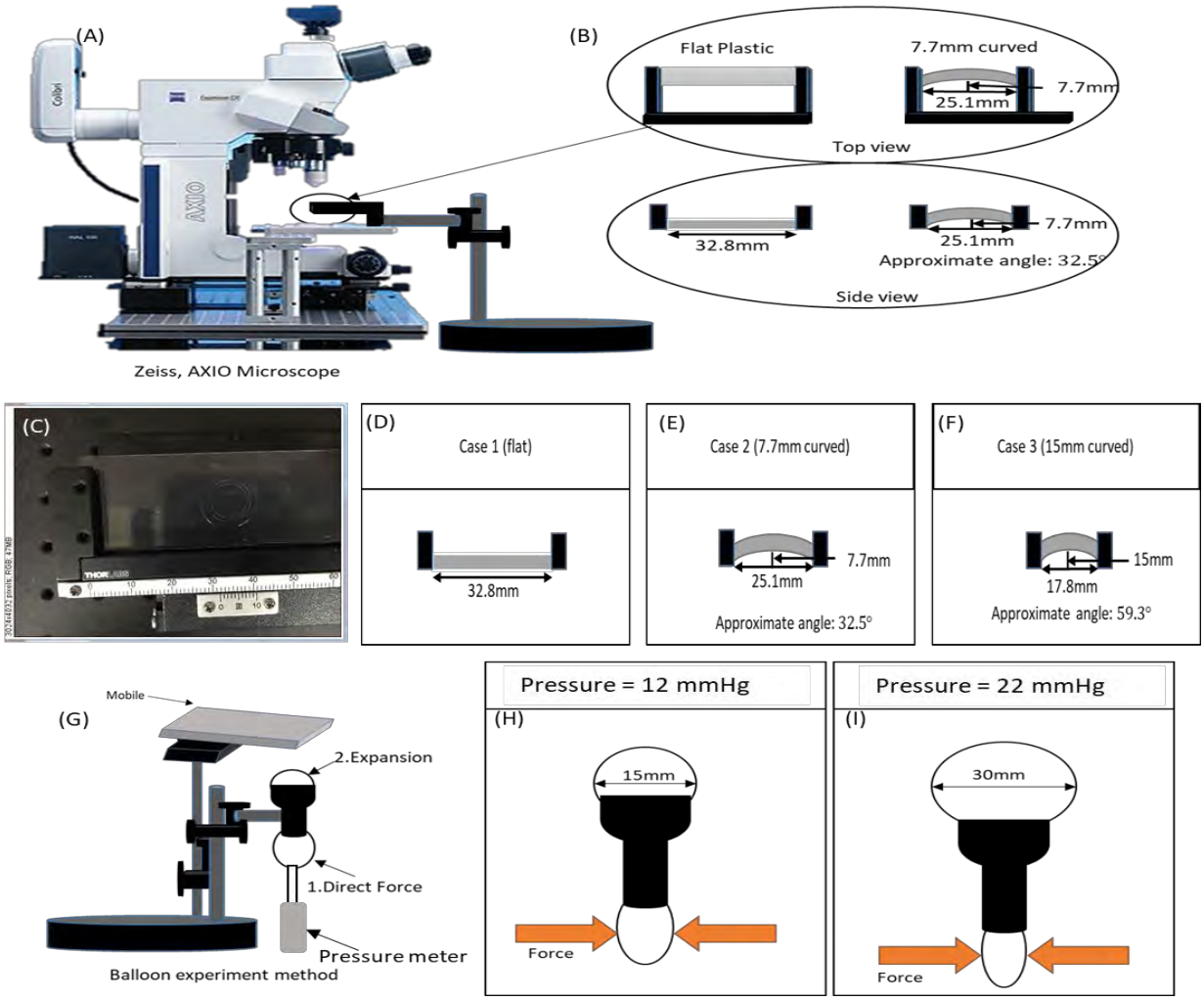

Figure 6.2: (A) a schematic presentation of the microscope setup; (B) top and side view of sample images during the change of the curvature; (C) shows a real image taken by the microscope; (D-F) show an illustration of the testing cases; (G) a schematic presentation of the pressure increasing experiment using a balloon; (H-I) show an illustration of the testing cases with pressure at 12 mmHg and 22 mmHg, which are the normal IOP and the glaucoma's IOP, respectively

6.3 RESULTS AND DISCUSSION

Many trials were carried to optimize the microchannel fabrication process on the contact lens by using CO_2 laser. The laser power was swapped from 36 up to 48 W while the scanning speed was changed in the range of 440 – 520 $mm.s^{-1}$. However, the distance between the laser outlet and the contact lens was kept fixed at 50 mm. Table 6.1 summarizes the laser system operation conditions and the geometry of the fabricated ring-couples on each contact lens.

Table 6.1: lists all the testing scenarios.

Contact lens	Interspacing (mm)	Laser power (W)	Scanning speed ($mm \cdot s^{-1}$)
1	12 mm and 10 mm	48	520
2		48	480
3		44	520
4		44	480
5		40	600
6		40	440
7	12 mm and 9 mm	40	440
8	12 mm and 8 mm	40	440
9	12 mm and 8 mm	36	440

Microscope images of all laser-processed contact lenses are presented in Figure 6.3(A). Some laser-treated contact lenses were damaged and images of the successfully processed lenses are showed in Figure 6.3B. According to the microscopic images, the best results were achieved at laser operation conditions; laser power of 40 W and scanning speed of $440 mm.s^{-1}$. The experiment showed that the power and speed of the laser beam above the optimal settings leads to cracking and destroying the lenses. Also, the lower input power could not create convenient engraves on the lens's surface. The quality of the produced micro-channels was examined by Alicona optical microscope (Figure 6.4B-C). Following to the laser optimization process, the laser system was run at the optimum operation conditions for producing a ring-couple on each introduced contact lens. Three ring-couples each of interspace 1, 1.5, 2 mm were engraved on three contact lenses separately (Figure 6.4A). Also, a 3D optical microscope was used to analyse the channels' depth, obtained at optimum operation condition of the laser system (Figure 6.4D). The maximum depth was measured to be ~ 20 μm for the rings.

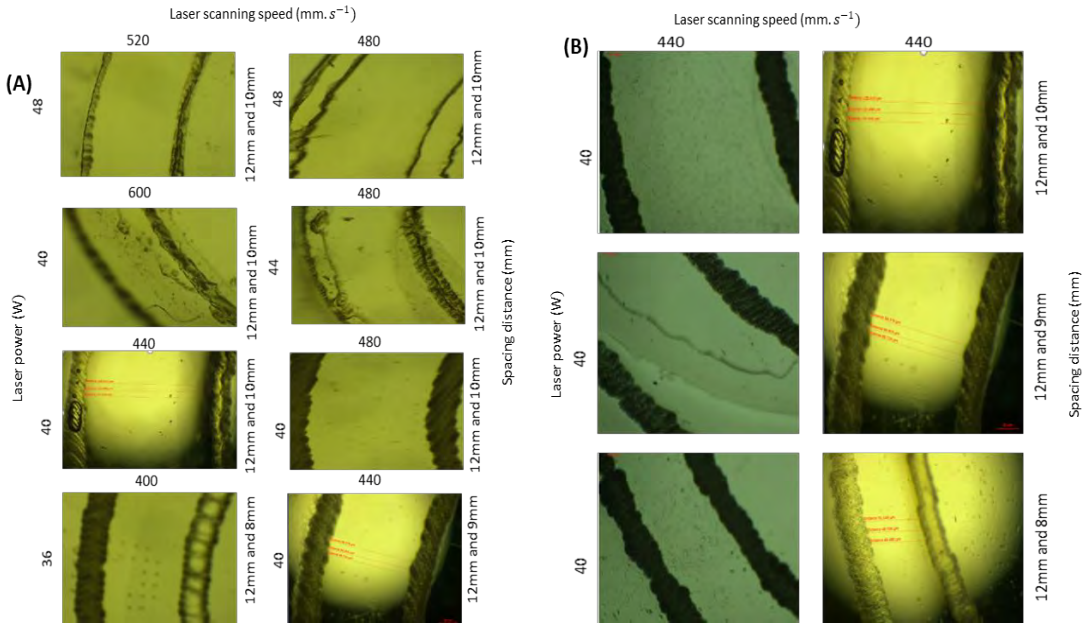

Figure 6.3: Images of contact lenses captured by an optical microscope after the laser treatment process; (A) images of all the laser-treated lenses at different laser operation conditions; (B) images of the contact lenses those survived the laser treatment process having different spacing gaps between the microchannel, the red lines in the images were drawn to measure the distance between the rings using the microscope's built-in software

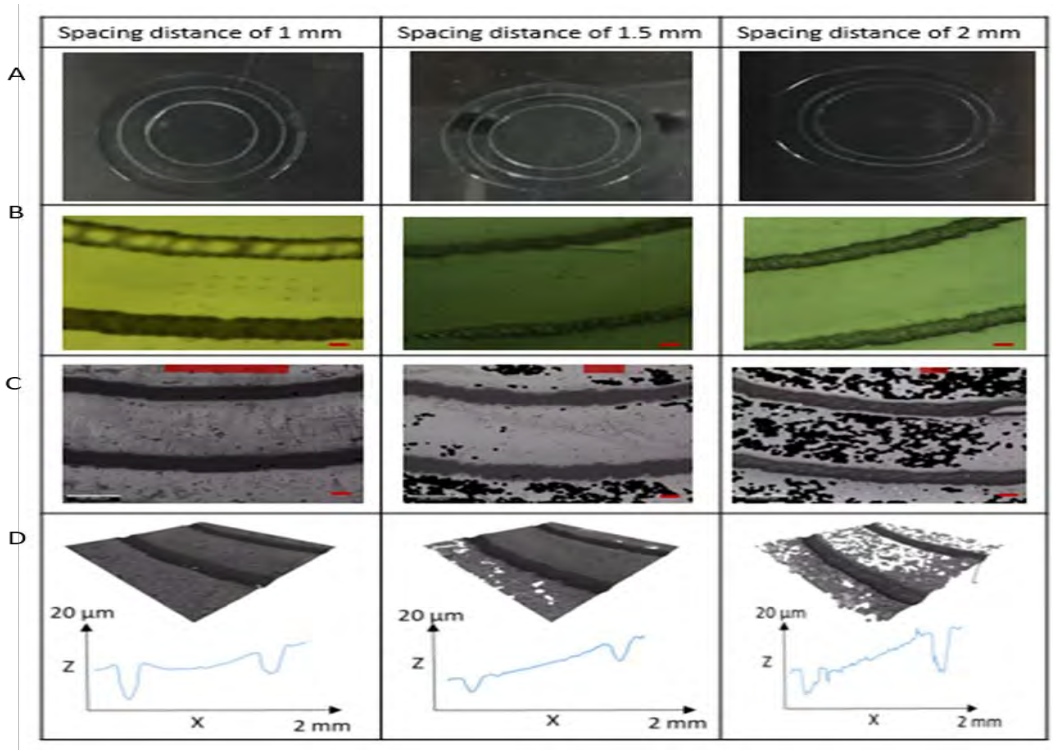

Figure 6.4: Pictures of the laser-treated contact lenses: (A) photographs of CO_2 laser-engraved rings on the lenses produced at laser power of 40 W and scanning speed of 440 mm.s^{-1}; (B-C) microscopic images of laser-modified contact lenses; (D) 3D microscopic images of the channels to study the depth

Performance of the laser treated lenses was tested. The lens was fixed on a plastic flexible sheet and the interspace between the ring-couple was measured under the microscope while the lens was lying flat. The interspace measurements were repeated while the lens was curved at different radius of curvatures. Changing the curvature of the lens affected the interspacing between the engraved rings. The interspaces of the ring-couples in all examined lenses showed an increase with changing the lens conditions from flat to curved. Changing the conditions of the lens's surface from flat to curved with a radius of curvature 7.7 mm led to increasing the interspace between the channels by up to ≈ 12%. The interspacing distance was increasing with the lens's surface curvature. For the lens with interspacing of 1.5 mm, increasing the radius of curvature to 15 mm resulted in an increase in the interspace by ≈ 20%. However, it increased by ≈ 10% for the contact lens with interspacing of 1 mm and 2 mm (Figure 6.5A). The interspace readings can be recorded by examining either the engraved surface of the lens or the intact surface. Figure 6.5B illustrates that the readings taken from the intact lens's surface are relatively similar to the results taken from the laser-treated side. As the interspacing increased by up to ≈ 10% and ≈ 20% at radius of curvatures 7.7 mm and 15 mm, respectively.

Performance of the laser-treated lenses was re-checked by a different method. The lens was fixed on a balloon surface and the interspace between the ring-couple was measured using a smartphone. The test was carried out at normal IOP value, 12 mmHg, and in glaucoma condition, 22 mmHg. It was found that the interspacing distance was increasing with the pressure (Figure 6.5C-D). The interspacing increased up to 4%, 10%, and 6% due to increasing the balloon internal pressure for the samples of interspacing distances 1, 1.5, and 2 mm, respectively. Also, results taken from the untreated surfaces of the contact lenses were similar to those measured at the treated surface (Figure 6.5D).

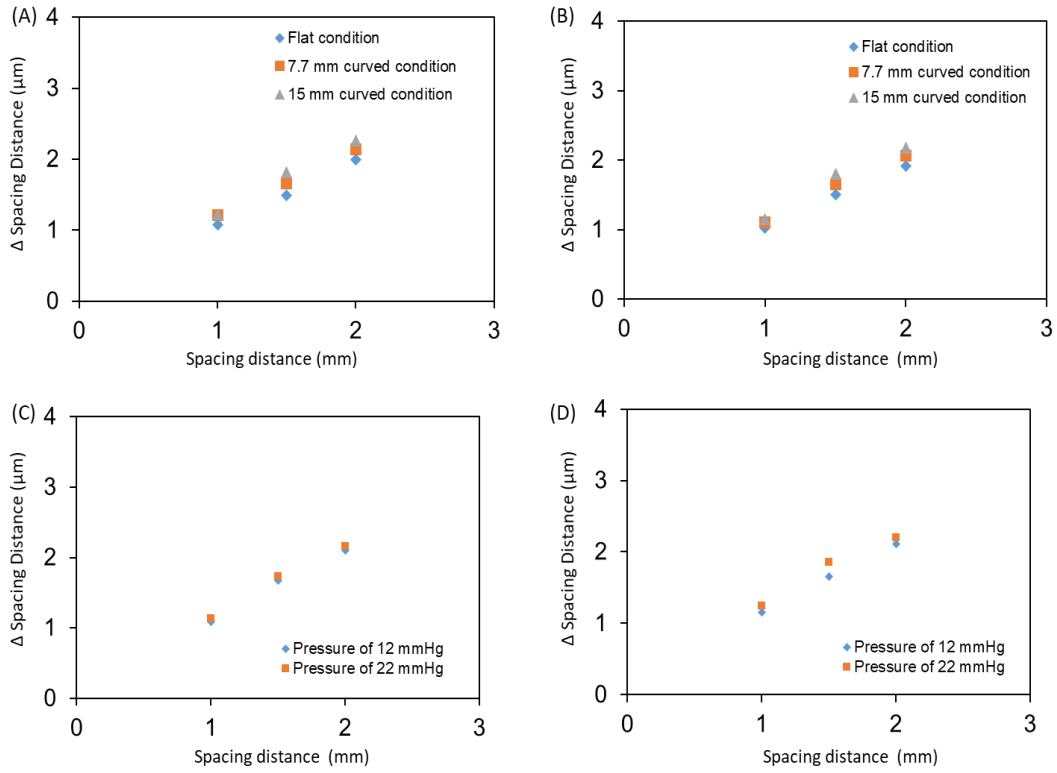

Figure 6.5: The interspace measurements for the laser-treated contact lenses: (A) the change of the interspacing between the channels due to the increase of the radius of curvature from the flat condition(0 mm) to 7.7 mm, and 15 mm; (B) the change of the interspacing between the channels measured at the untreated surface of the lenses; (C) the change of the interspacing between the microchannels measured from the laser-treated side of the contact lens at pressure range of 12 – 22 mmHg; (D) the change of the interspacing between the channels, measurements were taken from the untreated side of the contact lens

6.4 CONCLUSION

We have developed a cost-effective, and minimally invasive method for monitoring the intraocular eye pressure. Commercial contact lenses were laser-treated to create ring-couples. The ring-couples were fabricated on the contact lenses at a laser power of 40 W and a scanning speed of 440 mm.s^{-1} with channel depths of up to 20 µm. The fabricated lenses showed the ability to change the interspacing distance with changing their curvature. The fabricated rings demonstrated a good response to the changes of the different surface curvature level as the

interspace between the ring-couple changed up to 20% upon increasing the pressure from 12 to 22 mmHg. The proposed contact lens is reusable and it could be used as a continuous and non-invasive technique to monitor IOP for glaucoma patients. Smartphones can be used as readers to capture the interspacing changes, and thus providing the opportunity to obtain rapid results at home.

REFERENCES

[1] H. A. Quigley, "Number of people with glaucoma worldwide," *Br. J. Ophthalmol.*, vol. 80, pp. 389–393, 1996.

[2] S. Resnikoff *et al.*, "Global data on visual impairment in the year 2002," *Bull. World Health Organ.*, vol. 82, no. 11, pp. 844–851, 2004.

[3] J. Liu and C. Roberts, "Influence of corneal biomechanical properties on intraocular pressure measurement:: Quantitative analysis," *J. Cataract Refract. Surg.*, vol. 31, pp. 146–155, Feb. 2005.

[4] H. A. Quigley and S. Vitale, "Models of open-angle glaucoma prevalence and incidence in the United States," *Investig. Ophthalmol. Vis. Sci.*, vol. 38, no. 1, pp. 83–91, 1997.

[5] K. Mansouri, F. A. Medeiros, A. Tafreshi, and R. N. Weinreb, "Continuous 24-hour Intraocular Pressure Monitoring With a Contact Lens Sensor: Safety, Tolerability, and Reproducibility in Glaucoma Patients," *Arch Ophthalmol*, vol. 130, no. 12, 2012.

[6] T. Realini, N. Weinreb, and S. Wisniewski, "Short-term repeatability of diurnal intraocular pressure patterns in glaucomatous individuals," *Ophthalmology*, vol. 118, no. 1, pp. 47–51, 2011.

[7] K. Mansouri and R. N. Weinreb, "Continuous 24 hour intraocular pressure monitoring for glaucoma with a contact lens sensor - Time for a paradigm change," *Swiss Med. Wkly.*, vol. 142, no. MARCH, 2012.

[8] Y. Barkana, S. Anis, J. Liebmann, C. Tello, and R. Ritch, "Clinical Utility of Intraocular Pressure Monitoring Outside of Normal Office Hours in Patients With

Glaucoma," *JAMA Ophthalmol.*, vol. 124, no. 6, pp. 793–797, Jun. 2006.

[9] E. Renard *et al.*, "Twenty-four hour (nyctohemeral) rhythm of intraocular pressure and ocular perfusion pressure in normal-tension glaucoma," *Investig. Ophthalmol. Vis. Sci.*, vol. 51, no. 2, pp. 882–889, 2010.

[10] E. Hughes, P. Spry, and J. Diamond, "24-Hour Monitoring of Intraocular Pressure in Glaucoma Management: A Retrospective Review," *J. Glaucoma*, vol. 12, no. 3, 2003.

[11] J. H. K. Liu and R. N. Weinreb, "Monitoring intraocular pressure for 24 h," *Br. J. Ophthalmol.*, vol. 95, no. 5, pp. 599–600, 2011.

[12] T. Kida, J. H. K. Liu, and R. N. Weinreb, "Effect of 24-hour corneal biomechanical changes on intraocular pressure measurement," *Investig. Ophthalmol. Vis. Sci.*, vol. 47, no. 10, pp. 4422–4426, 2006.

[13] Y. H. Lee, C. S. Kim, and S. pyo Hong, "Rate of visual field progression in primary open-angle glaucoma and primary angle-closure glaucoma.," *Korean J. Ophthalmol.*, vol. 18, no. 2, pp. 106–115, 2004.

[14] K. Mansouri, F. A. Medeiros, A. Tafreshi, and R. N. Weinreb, "Continuous 24-hour monitoring of intraocular pressure patterns with contact lens sensor: Safety, tolerability, and reproducibility in patients with glaucoma," *Arch. Ophthalmol.*, vol. 130, no. 12, pp. 1534–1539, 2012.

[15] N. Ehlers, T. Bramsen, and S. Sperling, "Applanation Tonometry and Central Corneal Thickness," *Acta Ophthalmol.*, vol. 5, no. 512, pp. 34–43, 1975.

[16] M. C. Lin *et al.*, "Scalloped channels enhance tear mixing under hydrogel contact lenses," *Optom. Vis. Sci.*, vol. 83, no. 12, pp. 874–878, 2006.

[17] A. Chauhan and C. J. Radke, "Settling and deformation of a thin elastic shell on a thin fluid layer lying on a solid surface," *J. Colloid Interface Sci.*, vol. 245, no. 1, pp. 187–197, 2002.

[18] M. Leonardi, P. Leuenberger, D. Bertrand, A. Bertsch, and P. Renaud, "First steps toward noninvasive intracular pressure monitoring with a sensing contact lens," *Investig. Ophthalmol. Vis. Sci.*, vol. 45, no. 9, pp. 3113–3117, 2004.

[19] M. V. Monticelli, A. Chauhan, and C. J. Radke, "The effect of water hydraulic permeability on the settling of a soft contact lens on the eye," *Curr. Eye Res.*, vol. 30,

no. 5, pp. 329–336, 2005.

[20] J. L. Creech, A. Chauhan, and C. J. Radke, “Dispersive mixing in the posterior tear film under a soft contact lens,” *Ind. Eng. Chem. Res.*, vol. 40, no. 14, pp. 3015–3026, 2001.

[21] R. N. Weinreb and J. H. K. Liu, “Nocturnal Rhythms of Intraocular Pressure,” *Arch. Ophthalmol.*, vol. 124, no. 2, pp. 269–270, Feb. 2006.

[22] C. R. Schnell, C. Debon, and C. L. Percicot, “Measurement of intraocular pressure by telemetry in conscious, unrestrained rabbits,” *J. Toxicol. - Cutan. Ocul. Toxicol.*, vol. 18, no. 3, p. 244, 1999.

[23] J. H. K. Liu, X. Zhang, D. F. Kripke, and R. N. Weinreb, “Twenty-four-hour intraocular pressure pattern associated with early glaucomatous changes,” *Investig. Ophthalmol. Vis. Sci.*, vol. 44, no. 4, pp. 1586–1590, 2003.

[24] J. H. K. Liu, F. A. Medeiros, J. R. Slight, and R. N. Weinreb, “Diurnal and nocturnal effects of brimonidine monotherapy on intraocular pressure,” *Ophthalmology*, vol. 117, no. 11, pp. 2075–2079, 2010.

[25] G. E. Dunbar, B. Y. Shen, and A. A. Aref, “The Sensimed Triggerfish contact lens sensor: Efficacy, safety, and patient perspectives,” *Clin. Ophthalmol.*, vol. 11, pp. 875–882, 2017.

[26] J. H. K. Liu and R. N. Weinreb, “Monitoring intraocular pressure for 24 h,” *Br. J. Ophthalmol.*, vol. 95, no. 5, pp. 599–600, 2011.

Chapter 7: Conclusions

7.1 CONCLUSION

The aim of this research was accomplished by the fabrication of three different sensors to detect glucose, pH level and intraocular pressure (IOP). Two methods were used to develop the sensors. Firstly, imprinted micro-structures were fabricated on hydrogel material. The imprinted structures helped to monitor glucose using phenylboronic acid functionalized hydrogel films, and to detect pH levels using a Fresnel lens stamped on 2-hydroxyethyl methacrylate (HEMA). Secondly, CO_2 laser ablation was used to develop two micro circular channels on the surface of commercial contact lenses. The CO_2 laser removal was also used to modify the surface properties of a contact lens by engraving 1D and 2D channels on the surface and then investigating the wettability of the lens.

A novel glucose sensor based imprinted glucose responsive hydrogel was developed. The hydrogel was made on poly-acrylamide, *N*,*N*'-methylenebisacrylamide polymerized with a phenylboronic acid, 3-(acrylamido)phenylboronic acid. A micro-stamp of a hexagonal structure was fabricated from PDMS mirror-replica grating into the hydrogel mixture. Then the glucose detection was achieved through optical diffraction measurements from the stamped hydrogel in the presence of various glucose levels. The sensor was able to detect a glucose concentration from 1 mM to 200 mM within a response time of 15 min. The proposed photonic sensors can be used in point-of-care tools, implantable devices, and continuous wearable glucose detection systems.

In addition, a new pH monitoring method was presented here based on a patterned Fresnel lens on the surface of hydrogel, mainly made of 2-hydroxyethyl methacrylate (HEMA), which is the fundamental material used to manufacture commercial contact lenses. The HEMA substance was incorporated with ethylenedioxy-N-methylamphetamine (EDMA), acrylic acid (AA) and 2-dimethoxy-2-phenylacetophenone (DMPA) to form the pH-sensitive hydrogel. Then, the combination was poured on a Fresnel lens structure to fabricate two sets of samples, a sample attached to the glass and a free standing sample. Both sensors had a pH sensitivity range from 4.5 to 7.4 and a response time of 5 minutes. The sensors showed an increase in sensitivity after 10 days storage in a buffer solution of pH 7.4. The increase in temperature from 20 $^{\circ}$C to 40 $^{\circ}$C had no significant impact on the sensors' performance. The proposed hydrogel-based sensors are a simple, fast and cost-effective method to detect pH changes.

Laser ablation was applied to commercial contact lenses, Narafilcon, 1-day Acuvue® TruEye®, Johnson & Johnson, to modify their surface in order to improve the wettability of the lenses. Carbon dioxide laser (CO_2-laser), HPC LS 3040, was utilized to perform 1D and 2D arrays on selective areas of the lenses. Different laser parameters (the space gap between the patterns; laser power; and scan speed) were applied to investigate the effect of surface roughness on the hydrophilicity and transmission of the lenses. It was found that the laser parameters of 0.3 mm space gap, 9 W power at 200 mm s^{-1} scanning speed are the best settings that can be applied to commercial contact lenses to improve the wettability area. The laser removal process had a maximum depth of 40 μm. Surface treatment of contact lenses may be useful for a wide range of applications such as LED lights, communication systems, biosensing applications, and drug release control. However, our optical transmittance measurements showed a drop on the light transmittance by 45% for the treated lenses, due to the large exposure and density of the laser energy.

Furthermore, a CO_2 laser was used to structure two ring-shaped channels on the surface of a commercial contact lens (ACUVUE TrueEye) with diameter of 14.2 mm. It was found that the optimal laser setting was a power of 40 W with a scanning speed of 440 $mm.s^{-1}$, creating a maximum depth of 20 μm. Three lens were fabricated with interspacing between the channels of 1 mm, 1.5 mm and 2 mm. The interspacing between the designed channels changed in respect to the change in the lens position, from a flat position to up to a 15-mm curvature position. The distance increased by up 20% when the lenses' curvature changed to 7.7 mm and 15 mm, which are respectively the ideal radius of the cornea curvature, and the extreme risk radius of the cornea curvature. Additionally, the space between the two rings increased when the pressure was boosted up from 12 mmHg to 22 mmHg, which are the normal IOP of a healthy eye and the IOP of a glaucoma patient's eye, respectively. The proposed lenses are reusable, fast to fabricate, and cost-effective. Moreover, the lenses showed a response in detecting the pressure changes, which may be used for detection of IOP increases in glaucoma treatment.

Finally, stamping and laser ablation methods were demonstrated to fabricate hydrogel-based sensors. However, each method has its own advantages and limitations. Stamping techniques are reusable, suitable for mass production, cost-effective, have a fast response and are non-invasive. Two different structures were stamped on the hydrogel substance. Firstly, a hexagonal diffraction grating was imprinted on hydrogel with phenylboronic acid to monitor the glucose changes. The second stamped structure was a Fresnel lens which was copied on the surface of the hydrogel. Both micro-structures and the use of hydrogels showed the capability of manufacturing good quality sensors with a fast response time. However, the range of these sensors may need to be increased; for example to detect glucose concentrations below 1 mM or a pH level between 7 and 7.45, where the sensors may be suitable for biological use. The

main limitation of this process was that the hydrogel preparation may be time consuming. The pH-sensitive hydrogel needed about 5 minutes under the UV light; whereas the glucose-sensitive hydrogel needed about one hour of UV curing. It required more time because the hexagonal grating cannot be copied directly into the phenylboronic-acid-based hydrogel. Moreover, the pH hydrogel-based sensor was equilibrated by keeping the samples overnight in a PBS of pH 7.4.

On the other hand, the CO_2 laser ablation method is modern, fast, and no skilled staff are required. Additionally, it is the least expensive ablation laser system compared to other systems like the excimer laser, and the femtosecond laser. The contact lens treatment was carried out by two different CO_2 lasers: CO_2 laser (HPC LS 3040) and Rayjet CO_2 laser. The CO_2 laser (HPC LS 3040) was used to manipulate the surface of contact lenses that are available on the market. We managed to improve the surface wettability by treating a selective area of the lens. However, the laser power damaged some lenses due to the high light exposure. Also, the creation of the 2D patterns led to the lenses being destroyed due to the thermal effects of repeating the micro-patterning on the same spots. Hence, a femtosecond laser would offer a better result for 2D micro-structures because of the high resolution of such a laser. Moreover, the Rayjet CO_2 laser was used to fabricate micro-channels on the contact lens to measure the IOP for glaucoma patients. The Rayjet laser showed relatively better results in comparison to the other laser system here. The CO_2 laser (HPC LS 3040) has a fixed z-axis of 7.4 mm; while the z-axis in the Rayjet removal was manually adjustable. In addition, the Rayjet provides access to graphic design software called CorelDraw, used for designing the desired structures. Furthermore, the Rayjet laser can work with other software and even with Microsoft PowerPoint.

7.2 CONTRIBUTION TO KNOWLEDGE

1. A new optical glucose sensor based on a hexagonal diffraction grating imprinted on flexible hydrogel has been developed. The sensor detected the changes in the diffraction angle within 15 min due to the increasing glucose concentrations (1–200 mM). This change could also be detected clearly under an optical microscope – the minimum increase in the thickness of the hydrogel sensor was ≈ 2% for the lowest concentration of 1 mM.

2. A pH sensor has also been manufactured using a Fresnel lens structure stamped on pH-sensitive hydrogel. The sensor detected changes within seconds of contact with the pH solutions. These pH sensors were also found to be reusable by repetition of the experimental process. The fabricated hydrogel was based on a composition of hydroxyethyl methacrylate (HEMA). The proposed sensors exhibited good sensitivity with a quick response time.

3. A new laser treatment method, using a CO_2-laser, was demonstrated to improve the wettability of commercial contact lenses. The approach was adopted to increase the surface area at selected places on the contact lens. Improved wetting properties were obtained by increasing the density of the surface patterns. The wettability was measured by depositing a controlled volume of deionized (DI) water onto a fully-hydrated lens. The correlation between the surface area and the inherent wettability/contact angle was studied. The wettability improvement led us to fabricate channels in contact lenses via CO_2-laser treatment.

4. The laser engraving treatment has been used to create a ring-shaped channel on commercial contact lenses to measure IOP changes. The objective of the project is to critically assess the channel design, as well as to classify and evaluate the effectiveness

and viability of the channel application for glaucoma patients. The fabricated lenses were able to respond to the change of IOP in the range of 12-22 mmHg.

7.3 FUTURE WORK

The master hexagonal diffraction grating has been successfully copied in poly(HEMA). This poly(HEMA) is the main compound used to fabricate commercial contact lenses. The master grating was patterned initially in a PDMS surface and then replicated into the poly(HEMA) hydrogel (Figure 7.1A). The hydrogel was made of 2-hydroxyethyl methacrylate (HEMA), ethylene glycol dimethacrylate (EGDMA) and a photo-initiator (of 2-hydroxy-2-methylpropiophenone). The proposed fabricated hydrogel was able to react to the temperature changes from 20°C to 40°C. Diffraction patterns generated by the blue laser of 450 nm showed that the diffraction angles between zero and the 1st-order peaks for blue light shifted due to variation in the temperature Figure 7.1(B-C). Moreover, when the temperature increases, in the interspace of the 1st-order diffraction decreases see Figure 7.1(D).

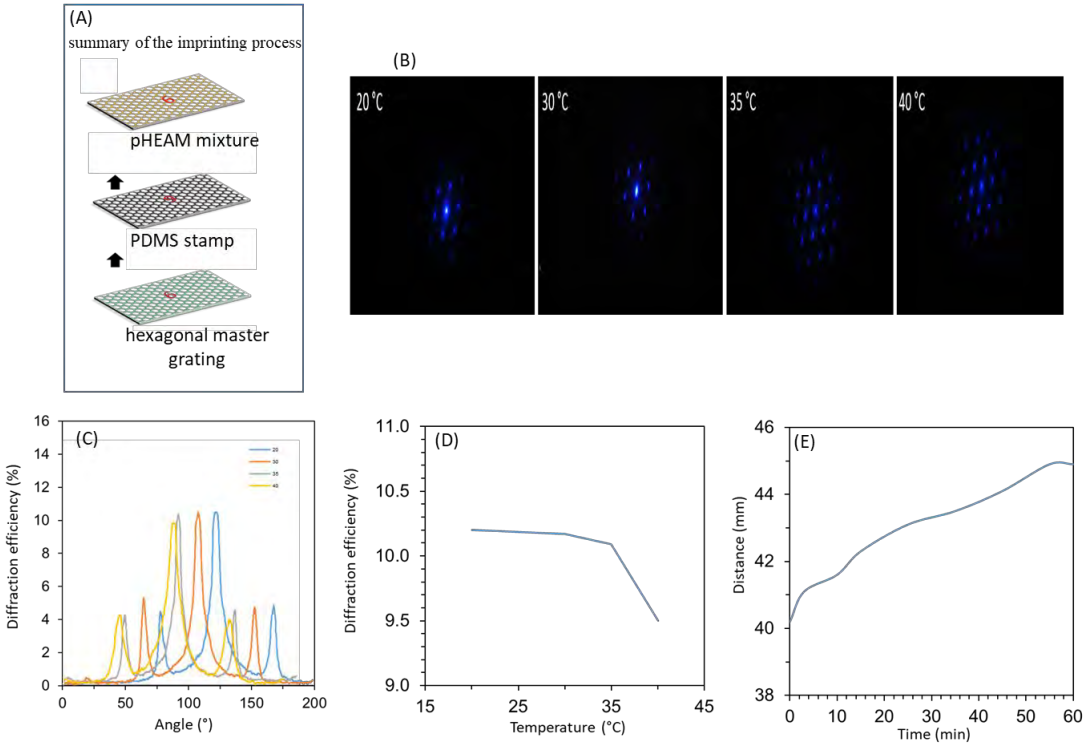

Figure 7.1: Fabrication of hydrogel-based sensor to detect the temperature changes: (A) a summary of the replication process; (B) diffraction patterns generated by blue laser light (450 nm wavelength) transmitted through the sample due the increase of temperature 20, 30, 35, and 40 °C; (C) the shift of the angle-resolved intensity graphs representing diffraction patterns generated by the 2smaple illuminated by the blue laser due to the variation in temperature; (D) the change in the interspace of the 1st-order with increasing temperature; (E) time-response of the sensor

Furthermore, fibre optic cables were used to create micro-channels within the contact lenses' hydrogel. This technique may be used in a wide range of biomedical applications, such as controlling the time of drugs delivery release.

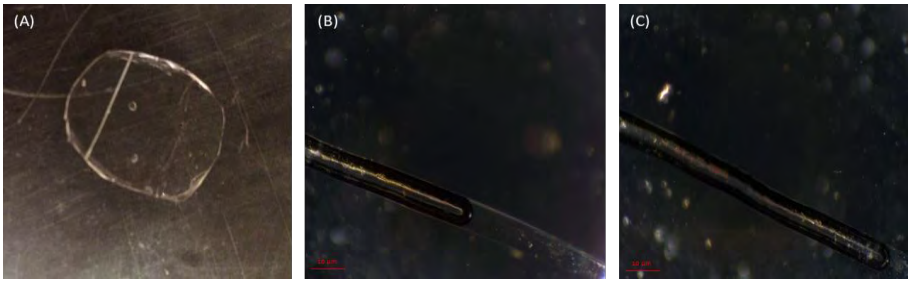

Figure 7.2: Fabricated channel inside hydrogel sample: (A) picture of the sample; (B) and (C) microscopic images of the channel